UC San Diego

UC San Diego Electronic Theses and Dissertations

Title

Cleaning, Passivation, and Functionalization of SiGe(001) and (110) Surfaces for ALD Nucleation

Permalink

https://escholarship.org/uc/item/8sq6g9d9

Author

Park, Sang Wook

Publication Date

2016

Peer reviewed|Thesis/dissertation

eScholarship.org Powered by the California Digital Library
University of California

UNIVERSITY OF CALIFORNIA, SAN DIEGO

Cleaning, Passivation, and Functionalization of SiGe (001) and (110) Surfaces for ALD Nucleation

A dissertation submitted in partial satisfaction of the requirements for the degree
Doctor of Philosophy

in

Materials Science and Engineering

by

Sang Wook Park

Committee in Charge:

Professor Andrew C. Kummel, Chair
Professor Ratnesh Lal
Professor Yu-Hwa Lo
Professor William C. Trogler
Professor Paul K. Yu

2016

Copyright ©

Sang Wook Park, 2016

All Rights Reserved

The Dissertation of Sang Wook Park is approved, and it is acceptable in quality and form for publication on microfilm and electronically:

Chair

University of California, San Diego

2016

DEDICATION

To my Wife and Daughters, whose endless love always encourages and supports me in all aspects of life.

EPIGRAPH

Science is but a perversion of itself unless it has as its ultimate goal the betterment of humanity.

Nikola Tesla

TABLE OF CONTENTS

LIST OF SYMBOLS AND ABBREVIATIONS

Å	angstrom
ALD	atomic layer deposition
BE	binding energy
CB	conduction band
CVD	chemical vapor deposition
DFT	density functional theory
DI	deionized
D_{it}	density of interface traps
DOS	density of states
e	electron
E_f	Fermi level
FinFET	Fin field-effect transistor
I	electric current
KE	kinetic energy
L	Langmuir
LDOS	local density of states
MBE	molecular beam epitaxy
MIS	metal insulator semiconductor
MOS	metal oxide semiconductor
MOSCAP	metal oxide semiconductor capacitor
MOSFET	metal oxide semiconductor field effect transistor

nm	nanometer
pA	picoamps
PAW	projector augmented wave
PBE	Perdew-Burke-Emzerhof
PBN	pyrolitic boron nitride
PDA	post deposition anneal
PP	pseudo potential
SCE	short-channel effect
SRC	Semiconductor Research Corporation
STM	scanning tunneling microscopy
TDMAT	tetrakis(dimethylamino)titanium
TMA	trimethylaluminum
UHV	ultra high vacuum
V	volts
VASP	Vienna ab-initio simulation package
VB	valence band
V_{th}	threshold voltage
XPS	x-ray photoelectron spectroscopy
υ	frequency
Φ_{spec}	spectrometer work function

LIST OF FIGURES

LIST OF TABLES

ACKNOWLEDGEMENTS

First of all, I would like to acknowledge my advisor, Professor Andrew C. Kummel, who has motivated me to dive myself into surface science. Under his sincere guidance, I was able to focus on my experiments and present my research to many scientists in various conferences.

I also would like to acknowledge my former coworker, Dr. Tobin Kaufman-Osborn who has led me to overcome challenges I was facing. As a trainer and friend, he has taught me to develop my ability to solve the difficulties in creative and logical ways and drove me to be relaxed and comfortable in my San Diego life. Dr. Tyler Kent was also a nice friend who helped me to come up with solutions through intensive discussions. I also want to thank Jong Youn Choi for his positive and honest attitude toward research and life. As a good teammate working on our chamber together, he allowed me to enjoy the vacuum science through numerous hands-on experiments and discussions. I also would like to thank all of other teammates in Kummel group who shared unforgettable memories with me; Hyunwoong Kim, Iljo Kwak, Dr. Evgeniy Chagarov, Mary Edmonds, Steven Wolf, Christopher Ahles, Kasra Sardashti, Dr. Sergio Sandova, Natalie Mendez, and James Wang.

I also would like to thank my committee members for their sincere guidance help in my Senate and Thesis Defense. The committee members are Professor Paul Yu, Professor William Trogler, Professor Yu-hwa Lo, and Professor Ratnesh Lal.

My collaborators have helped me writing my doctor's thesis. Bhagawan Sahu, Shariq Siddiquui, Naomi Yoshida, Adam Brandt, Jessica Kachian provided me

numerous high quality SiGe wafers as well as clear directions and discussions toward the experiments.

I also would like to deliver my endless thanks to my family; Chloe Kim, Alison, and Catherine Park for their support for four years in San Diego.

This work was funded by the Semiconductor Research Corporation (SRC), GLOBALFOUNDRIES, and Applied Materials.

Chapter 2, in part or in full, is a reprint of the following material:

S. W. Park, T. Kaufman-Osborn, H. Kim, S. Siddiquui, B. Sahu, N. Yoshida, A. Brandt, A. C. Kummel "Combined wet and dry cleaning of SiGe(001)" Journal of Vacuum Science and Technology A., 33 (4) (2015). The dissertation author was the primary investigator and author of this paper.

Chapter 3, in part or in full, is a reprint of the following material:

S. W. Park, H. Kim, E. Chagarov, B. Sahu, S. Siddiquui, N. Yoshida, J. Kachian, A. C. Kummel "Formation of Chemically Selective Si-O-Al on SiGe(110) and SiGe(001)" Surface Science (*In Press*) (2016). The dissertation author was the primary investigator and author of this paper.

Chapter 4, in part or in full, is a reprint of the following material:

S. W. Park, J. Y. Choi, B. Sahu, S. Siddiquui, N. Yoshida, J. Kachian, A. C. Kummel "Formation of atomically ordered and chemically selective Si-O-Ti monolayer on $Si_{0.5}Ge_{0.5}$(110) for a MIS structure via H_2O_2(g)" (*Manuscript in preparation*). The dissertation author was the primary investigator and author of this paper.

VITA

EDUCATION

2008 Bachelor of Science in Materials Science and Engineering, Hanyang University

2010 Master of Science in Materials Science and Engineering, Stanford University

2016 Doctor of Philosophy in Materials Science and Engineering, University of California, San Diego

PUBLICATIONS

S. W. Park, J. Y. Choi, B. Sahu, S. Siddiquui, N. Yoshida, J. Kachian, A. C. Kummel "Formation of atomically ordered and chemically selective Si-O-Ti monolayer on $Si_{0.5}Ge_{0.5}$(110) for a MIS structure via H_2O_2(g) functionalization" *(manuscript in preparation)*

S. W. Park, H. Kim, E. Chagarov, B. Sahu, S. Siddiquui, N. Yoshida, J. Kachian, A. C. Kummel "Formation of Chemically Selective Si-O-Al on SiGe(110) and (001) for ALD Nucleation Using H_2O_2(g)" Surface Science *(In Press)* (2016)

K. Sardashti, K-T Hu, H. Kim, S. Park, K. Tang, S. Madisetti, P. McIntyre, S. Oktyabrsky, S. Siddiqui, B. Sahu, N. Yoshida, J. Kachian, A. C. Kummel "Sulfur passivation for formation of Si terminated Al_2O_3/SiGe(001)" Applied Surface Science, 366, p455–463 (2016)

S. W. Park, T. Kaufman-Osborn, H. Kim, S. Siddiquui, B. Sahu, N. Yoshida, A. Brandt, A. C. Kummel "Combined wet and dry cleaning of SiGe(001)" Journal of Vacuum Science and Technology A., 33 (4) (2015).

S. W. Park, H. Kim, E. Chagarov, A. C. Kummel "Passivation and Functionalization of SiGe(001) and (110) via atomic hydrogen, and HOOH Dosing for ALD Nucleation" Techcon 2015 Austin, TX

S. W. Park, T. Kaufman-Osborn, E. Chagarov, A. C. Kummel "Functionalization of SiGe via H_2O_2(g) Dosing" Techcon 2014 Austin, TX

T. Kaufman-Osborn, E. Chagarov, S. W. Park, B. Sahu, S. Siddiqui, and A. C Kummel. "Atomic imaging and modeling of passivation, functionalization, and atomic

layer deposition nucleation on the SiGe(001) surface via H_2O_2(g) and trimethylaluminum dosing." Surface Science, 630, pp. 273-279 (2014)

S. W. Park, K. Pickrahn, Y. Gorlin, H. Lee, T. Jaramillo, S. Bent "Active MnO_x Electrocatalysts Prepared by Atomic Layer Deposition for Oxygen Evolution and Oxygen Reduction Reactions" Advanced Energy Materials, 2, pp. 1269-1277 (2012)

B. S. Kim, S. W. Park, P. T. Hammond "Hydrogen-Bonded Layer-by-Layer Assembled Biodegradable Polymer Micelles as Drug Delivery Vehicles" ACS Nano 2 (2008)

FIELD OF STUDY

Major Field: Materials Science and Engineering

Studies in Surface Science and Physical Chemistry
Professor Andrew C. Kummel

ABSTRACT OF THE DISSERTATION

Cleaning, Passivation, and Functionalization of SiGe (001) and (110) Surfaces for ALD Nucleation

by

Sang Wook Park

Doctor of Philosophy in Materials Science and Engineering

University of California, San Diego, 2016

Professor Andrew C. Kummel, Chair

SiGe is a promising material for channel or contact applications because of its high hole and electron mobility and capacity for both compressive and tensile strain by integration with Ge-rich and Si-rich layers. The high hole mobility of SiGe can be used for p-channel FET as an alternative to Si. The larger lattice constant of SiGe compared to Si can provide tensile or compressive stress into the Si channel thereby enhancing the electron or hole mobility, respectively. Moreover, the multi-gate structure, which utilizes multiple crystalline planes such as (001) and (110) can be

employed to overcome the challenges such as SCEs resulting from single-gate MOS devices.

In this work, cleaning, passivation, and functionalization of SiGe(001) and (110) surfaces were developed and studied using *in-situ* XPS, STM, and STS. XPS was utilized to understand the chemical compositions, oxidation states, and thickness of thin films on SiGe(001) and (110) surfaces. STM was used to study the topological structures and bonding configurations on the surfaces. STS was performed to probe the electronic structures such as pinning or unpinning effects by characterizing the density of states.

In order to avoid the oxygen and carbon contaminations after *ex-situ* native oxide removal, a combined wet and dry cleaning was performed. Wet *in-situ* HF clean method was successful to remove native oxides on SiGe(001) and contained no oxygen. Dry clean of atomic H via a thermal gas cracker method was found to be effective to remove the residual carbon contaminations. Sputter-cleaned SiGe(001) surface was terminated with only Ge dimers while SiGe (110) surface was terminated with both Si and Ge adtoms verified by STM. $H_2O_2(g)$ was employed to passivate the SiGe surfaces and provide a high nucleation density for the metal ALD process confirmed by XPS. TMA was dosed onto the hydroxyl terminated SiGe surfaces to form a monolayer of Al_2O_3. TDMAT or $TiCl_4$ was also exposed onto the hydroxyl terminated SiGe surfaces to form a monolayer of TiO_x. Al atoms were bonded to one oxygen atom while Ti atoms were bonded to two oxygen atoms on the surfaces

studied by STM and XPS. Furthermore, PDA resulted in the formation of selective Si-O-Al or Si-O-Ti on SiGe(001) and (110) surfaces.

Chapter 1

Introduction

1.1 Ultra high vacuum chamber

All *in-situ* scanning tunneling microscopy (STM), and scanning tunneling spectroscopy (STS), X-ray photoelectron spectroscopy (XPS) studies were performed in a customized Omicron ultra-high vacuum (UHV) chamber. The STM chamber consists of an Omicron low temperature (LT) STM and the base pressure is 2 x 10^{-11} torr pumped by agilent technology ion pump and titanium sublimation pump (TSP). The preparation chamber is composed of Omicron monochromatic XPS, Veeco atomic hydrogen source, low energy electron diffractometer (LEED), and Extrel mass spectrometer. The base pressure of the preparation chamber is 1 x 10^{-10} torr pumped by agilent technology ion pump and TSP. The sample could be annealed at elevated temperatures using a pyrolytic boron nitride (PBN) heater in the manipulator. To avoid the molecular desorption from the manipulator body during the annealing process, liquid nitrogen was utilized to cool down the manipulator body. Dosing of different kinds of oxidant and reductant precursors was performed in load lock/atomic layer deposition (ALD) chamber. Because the base pressure of load lock/ALD chamber is 1 x 10^{-7} torr pumped by two turbo pump and backed by mechanical pumps, samples could be dosed with the maximized cleanness and transferred to the preparation chamber without any air exposure. Different types of oxidants such as H_2O or H_2O_2 from Fischer Scientific and reductant such as trimethylaluminum (TMA) from Strem

Chemicals were utilized in the ALD chamber. A schematic diagram of the UHV chamber system is demonstrated in Fig. 1.1.

1.2 X-ray photoelectron spectroscopy

XPS is a technique to analyze the chemical properties from the surface by utilizing a characteristic x-ray and measuring the intensities and kinetic energies of the emitted electrons via a hemispherical analyzer (HSA) and a detector. Since each emitted electron has a specific kinetic energy depending on elements and orbitals, XPS can provide the chemical structures of the surface. When the surface elements form bonds with other atoms which are more electronegative or electropositive, the chemical shifts separated by a few eV from the main peak can be observed and this provides bonding configurations. Moreover, due to the exponential attenuation of the peak intensities in the presence of the overlayer, the thickness and coverage of a thin film can be estimated. Since the binding energy of the emitted electrons is equal to the energy of the characteristic X-ray ($h\upsilon$) minus the kinetic energy of the electrons and the work function of spectrometer (Φ_s), the binding energy of the electrons can be obtained.[1]

$$BE = h\upsilon - KE - \Phi_s \qquad (1.2.)$$

A schematic diagram of the XPS system is demonstrated in Fig. 1.2.

1.3 Scanning tunneling microscopy

STM is a technique to study the surface morphology by utilizing a vacuum tunneling between a tip and the sample of interest.[2] As shown in Fig. 1.3(a), by applying a bias between a metallic tip and the sample, a tunneling current can be achieved thereby investigating the morphology of the sample with a high resolution in the angstrom (Å) range. Since a vacuum tunneling is exponentially proportional to the distance between a tip and the sample, a feedback loop should be used to maintain a constant tunneling current and moves a metallic tip forward and backward depending on the surface morphology.

During the STM imaging process, two different states of the sample can be obtained by applying a positive or negative bias to the sample with regard to a tip. As demonstrated in Fig. 1.3(b), when a positive bias is applied to the sample, fermi level (E_f) of a tip is higher than the conduction band (CB) of the sample and electrons tunnel from a tip to the sample providing the empty state images of the sample. In comparison, when a negative bias is applied to the sample, E_f of a tip is lower than the valence band (VB) of the sample allowing electrons tunnel from the sample to a tip resulting in the filled state images as shown in Fig. 1.3(c).

1.4 Scanning tunneling spectroscopy

STS is a technique to investigate the electronic structures by measuring a tunneling current depending on the sample bias. In order to obtain the I/V spectra, the sample was biased ranging from negative to positive values and a tip was moved

forward and backward during the scan for the increased sensitivity with regard to small currents. Simultaneously, by applying a modulation signal through an external lock-in amplifier, the dI/dV data were directly obtained along with I/V spectra. In this dissertation, the raw I/V spectra were smoothed through a low-pass filter and this led to a broadened I/V, denoted as ($\overline{I/V}$). Moreover, a fitting program was performed to estimate the band edge energies with a linear function.[3,4] Since the (dI/dV)/($\overline{I/V}$) is proportional to the density of states (DOS)[5,6], the electronic properties such as the position of E_f and band gap states can be obtained by estimating the valence band maximum (VBM) and conduction band minimum (CBM).

1.7 Density functional theory

Density functional theory (DFT) is a technique to perform a computational quantum mechanical model to understand the electronic structure.[7] To verify the proposed bonding configurations and electronic structurers from the experimental results, DFT models were employed, followed by relaxation. In this dissertation, clean and hydroxyl-terminated SiGe(110) surfaces with 50% Si and 50% Ge atoms were investigated through DFT models. In addition, DOS of the structures were performed to estimate the positions of the E_f thereby determining the pinned or unpinned SiGe(110) surfaces depending on the termination conditions.

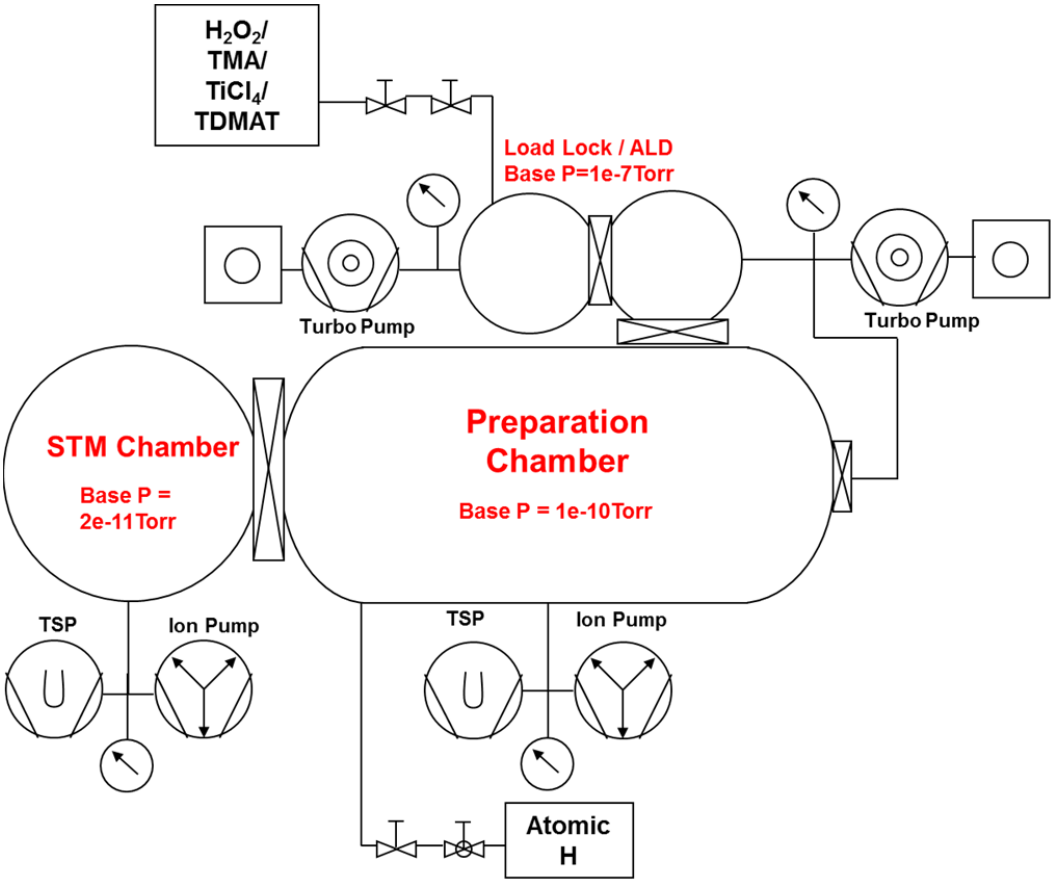

Figure 1.1 Schematic diagram of the Omicron UHV system.

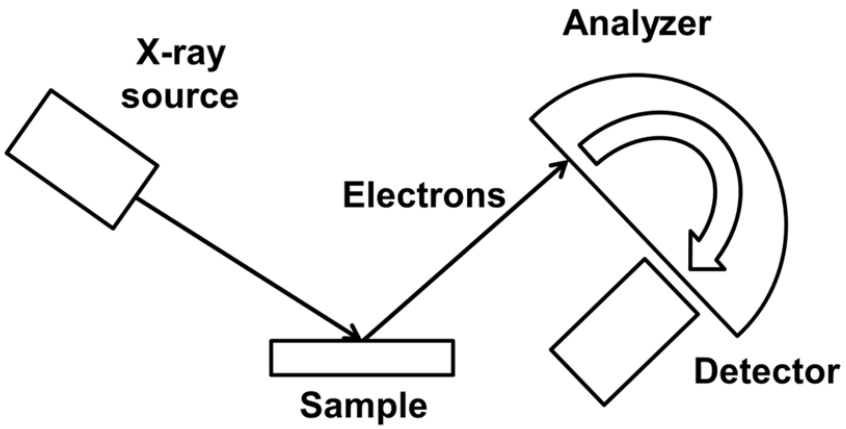

Figure 1.2 Schematic diagram of the XPS system.

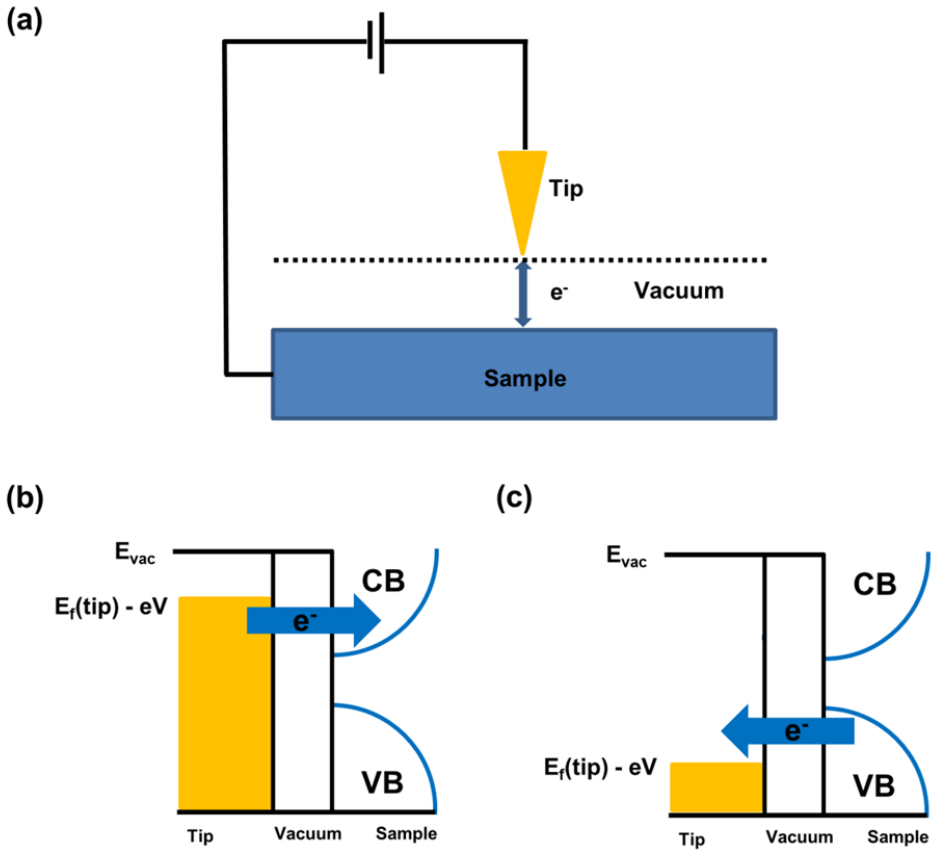

Figure 1.3 Schematic diagram of STM and STS. (a) Schematic diagram of the STM operation. (b) Band diagram of empty state image. (c) Band diagram of filled state image.

1.8 References

[1] D. Briggs and M. P. Seah, D. Briggs, & M. P. Seah,(Editors), John Wiley & Sons, Chichester 1983, xiv+ 533 (1983).

[2] G. Binnig and H. Rohrer, Surface Science **126,** 236 (1983).

[3] R. M. Feenstra, J. Y. Lee, M. H. Kang, G. Meyer, and K. H. Rieder, Physical Review B **73,** 035310 (2006).

[4] R. M. Feenstra, Physical Review B **50,** 4561 (1994).

[5] R. M. Feenstra, Surface Science **299–300,** 965 (1994).

[6] R. M. Feenstra, J. A. Stroscio, and A. P. Fein, Surface Science **181,** 295 (1987).

[7] E. A. Chagarov and A. C. Kummel, in *Fundamentals of III-V Semiconductor MOSFETs* (Springer, 2010), p. 93.

Chapter 2

Combined Wet and Dry Cleaning of SiGe(001)

2.1 Abstract

Combined wet and dry cleaning via hydrofluoric acid (HF) and atomic hydrogen on $Si_{0.6}Ge_{0.4}$(001) surface was studied at the atomic level using ultra-high vacuum (UHV) scanning tunneling microscopy (STM), scanning tunneling spectroscopy (STS), and x-ray photoelectron spectroscopy (XPS) to understand the chemical transformations of the surface. Aqueous HF removes native oxide, but residual carbon and oxygen are still observed on $Si_{0.6}Ge_{0.4}$(001) due to hydrocarbon contamination from post HF exposure to ambient. The oxygen contamination can be eliminated by shielding the sample from ambient via covering the sample in the HF cleaning solution until the sample is introduced to the vacuum chamber or by transferring the sample in an inert environment; however, both processes still leave carbon contaminant. Dry *in-situ* atomic hydrogen cleaning above 330˚C removes the carbon contamination on the surface consistent with a thermally activated atomic hydrogen reaction with surface hydrocarbon. A post-deposition anneal at 550˚C induces formation of an atomically flat and ordered SiGe surface observed by STM. STS verifies that the wet and dry cleaned surface has an unpinned Fermi level with no states between the conduction and valence band edge comparable to sputter cleaned SiGe surfaces.

2.2 Introduction

In order to overcome challenges when scaling down silicon-based complementary metal-oxide semiconductor (CMOS) devices, SiGe has received much attention due to its high carrier mobility and application in strain engineering. [1-3] SiGe has a higher hole mobility which makes it useful as a replacement for Si as a channel material in P-type metal-oxide-semiconductor (PMOS) transistors. [4-6] Additionally, the larger lattice constant of SiGe can be utilized to improve electron mobility in N-type metal-oxide-semiconductor (NMOS) transistors by inducing a biaxial tensile strain into Si channels. [7-12] However, integration of SiGe as a channel material requires a clean and well-ordered surface for gate oxide deposition. [13] As the thickness of gate oxide scales down for high performance and low power consumption, a high quality interface between the high-k metal oxide and SiGe determines the device performance characteristics such as leakage current, mobility, and interface trap density (D_{it}). [14,15]

Several cleaning procedures have been explored on SiGe surfaces. HCl solution cleaning is an ineffective method to remove native oxide because SiO_2 is inert to HCl solutions. [16] HF treatment removes all the surface oxides leaving the surface hydrogen terminated after transfer to UHV as shown by synchrotron high resolution XPS spectroscopy; however, an inert processing environment is required to avoid oxygen and carbon contamination since the hydrogen passivated Si(001) and Ge(001) surfaces after HF cleaning are not stable in the ambient air. [17-19] It is expected that GeH_x species are less stable than SiH_x species in ambient due to their weaker bonds. [19-21] Supercritical CO_2 containing HF and H_2O removes all native oxides on SiGe

surfaces; however, this method requires high HF concentrations resulting in rougher surfaces. [22]

The study seeks to understand the chemical transformations required to produce a clean and uniform SiGe(001) surface. A combined wet and dry cleaning procedure is employed to remove O and C, maximize the nucleation density of high-k atomic layer deposition (ALD), and prepare a good template for subsequent forming gas anneal. [23,24] XPS measurements show that two newly developed HF wet clean methods remove the SiGe oxides leaving the surface chemically passivated thereby avoiding substrate oxidation even during ambient exposure. Even though ambient exposure results in hydrocarbon contamination, it is readily removed by subsequent atomic H exposure. The atomic H cleaning also induces Si segregation onto the surface while maintaining a good electronic structure. Si termination is likely to be advantageous for device performance due to the low defect density of Si/high-k dielectric interfaces after forming gas annealing. [25] Furthermore, Si termination on Ge PMOS transistors minimizes the interface trap density (D_{it}). [26] In the present study, each experimental step is verified using *in-situ* x-ray photoelectron spectroscopy (XPS), scanning tunneling microscopy (STM), and scanning tunneling spectroscopy (STS).

2.3 Methods

N-type $Si_{0.6}Ge_{0.4}$(001) layers with 4×10^{19} cm^{-3} P doping grown on Si(001) were prepared by Applied Materials and diced into 12 × 4.5 mm pieces. Samples were

degreased with acetone, methanol, and deionized water using ultra sonication three times then dried with N_2 gas.

Samples were dipped into 2% HF solution for 2 minutes to remove native oxide and loaded within 5 minutes into a custom Omicron UHV chamber with a base pressure of 2×10^{-10}. Samples were annealed at 100, 200, and 500°C via direct heating. The sample temperatures were monitored by a pyrometer and heated at a rate of 1°C/sec. Chemical, topological, and electronic properties were verified via XPS, STM, and STS in each experiment.

Two methods, "Toluene Double Dip" and "HF Drop", were investigated to eliminate residual oxygen on the surface. It was hypothesized that residual oxygen on the surface came from ambient hydrocarbon; therefore, deposition of a clean hydrocarbon capping layer was investigated. For the "Toluene Double Dip" method, toluene was layered onto 2% HF solution to coat the SiGe upon removal from the HF solution; to insure no residual HF, after the samples were pulled out of the solution, samples were transferred to another toluene solution. SiGe surfaces remained covered with a layer of toluene to minimize air exposure during the transfer. In "HF Drop", after the normal HF clean without toluene, an additional 2% HF solution was dropped onto samples in the load lock under N_2 purge and evaporated in the load lock chamber during pump down to a base pressure of 2×10^{-8} Torr. After each cleaning method, the samples were annealed at 150°C and 300°C via resistive PBN heating; the surface composition after each step was determined by *in-situ* XPS.

After the drop clean method, SiGe samples were exposed to atomic hydrogen in the UHV chamber using a thermal gas cracker (Atomic Hydrogen Source, Veeco). The gas pressure was controlled via a leak valve and measured through an ion gauge; the exposure was calculated in terms of Langmuirs (1 Langmuir (L) = 1 x 10^{-6} Torr · 1 sec). During the gas dosing, the filament temperature of thermal gas cracker was 1800°C – 2200°C while SiGe(001) samples were maintained at 330°C using a resistive PBN heater. The exposure pressures were measured with an ion gauge and calculated in Langmuirs; therefore, the reported doses are based on the H_2 pressure and are an upper limit to the true exposure. The cracking efficiency is expected to be 30 % (Veeco), but it could not be verified.

Samples were transferred to a STM chamber with a base pressure of 1 × 10^{-11} Torr. The atomic and electronic structures of SiGe surface in each experiment were studied with *in-situ* STM and STS at 300K (LT-STM, Omicron Nanotechnology). Constant-current STM (Isp = 200pA) was operated with a sample bias between -1.8 and -2.0V to obtain filled state STM images. Variable-z mode STS was operated using a modulation signal (0.1V, 650 Hz) from an external lock-in amplifier (SR830 DSP, Stanford Research Systems) while sweeping the sample bias from -1.5 to +1.5V.

Chemical analysis was performed using an *in-situ* monochromatic XPS (XM 1000 MkII/SPHERA, Omicron Nanotechnology). Constant analyzer energy mode with a pass energy of 50eV and a line width of 0.1 eV using an Al Kα source (1486.7 eV) were employed. The takeoff angle was 30° from the sample surface, which is close to surface parallel, and an acceptance angle of + 7° was employed. For peak

shape analysis, CASA XPS v.2.3 was employed using a Shirley background subtraction.

2.4 Results and Discussion

2.4.1 Wet cleaning

$Si_{0.6}Ge_{0.4}$(001) surfaces were cleaned via a 2% HF solution method leaving the surface hydrogen terminated at room temperature as reported in a previous study using synchrotron radiation photoelectron spectroscopy. [16] Fig. 2.1(a) shows XPS results of SiGe(001) surface after 100, 200, and 500°C anneals. All XPS peaks are normalized by photoelectron cross-sections (Si 2p-0.817, Ge 3d-1.42, O 1s-2.93, C 1s-1) using Hartree-Slater atomic model. [27] Moreover, it is assumed that elements such as oxygen and carbon are present as adsorbates on the SiGe(001) substrate. Since the escape depth of electrons from the Si2p and Ge3d peak is approximately 1nm for a detection angle of 30° from the sample surface based on a model by Seah and Dench [28], for the 44% in the C/(Si+Ge) and 14% in the O/(Si+Ge) ratios shown in Fig. 2.1, the real surface concentrations correspond to approximately 2.3ML carbon and 0.7ML oxygen. These numerical values are obtained based on a simplified model in which the top 3 monolayers are purely composed of C and O atoms and the lower layers are composed of Si and Ge atoms and the attenuation is estimated using the formula $I=I_o\exp(-t/\lambda)$ (I: intensity in the presence of the overlayer, I_o: intensity in the absence of any covering layer, t: thickness of the layer, λ: inelastic mean free path). The presence of oxygen is likely due to Si because Si-O bonds are stronger than Ge-O

bonds and because H terminated Ge(001) exhibits only carbon contamination in ambient as shown by Rivillon et al. [19] Moreover, as shown by Hirose et al, Si(001) rapidly absorbs a submonolayer of oxygen in ambient due to defects and weakly bound hydrides consistent with Si in SiGe(001) being responsible for oxygen contamination. [21] It is expected that the H termination is desorbed for the 500°C anneal as shown in previous reports. [16,29] In the absence of strong adsorbate bonding, the surface of SiGe(001) is terminated by Ge atoms due to the segregation of Ge to the surface as reported in the previous studies. [30-32] Density functional theory (DFT) calculations theoretically verified that clean SiGe(001) surfaces are thermodynamically more stable when composed of Ge atoms compared to Si atoms. [33] The wet cleaned surface of SiGe(001) shows a high percentage of Ge atoms because the native oxide of SiGe is mainly composed of SiO_2, and the SiO_2 is removed by wet HF thereby exposing the accumulation of Ge underneath the native oxide as reported in the previous report. [34] Since the Si/Ge ratio is identical on all surfaces independent of annealing condition (Fig. 2.1), it is concluded that the wet cleaned surfaces are largely Ge enriched.

XPS data shows that wet HF cleaned SiGe surfaces contain residual oxygen and carbon. Since no SiO_x nor GeO_x components are present, the XPS data is consistent with the C and O being in the form of hydrocarbon due to air exposure during the transfer into the load lock. The surface concentration of carbon and oxygen decreases upon heating to 200°C. However, as the temperature is increased up to 500°C, the O is transferred to Si atoms forming surface SiO_x before the hydrocarbon

completely desorbs while in UHV adsorbate-free annealed SiGe(001), Ge is terminated. [33] In the previous study, it is reported that "reverse segregation" at the surface is induced between Si and Ge by atomic hydrogen exposure because the Si-H bond is much stronger than Ge-H bond. [35,36] A similar phenomenon of reverse segregation should be expected on the SiGe(001) surface if there is a full monolayer of oxygen because the Si-O bond is much stronger than the Ge-O bond.

Fig. 2.1(b) shows a filled-state STM image of a SiGe(001) surface after a 500°C anneal. The STM image shows that HF wet clean and 500°C anneal result in a surface with a root mean square (RMS) roughness of 0.40 nm. Since the wet clean surface contains only small domains and a high concentration of surface contaminants, a line trace analysis is needed to accurately determine the surface atomic space. To determine the vertical row spacing of HF wet cleaned and annealed SiGe(001) surface, line traces of four different areas are analyzed in Fig. 2.1(c). Line trace analysis shows an average row spacing of 1.2nm with a standard error (SE) of 0.055nm consistent with the row spacing of the ideal SiGe(001) surface.

2.4.2 Toluene double dip

In the present study, two methods of enhanced wet cleaning, "Toluene Double Dip" and "HF Drop", were investigated to eliminate residual oxygen on the SiGe(001) surface. Since residual oxygen mainly results from the air exposure during the sample transfer, each method was designed to protect the surface against oxidation by oxy-hydrocarbons from air by covering the surface with a hydrophobic toluene layer or

using an N_2 purge. Fig. 2(a) shows the schematic of the toluene double dip method. It was hypothesized that if toluene sticks to the residual reactive sites on the HF wet cleaned sample, this would inhibit adsorption of oxy-hydrocarbons. Toluene is a hydrophobic molecule with strong internal bonds which should adsorb onto hydrogen terminated SiGe(001) surface without any chemical reaction and easily evaporate in a vacuum chamber due to its high vapor pressure at RT. XPS data shows that toluene double dip results in no oxygen and low carbon contamination in Fig. 2.2(b). As the sample temperature was increased to 300°C, toluene capped SiGe(001) surface had only 4% oxygen which is 50% smaller than normal HF cleaned SiGe(001). The residual oxygen is probably due to contamination from the vacuum system since it was not present on the sample prior to annealing.

2.4.3 Wet and dry cleaning

For the "HF Drop" method, after HF wet clean, additional HF solution is dropped onto SiGe(001) surface in the load lock under N_2 purge, which is known to stabilize Ge-H bonds in ambient.[19] The HF is evaporated in a vacuum chamber during evacuation via a turbo pump. As shown in Fig. 2.3(a), after the HF drop clean, the SiGe(001) surface contains no oxygen, but still contains carbon comparable to *ex-situ* HF clean.

To remove the carbon from the HF drop cleaned SiGe(001) surface, atomic hydrogen was employed while the substrate temperature was maintained at 330°C. In the previous studies, atomic hydrogen cleaning at temperatures higher than 250°C

prevented preferential etching of Ge due to inhibition of GeH_2 formation at elevated temperature [37,38] and atomic hydrogen cleaning is known to induce a Si segregation on Ge-covered Si(001) by suppressing Ge segregation above the substrate temperature of 250°C. [36] Additionally, it was reported that atomic hydrogen suppresses the Ge surface segregation during molecular beam epitaxy (MBE) growth of Si/Ge heterostructures. [39] It is anticipated that similar phenomena should be observed on SiGe(001) when dosed with atomic hydrogen at 330°C. The SiGe(001) surface was dosed with 18,000L of atomic hydrogen while the substrate temperature was maintained at 330°C. XPS results in Fig. 2.3(a) show that almost all carbon is eliminated, but 6% of oxygen is introduced because the high temperature of tungsten filament of thermal gas cracker induces wall desorption of oxygen in the UHV chamber which forms SiOx on Si-enriched SiGe(001) surfaces. Fig. 2.3(b) shows the spectrum of Ge 3d and Si 2p peak after the wet HF drop method and dry atomic H clean. Si 2p peak shows the formation of shoulder at higher binding energy corresponding to SiOx after atomic H clean whereas Ge 3d peak shows no changes. This is consistent with the atomic H clean inducing or maintaining a Si enriched SiGe(001) surface.

Fig. 2.4 shows STM images of HF drop cleaned SiGe(001) after atomic H cleaning at 330°C and subsequent anneals at 330 and 550°C. Due to the small domain size and residual oxygen contamination, line trace analysis is needed to quantitatively determine the surface order. The SiGe(001) surfaces with only 330°C anneal (Fig. 2.4(a)) have a RMS roughness of 0.29 nm and an average row spacing of 1.2nm ± 0.049nm (SE) as shown in Fig. 2.4(c); this is the identical row spacing as the sputter

cleaned surface and, therefore, consistent with the ideal row spacing of SiGe(001) despite the small domain size and the residual surface contamination. Post clean annealing at 550°C decreases the RMS roughness from 0.29 to 0.23 nm while maintaining 1.2nm ± 0.044nm (SE) row spacing as shown in Fig. 2.4(d); in addition, the STM images show no etch pits. Compared to the HF wet cleaned surface, combined wet and dry cleaning results in a flatter and more uniform surface as shown by the 30% decrease in RMS roughness and the appearance of distinct rows with the spacing of the ideal sputter-cleaned surface. Lower RMS roughness and the absence of etch pits are considered critical to high channel mobility. [40-43]

STS measurements were taken to determine the effect of the cleaning processes on the electronic structure of n-type SiGe(001) surfaces. Pinning of $Si_{0.6}Ge_{0.4}$(001) results in a Fermi level near the valence band similar to Ge(001) so STS of n-type is sufficient to determine the unpinning of the surface. [44] STS measures the local density of states (LDOS) by lock-in measurement of the AC signal from AC modulation of the sample bias during an I-V (current-voltage) sweep of the DC sample bias to obtain (dI/dV)/(I/V) which is considered to be proportional to the LDOS. [45,46] STS curves in Fig. 2.5 show the HF drop cleaned surface after both atomic H cleaning and annealing at 550°C produces an unpinned surface with same electronic structure (HF Drop+Dry Atomic H Clean) as sputter cleaned surface (Sputter Clean). Moreover, no states are detected in the band gap region between conduction and valence band edges in contrast to normal HF cleaned surface with band gap states (Normal HF

Clean). This result demonstrates that a clean and unpinned SiGe surface is obtained through combined wet HF and dry atomic H cleaning method without sputter clean.

2.5 Conclusion

HF wet clean was utilized to remove the native oxide of $Si_{0.6}Ge_{0.4}(001)$ surface; however, normal *ex-situ* HF wet cleaned SiGe(001) contains residual oxygen as a form of hydrocarbon. Two methods, "Toluene Double Dip" and "HF Drop", were studied to eliminate residual oxygen. Toluene protects the surface against ambient deposition of oxy-hydrocarbon by toluene passivating the reactive SiGe surface defects. Since toluene has strong internal bonds, a high vapor pressure, and is hydrophobic, it leaves no significant dissociative chemisorption products on hydrogen terminated SiGe(001) surface and it prevents water condensation. The HF drop simulates HF clean with N_2 purge to minimize oxygen adsorption from ambient condition. HF drop clean eliminates oxygen from the SiGe(001) surface. In order to remove residual carbon, dry atomic hydrogen clean was investigated. The thermal atomic H clean at 330°C both removed residual carbon and formed a Si enriched SiGe(001) surface consistently with only SiO_x and no GeO_x forming post H clean upon oxygen exposure. STS verified combined wet and dry clean provides the same electronic structures as sputter cleaned SiGe(001).

2.6 Acknowledgments

This work was supported by the Semiconductor Research Corporation (Task 2451.001), NSF DMR 1207213, and Applied Materials. The SiGe wafers were provided by Applied Materials.

Chapter 2, in part or in full, is a reprint of the following material: S. W. Park, T. Kaufman-Osborn, H. Kim, S. Siddiquui, B. Sahu, N. Yoshida, A. Brandt, A. C. Kummel "Combined wet and dry cleaning of SiGe(001)" Journal of Vacuum Science and Technology A., 33 (4) (2015). The dissertation author was the primary investigator and author of this paper.

2.7 Supplemental materials

To provide more accurate insight into experimental uncertainties, the raw XPS spectra of Ge 2p, Ge 3d, Si 2p were fitted to show the chemical shift with an error range of ±0.1eV and the atomic ratios for the SiGe(001) surface are presented during the different cleaning methods. In addition, all XPS spectra are calibrated based on the C 1s peak at 284.5eV and the chemical shifts of the Ge 2p peaks under all conditions are discussed due to its higher surface sensitivity and accuracy resulting from small escape depth and strong peak intensity compared to Ge 3d and Si 2p peaks.

As shown in Fig. 2.6, the XPS spectral peaks after HF wet clean are broad with the Ge 2p having FWHM of 1.81eV compared to the sputter cleaned Ge 2p SiGe(001) surface with FWHM of 1.60eV. This is mainly because the adsorbates such as carbon and oxygen cause small chemical shifts. After the annealing at 100°C, the Ge 2p, Ge 3d, Si 2p become sharper with a FWHM of 1.51eV for Ge 2p consistent with

desorption of hydrocarbons and other weakly bound contaminants. Even after the 500°C annealing, the Ge 2p peak is at 1218.4eV, which is shifted by 1.0 eV from the bulk value of 1217.4eV on a sputter cleaned SiGe surface, consistent with desorption of hydrogen and bonding to remaining adsorbates. The energy shifts of the Ge 3d and Si 2p are not statistically significant due to the 10x lower signal to noise ratio and lower surface sensitivity of these peaks. The sensitivity corrected intensity ratios from Fig. 2.1(a) are provided in table 2.1.

XPS spectra after toluene double dip method are shown in Fig. 2.7. Compared to wet HF cleaned and 100°C annealed SiGe(001), the non-annealed double dip clean surface contains low ratios of carbon and oxygen adsorbates as shown in Table 2.2; the fraction of O is reduced from 0.14 to 0 and the fraction of C is reduced from 0.44 to 0.15 after toluene double dip method. The Ge 2p peak is at 1218.2eV, which is shifted by 0.8 eV from the 1217.4eV Ge 2p peak on a sputter cleaned SiGe surface, consistent with bonding to adsorbates and possibly some hydrogen. After 300°C annealing, the Ge 2p peak still remains at the same position indicating the surface is still terminated with hydrogen and adsorbates. The sensitivity corrected intensity ratios from Fig. 2.2(b) are provided in table 2.2.

XPS spectra after wet and dry atomic H clean are shown in Fig. 2.8. The Ge 2p peak after *in-situ* wet clean is at 1218.3eV, which is almost identical to 1218.2eV on a toluene double dip cleaned SiGe surface, consistent with bonding primarily to the remaining adsorbates. The dry atomic H clean shifts the Ge 2p peak to 1217.7eV, which is identical to the sputter cleaned surface after atomic H dose, consistent with

all Ge surface atoms being Ge-H bonded. As shown in table 2.3, the fraction of C is reduced from 0.48 to 0.02 while the fraction of O is increased from 0 to 0.06 mainly due to adsorption of oxygen from operation of the high temperature atomic H source in the UHV chamber. The sensitivity corrected intensity ratios from Fig. 2.3(a) are provided in table 2.3.

XPS spectra after sputter and dry atomic H clean are shown in Fig. 2.9. The Ge 2p peak after sputter clean is at 1217.4eV, which is lowest binding energy for any surface preparation condition, consistent with a clean surface without any hydrocarbon or hydrogen adsorbates at the surface as reported in the previous study. [47] After atomic H dose, the Ge 2p peak is shifted to higher binding energy by 0.3eV from a sputter cleaned SiGe(001) surface mainly due to the hydrogen termination at the surface as shown in the previous study. [16] After 500°C annealing, the Ge 2p peak is shifted back by 0.3 eV to 1217.4eV binding energy since hydrogen atoms are desorbed and no adsorbates are present. Positions of peaks after each experimental step are compiled in Table 2.4.

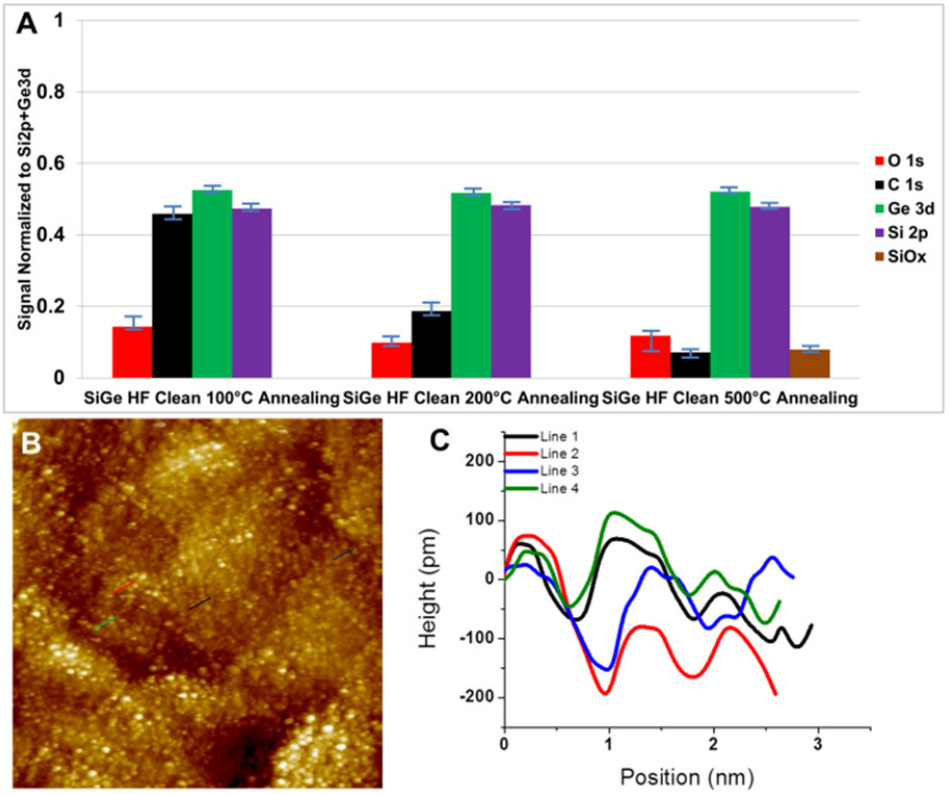

Figure 2.1 XPS and STM of wet cleaned SiGe(001) (a) XPS data of HF wet cleaned SiGe(001) surface followed by annealing at 100, 200, and 500°C. The ratio of each chemical element is normalized to the sum of all components of Si 2p and Ge 3d peaks. (b) Filled state STM image (50 x 50 nm^2, V_s= -1.8V, I_t=200pA) of wet cleaned and 500°C annealed SiGe(001) (c) Line trace analysis of four different areas on STM image (left). Vertical order is shown and average of row spacing is 1.2nm with a standard error of 0.055nm.

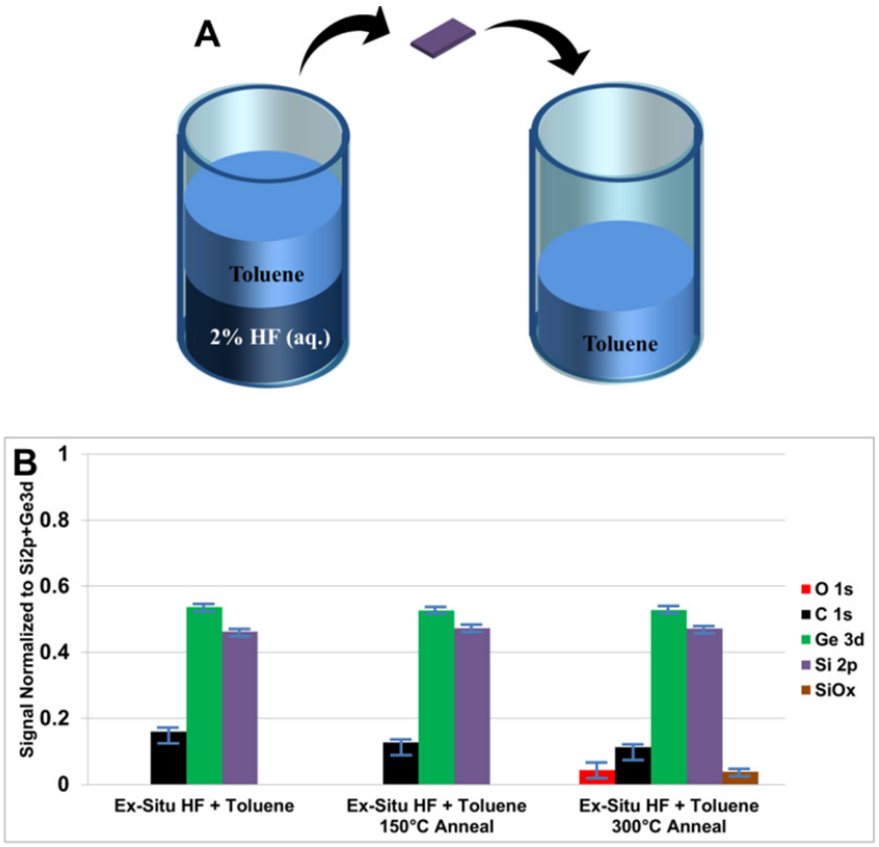

Figure 2.2 Schematic image and XPS of toluene double dip method (a) Schematic diagram of toluene double dip method. Wet HF cleaned SiGe(001) samples are pulled through a layer of toluene then dipped into another toluene solution. (b) XPS data of toluene double dip method followed by 150 and 300°C anneal.

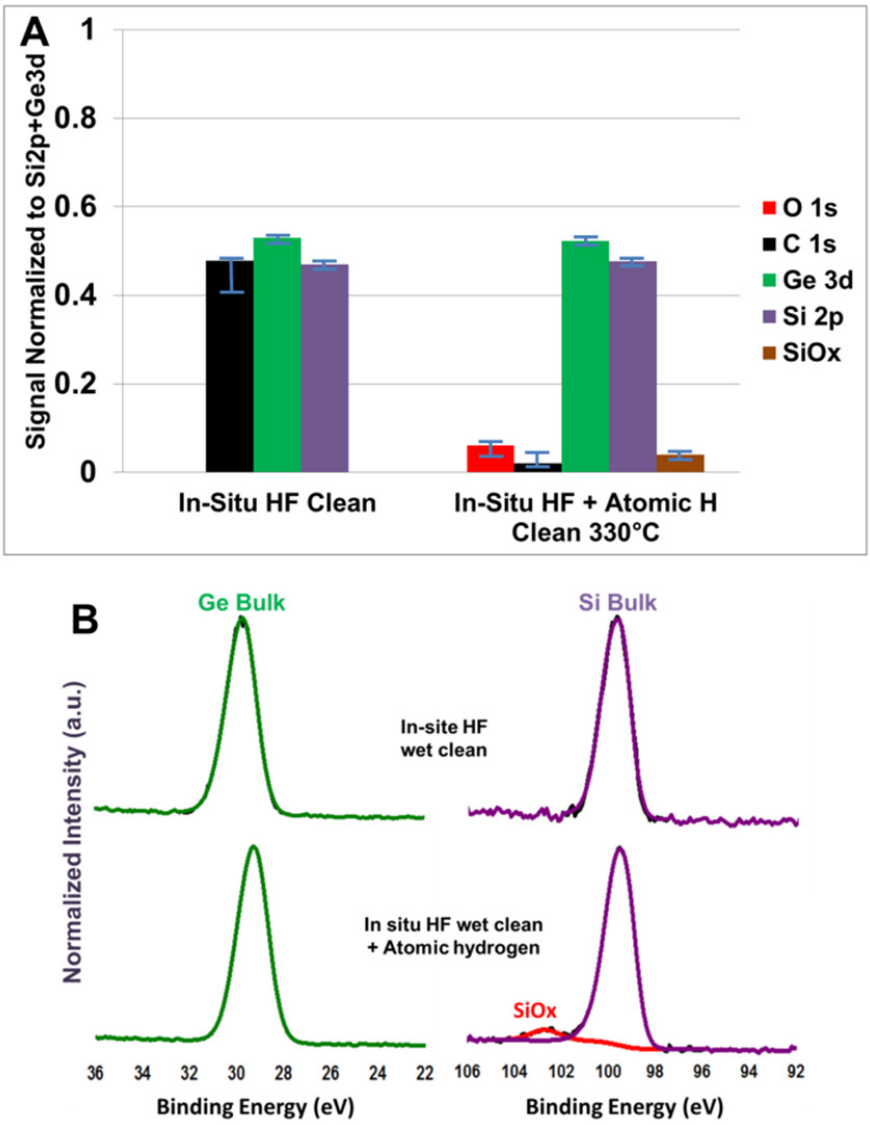

Figure 2.3 XPS analysis of wet plus dry cleaned SiGe(001) (a) XPS data of HF drop method followed by 18,000L atomic H clean shows atomic H removes carbon from SiGe(001) surface. (b) XPS analysis before and after atomic H clean show the change of spectrum in Ge 3d and Si 2p peaks shows the absence of any initial Si and Ge oxides and only 6% SiOx due to oxygen contamination during the atomic H clean.

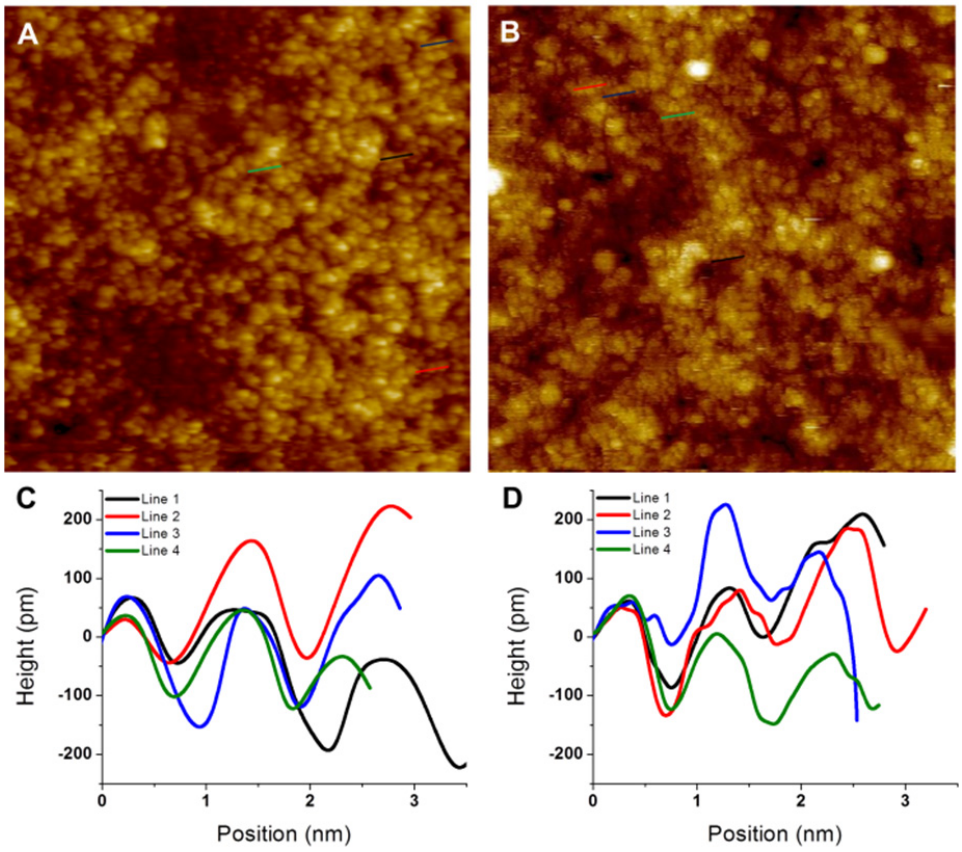

Figure 2.4 STM images of wet and dry cleaned SiGe(001) (a) Filled state STM image (50 x 50 nm^2, V_s= -1.8V, I_t=200pA) after 330°C anneal (b) STM image (50 x 50 nm^2, V_s= -1.8V, I_t=200pA) after 550°C anneal. (c) Line traces of four different areas on STM image of SiGe(001) after 330°C anneal (a) and average of row spacing is 1.2nm with a standard error of 0.049nm. (d) Line traces of four different areas on STM image of SiGe(001) after 550°C anneal (b) and average of row spacing is 1.2nm with a standard error of 0.043nm.

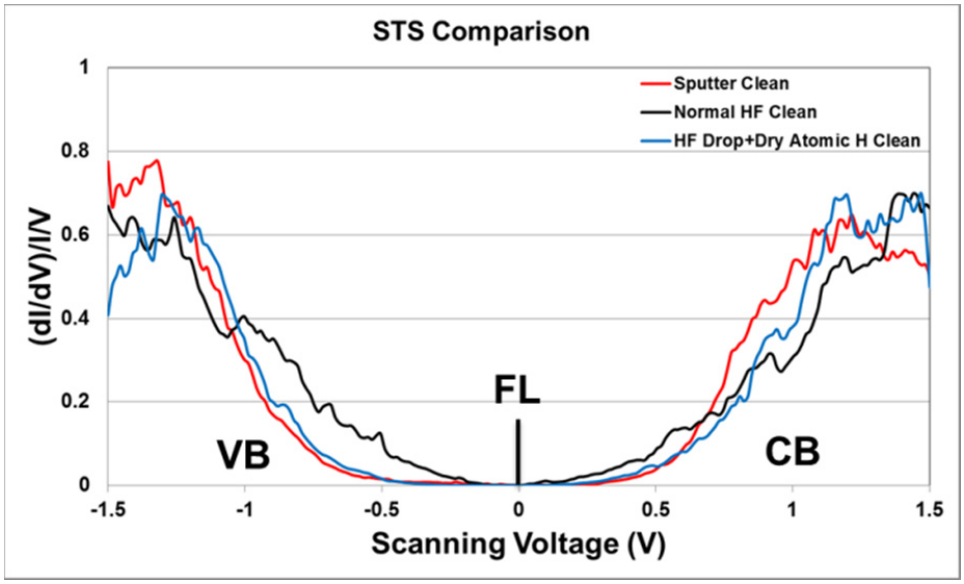

Figure 2.5 STS measurements of wet and dry cleaned SiGe(001). Combined HF drop and dry atomic H clean (HF Drop+Dry Atomic H Clean) shows no bandgap states compared to normal HF clean (Normal HF Clean) and results in identical LDOS as sputter cleaned SiGe(001) surface (Sputter Clean)

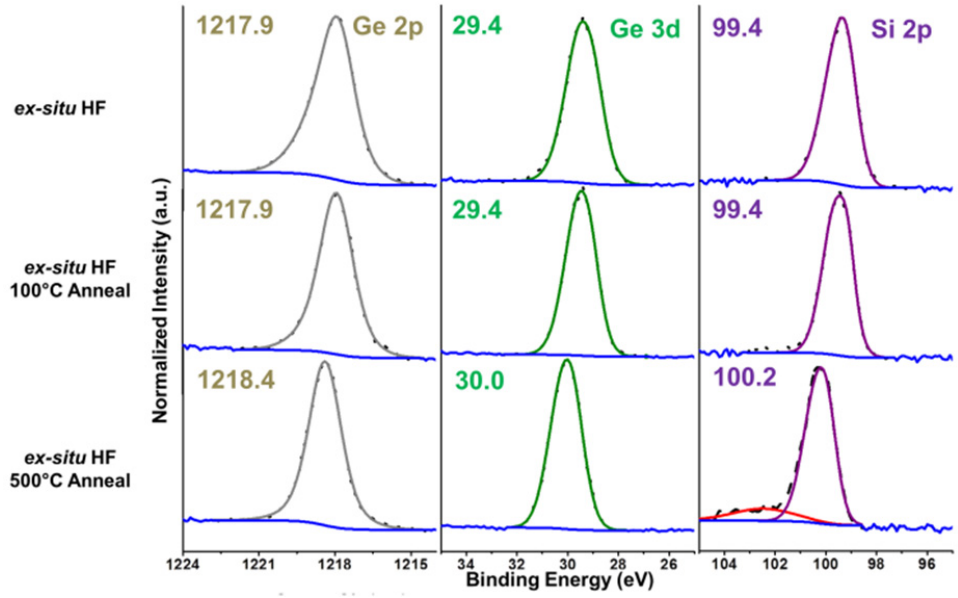

Figure 2.6 XPS spectra of Ge 2p, Ge 3d, and Si 2p on wet cleaned SiGe(001) followed by annealing. Annealing at 100°C reduces the peak widths. Annealing at 500°C induces the Ge peak to be symmetric but causes formation of a SiO_x peak. The numerical values in XPS spectra belong to peak positions.

Table 2.1 Atomic ratios for wet cleaned SiGe(001) followed by annealing. All ratios are corrected by photoelectron cross-sections and normalized by Ge 3d+Si 2p peaks.

	ex-situ HF + 100°C Anneal	*ex-situ* HF + 200°C Anneal	*ex-situ* HF + 500°C Anneal
O 1s	0.14±0.03	0.10±0.02	0.12±0.04
C 1s	0.44±0.03	0.18±0.02	0.07±0.02
Ge 3d	0.52±0.01	0.51±0.01	0.52±0.01
Si 2p	0.48±0.01	0.49±0.01	0.48±0.01
SiO_x	0.00	0.00	0.08±0.01
Ge + Si	1.00	1.00	1.00

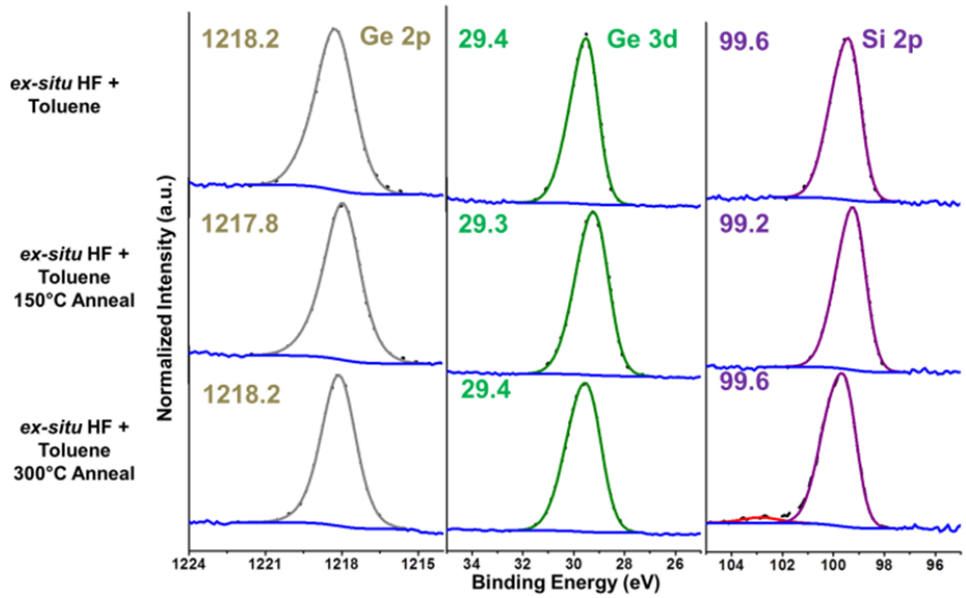

Figure 2.7 XPS spectra of Ge 2p, Ge 3d, and Si 2p of toluene double dip method followed by annealing. Annealing at 300°C induces the Ge peak to be symmetric but causes formation of a SiO_x peak. The numerical values in XPS spectra belong to peak positions.

Table 2.2 Atomic ratios for toluene double dip method followed by annealing. All ratios are corrected by photoelectron cross-sections and normalized by Ge 3d+Si 2p peaks.

	ex-situ HF + Toluene as-loaded	*ex-situ* HF + Toluene + 150°C Anneal	*ex-situ* HF + Toluene + 300°C Anneal
O 1s	0	0	0.04±0.02
C 1s	0.15±0.02	0.12±0.02	0.11±0.02
Ge 3d	0.53±0.01	0.53±0.01	0.53±0.01
Si 2p	0.47±0.01	0.47±0.01	0.47±0.01
SiO_x	0.00	0.00	0.03±0.01
Ge + Si	1.00	1.00	1.00

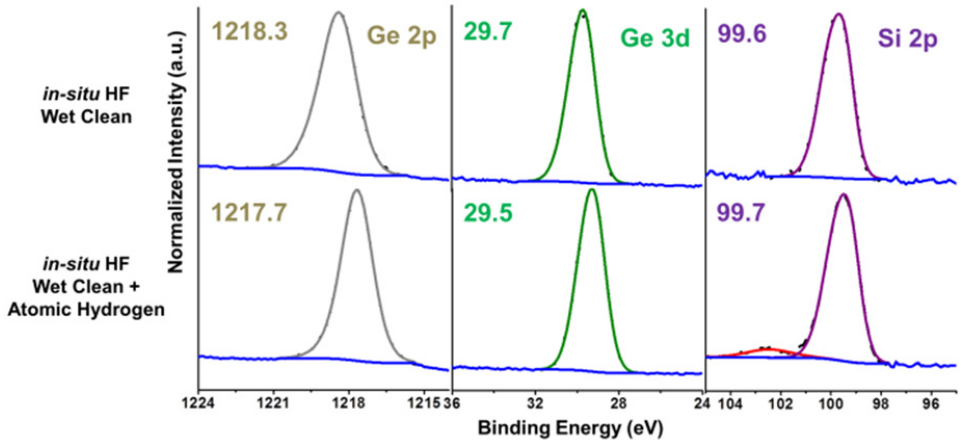

Figure 2.8 XPS spectra of Ge 2p, Ge 3d, and Si 2p of wet and dry clean followed by annealing. The Atomic H causes the Ge peak to become symmetric but induces formation of a small SiO_x peak. The numerical values in XPS spectra belong to peak positions.

Table 2.3 Atomic ratios for wet plus dry clean. All ratios are corrected by photoelectron cross-sections and normalized by Ge 3d+Si 2p peaks.

	in-situ HF as-loaded	*in-situ* HF + Atomic Hydrogen
O 1s	0.00	0.06±0.02
C 1s	0.48±0.05	0.02±0.02
Ge 3d	0.53±0.01	0.53±0.01
Si 2p	0.47±0.01	0.47±0.01
SiO_x	0.00	0.04±0.01
Ge + Si	1.00	1.00

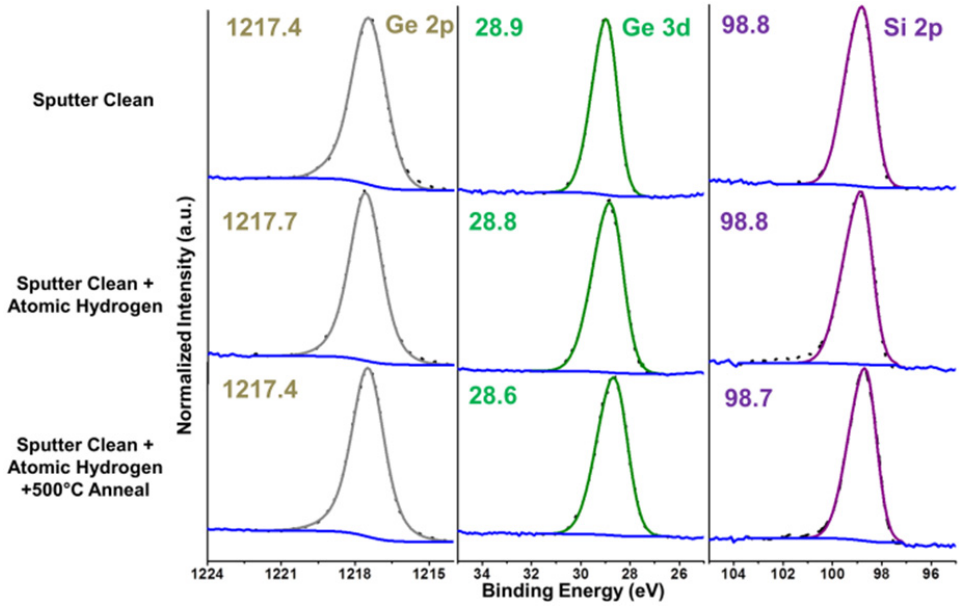

Figure 2.9 XPS spectra of Ge 2p, Ge 3d, and Si 2p of sputter and dry clean followed by annealing. The numerical values in XPS spectra belong to peak positions. The Atomic H shifts the Ge 2p peak to higher binding energy and 500°C anneal shifts the peak back to a lower binding energy consistent with the sputter cleaned position. The energy shifts of the Ge 3d and Si 2p are not statistically significant due to the 10x lower signal to noise ratio of these peaks.

Table 2.4 Positions of Ge 2p, Ge 3d, and Si 2p bulk peaks after each experimental step. Peak positions were calibrated based on the C 1s peak with an error range of ±0.1eV. Ge 2p peak shifts under all conditions are significant due to their higher surface sensitivity and stronger peak intensities compared to Ge 3d and Si 2p peaks; the accuracies of the peak shifts for Ge 3d and Si 2p are close to ±0.3eV due to the lower signal to noise ratios.

	Ex-situ **HF Wet Clean as-loaded**	***Ex-situ*** **HF Wet Clean + 100°C Anneal**	***Ex-situ*** **HF Wet Clean + 300°C Anneal**	***Ex-situ*** **HF Wet Clean + Toluene as-loaded**	***Ex-situ*** **HF Wet Clean + Toluene + 150°C Anneal**	***Ex-situ*** **HF Wet Clean + Toluene + 300°C Anneal**	***In-situ*** **HF Wet Clean as-loaded**	***In-situ*** **HF Wet Clean + Atomic H**	**Sputter Clean as-loaded**	**Sputter Clean + Atomic H**	**Sputter Clean + Atomic H + 500°C Anneal**
Ge 2p	**1217.9**	**1217.9**	**1218.4**	**1218.2**	**1217.8**	**1218.2**	**1218.3**	**1217.7**	**1217.4**	**1217.7**	**1217.4**
Ge 3d	**29.4**	**29.4**	**30.0**	**29.4**	**29.3**	**29.4**	**29.7**	**29.5**	**28.9**	**28.8**	**28.6**
Si 2p	**99.4**	**99.4**	**100.2**	**99.6**	**99.2**	**99.6**	**99.6**	**99.7**	**98.8**	**98.8**	**98.7**

2.8 References

[1] F. Schaffler, Semiconductor Science and Technology **12,** 1515 (1997).

[2] M. L. Lee, E. A. Fitzgerald, M. T. Bulsara, M. T. Currie, and A. Lochtefeld, Journal of Applied Physics **97** (2005).

[3] D. J. Paul, Semiconductor Science and Technology **19,** R75 (2004).

[4] T. Mizuno, N. Sugiyama, H. Satake, and S. Takagi, 2000 Symposium on Vlsi Technology, Digest of Technical Papers**,** 210 (2000).

[5] T. Mizuno, S. Takagi, N. Sugiyama, H. Satake, A. Kurobe, and A. Toriumi, Ieee Electron Device Letters **21,** 230 (2000).

[6] M. L. Lee, C. W. Leitz, Z. Cheng, A. J. Pitera, T. Langdo, M. T. Currie, G. Taraschi, E. A. Fitzgerald, and D. A. Antoniadis, Applied Physics Letters **79,** 3344 (2001).

[7] S. Datta, J. Brask, G. Dewey, M. Doczy, B. Doyle, B. Jin, J. Kavalieros, M. Metz, A. Majumdar, M. Radosavljevic, and R. Chau, Proceeding of the 2004 Bipolar/Bicmos Circuits and Technology Meeting**,** 194 (2004).

[8] S. Datta, G. Dewey, M. Doczy, B. S. Doyle, B. Jin, J. Kavalieros, R. Kotlyar, M. Metz, N. Zelick, and R. Chau, 2003 Ieee International Electron Devices Meeting, Technical Digest**,** 653 (2003).

[9] N. Griffin, D. D. Arnone, D. J. Paul, M. Pepper, D. J. Robbins, A. C. Churchill, and J. M. Fernandez, Journal of Vacuum Science & Technology B **16,** 1655 (1998).

[10] M. V. Fischetti, Journal of Applied Physics **89,** 1232 (2001).

[11] K. K. Rim, J. L. Hoyt, and J. F. Gibbons, Ieee Transactions on Electron Devices **47,** 1406 (2000).

[12] S. H. Olsen, A. G. O'Neill, S. Chattopadhyay, L. S. Driscoll, K. S. K. Kwa, D. J. Norris, A. G. Cullis, and D. J. Paul, Ieee Transactions on Electron Devices **51,** 1245 (2004).

[13] K. J. Kuhn, A. Murthy, R. Kotlyar, and M. Kuhn, Sige, Ge, and Related Compounds 4: Materials, Processing, and Devices **33,** 3 (2010).

[14] K. Saraswat, C. O. Chui, T. Krishnamohan, D. Kim, A. Nayfeh, and A. Pethe, Materials Science and Engineering B-Solid State Materials for Advanced Technology **135,** 242 (2006).

[15] Y. Taur and T. H. Ning, *Fundamentals of modern VLSI devices*, 2nd ed. (Cambridge University Press, Cambridge ; New York, 2009).

[16] Y. Sun, Z. Liu, S. Y. Sun, and P. Pianetta, Journal of Vacuum Science & Technology A **26,** 1248 (2008).

[17] Y. J. Chabal, G. S. Higashi, K. Raghavachari, and V. A. Burrows, Journal of Vacuum Science & Technology A **7,** 2104 (1989).

[18] X. Zhang, E. Garfunkel, Y. J. Chabal, S. B. Christman, and E. E. Chaban, Applied Physics Letters **79,** 4051 (2001).

[19] S. Rivillon, Y. J. Chabal, F. Amy, and A. Kahn, Applied Physics Letters **87,** 2531011 (2005).

[20] E. Yablonovitch, D. L. Allara, C. C. Chang, T. Gmitter, and T. B. Bright, Physical Review Letters **57,** 249 (1986).

[21] F. Hirose, M. Nagato, Y. Kinoshita, S. Nagase, Y. Narita, and M. Suemitsu, Surface Science **601,** 2302 (2007).

[22] B. Xie, G. Montano-Miranda, C. C. Finstad, and A. J. Muscat, Materials Science in Semiconductor Processing **8,** 231 (2005).

[23] M. L. Reed and J. D. Plummer, Journal of Applied Physics **63,** 5776 (1988).

[24] K. L. Brower, Applied Physics Letters **53,** 508 (1988).

[25] M. Caymax, F. Leys, J. Mitard, K. Martens, L. J. Yang, G. Pourtois, W. Vandervorst, M. Meuris, and R. Loo, Journal of the Electrochemical Society **156,** H979 (2009).

[26] M. Caymax, F. Leys, J. Mitard, K. Martens, L. J. Yang, G. Pourtois, W. Vandervorst, M. Meuris, and R. Loo, Advanced Gate Stack, Source/Drain, and Channel Engineering for Si-Based Cmos 5: New Materials, Processes, and Equipment **19,** 183 (2009).

[27] J. H. Scofield, Journal of Electron Spectroscopy and Related Phenomena **8,** 129 (1976).

[28] M. P. Seah and W. A. Dench, Surface and Interface Analysis **1,** 2 (1979).

[29] P. Gupta, V. L. Colvin, and S. M. George, Physical Review B **37,** 8234 (1988).

[30] D. J. Godbey and M. G. Ancona, Journal of Vacuum Science & Technology B **11,** 1392 (1993).

[31] D. J. Godbey and M. G. Ancona, Applied Physics Letters **61,** 2217 (1992).

[32] G. G. Jernigan, P. E. Thompson, and C. L. Silvestre, Surface Science **380,** 417 (1997).

[33] T. Kaufman-Osborn, E. A. Chagarov, S. W. Park, B. Sahu, S. Siddiqui, and A. C. Kummel, Surface Science **630,** 273 (2014).

[34] H. K. Liou, P. Mei, U. Gennser, and E. S. Yang, Applied Physics Letters **59,** 1200 (1991).

[35] Y. Kobayashi, K. Sumitomo, K. Shiraishi, T. Urisu, and T. Ogino, Surface Science **436,** 9 (1999).

[36] E. Rudkevich, F. Liu, D. E. Savage, T. F. Kuech, L. McCaughan, and M. G. Lagally, Physical Review Letters **81,** 3467 (1998).

[37] Y. J. Zheng, P. F. Ma, and J. R. Engstrom, Journal of Applied Physics **90,** 3614 (2001).

[38] J. Y. Lee, S. J. Jung, J. Y. Maeng, Y. E. Cho, S. Kim, and S. K. Jo, Applied Physics Letters **84,** 5028 (2004).

[39] G. Ohta, S. Fukatsu, Y. Ebuchi, T. Hattori, N. Usami, and Y. Shiraki, Applied Physics Letters **65,** 2975 (1994).

[40] K. Sawano, K. Kawaguchi, T. Ueno, S. Koh, K. Nakagawa, and Y. Shiraki, Materials Science and Engineering B-Solid State Materials for Advanced Technology **89,** 406 (2002).

[41] T. Yamanaka, S. J. Fang, H. C. Lin, J. P. Snyder, and C. R. Helms, Ieee Electron Device Letters **17,** 178 (1996).

[42] S. J. Fang, H. C. Lin, J. P. Snyder, C. R. Helms, and T. Yamanaka, Physics and Chemistry of Sio(2) and the Si-Sio(2) Interface-3, 1996 **96,** 329 (1996).

[43] T. Ohmi, K. Kotani, A. Teramoto, and M. Miyashita, Ieee Electron Device Letters **12,** 652 (1991).

[44] T. Kaufman-Osborn, E. A. Chagarov, and A. C. Kummel, Journal of Chemical Physics **140** (2014).

[45] R. M. Feenstra, Surface Science **299–300,** 965 (1994).

[46] R. M. Feenstra, J. A. Stroscio, and A. P. Fein, Surface Science **181,** 295 (1987).

[47] J. S. Hovis, R. J. Hamers, and C. M. Greenlief, Surface Science **440,** L815 (1999).

Chapter 3

Chemically Selective Formation of Si-O-Al on SiGe(110) and (001) for ALD Nucleation Using H_2O_2(g)

3.1 Abstract

Passivation and functionalization via atomic hydrogen, hydrogen peroxide (H_2O_2(g)), and trimethylaluminum (TMA) on clean silicon-germanium ($Si_{0.5}Ge_{0.5}$(110) and $Si_{0.47}Ge_{0.53}$(001)) surfaces were studied and compared at the atomic level using ultra-high vacuum (UHV) scanning tunneling microscopy (STM), scanning tunneling spectroscopy (STS), and X-ray photoelectron spectroscopy (XPS) to understand the topological, electronic, and chemical structures of the surfaces. STM and XPS indicate that a sputter-cleaned SiGe(110) surface is terminated with adatoms, while a SiGe(001) surface is terminated with germanium dimers. STS demonstrates that the Fermi level on a clean SiGe(110) surface is pinned near mid-gap due to surface dangling bonds, while the Fermi level on a clean SiGe(001) surface is consistent with unpinning. A saturation dose of H_2O_2(g) at 25°C chemisorbs to SiGe surfaces, leaving the Fermi level at the surface consistent with unpinning, and the surface is functionalized mainly with Si-OH, Ge-OH, and Si-O-Ge bonds on both SiGe(110) and (001). After a subsequent TMA dose at 25°C, XPS and STM verify that a thermally stable and well-ordered monolayer of Al_2O_3 is formed on SiGe(110) and (001) surfaces, resulting in the formation of Al-O-Si bonds. The H_2O_2(g) functionalization provides three times more oxygen sites on the surface and three

times as great a TMA nucleation density than does H_2O(g) at both 25°C and 120°C. STS demonstrates that H_2O_2(g)- and TMA-dosed SiGe surfaces show a Fermi level consistent with unpinning and a local density of states (DOS) without any states between the conduction and valence band edge, indicating an ideal template for further atomic layer deposition (ALD) nucleation of high-*k* materials on SiGe(110) and (001) surfaces.

3.2 Introduction

With the decreasing size of complementary metal-oxide semiconductor (CMOS) devices, new structures and materials are required and have been investigated. "Fin" field-effect transistor (FinFET) devices are among of these new structures; they are three-dimensional and utilize multiple crystalline planes[1,2]. The multi-gate structure of a FinFET suppresses short-channel effects (SCEs) common to highly scaled, single-gate metal-oxide-semiconductor field-effect transistors (MOSFETs)[3,4]. For highly scaled devices, silicon-germanium (SiGe) is considered a promising material due to easy integration of strain engineering and higher mobility. The larger lattice constant of SiGe as compared to that of silicon (Si) alone can be employed to enhance electron mobility in n-channel metal-oxide-semiconductor (nMOS) transistors by applying biaxial tensile stress to the Si channel layers[5,6]. Additionally, the use of epitaxial SiGe materials in source-drain regions provides uniaxial compressive stress into the Si channel, thereby improving hole mobility in p-channel metal-oxide-semiconductor (pMOS) transistors [7]. The higher hole mobility of

SiGe makes it a good alternative to Si for p-channel field-effect transistor (pFET) channels[8-10]. However, integration of SiGe as a channel material requires a clean and well-ordered surface for gate oxide deposition by suppressing GeO_x formation at the oxide/SiGe interface.

In order to employ SiGe as a channel material, a high quality interfacial layer between SiGe and a gate oxide needs to be formed[11]. Ge segregation to the surface of Si-capped Ge(001) pMOS transistors results in degraded device performance, such as low hole mobility and high interfacial trap density (D_{it}), due to the poor quality of Ge oxides[12]. Consequently, an oxide/SiGe interface with only Si atoms is expected to provide a better electronic structure.

To form the improved interfacial layer with low defect density between gate oxides and channel surfaces, a proper passivation should be employed before the deposition of gate oxides[13]. Oxidation via ozone is known to passivate the Ge surface through the formation of GeO_2, thereby minimizing D_{it}[14]. Lee et al.[15] reported passivation of Ge(001) via H_2O eliminated dangling-bond states due to the termination of Ge atoms by hydroxyl groups (–OH) and –H. Recent studies have demonstrated that H_2O_2(g) should be a good choice for passivating and functionalizing the SiGe surface with hydroxyls because the H_2O_2(g) nucleation density is 3 times greater than that of H_2O(g) on the Ge(001) surface[16]. Moreover, high coverage by hydroxyls is required to increase the gate oxide-nucleation density, thereby improving device performance (as indicated by low D_{it} and low on-state leakage).

Extensive studies have been performed to understand Si segregation on SiGe surfaces because its advantages for device performance. Chlorine plasma was reported to cause Si segregation on SiGe(001) surfaces via selective radical etching of Ge[17]. In addition, segregation of Si atoms on SiGe(001) surfaces by means of dichlorodifluoromethane (CF_2Cl_2) reactive-ion selective etching with directional etching characteristics has been reported[18]. Bestwick et al.[19] demonstrated that hydrogen bromide (HBr) plasma was effective for achieving a Si-rich SiGe surface by forming one monolayer of brominated Si on SiGe(001) again due to selective Ge etching[20].

An atomic hydrogen (H) dose at elevated temperatures generates Si segregation on Ge-covered Si(001) without preferential etching of Ge atoms. Rudkevich et al.[21] reported a "reversible exchange" between Ge and Si atoms on a Ge-covered Si(001) surface when the surface is exposed to atomic H at temperatures above 250°C; based on discrete Fourier transform (DFT) calculations, the Si-H terminated surface has an energy that is 30meV/atom lower than that of the Ge-H terminated surface. In addition, several studies have demonstrated the effectiveness of H in suppressing Ge segregation during SiGe epitaxial growth while leaving the surface terminated with hydrogen[22-24]. The Si-H bond being stronger than the Ge-H bond is considered to be the thermodynamic driving force segregating Si to the surface. An atomic H dose at substrate temperatures above 250°C prevents the etching of Ge atoms on Ge(001) and Ge overlayers on Si(001) surfaces[25,26]. Moreover, an atomic H dose at 300°C produces no etching of Si atoms on Si(001)[27]. Stesmans [28]

reported hydrogen passivation provided a significant improvement in the reduction of the dangling bonds, thereby decreasing the density of interfacial states via the formation of Si-H bonds on the interface of Si/SiO_2.

While previous related studies had explained passivation of Ge(001) and SiGe(001) with $H_2O_2(g)$ [13,15,16], the focus of the present study is the unique passivation of SiGe(110) by $H_2O_2(g)$. The passivation of SiGe is distinct from Ge because of the –OH bonding, which induces surface segregation of Si atoms. The reaction of SiGe(110) with $H_2O_2(g)$ is distinct from the reaction of SiGe(001) with $H_2O_2(g)$ due to the SiGe(110) adatom chemistry and small domains of the SiGe(110) surface. This study seeks to understand and compare the chemical, topological, and electronic properties of SiGe(110) and (001) surfaces for the multi-gated device application; the surface chemistry of SiGe(110) is dominated by adatoms which pin the clean surface while the surface chemistry of SiGe(001) is dominated by surface dimers which unpin the clean surface. Passivation by means of atomic H and H_2O_2 is employed to unpin the Fermi level and induce formation of a Si-terminated SiGe(110) surface. Scanning tunneling microscopy (STM) and X-ray photoelectron spectroscopy (XPS) verify that atomic H produces the Si-segregated SiGe(110) surface while preventing etching. Functionalization by $H_2O_2(g)$ and a subsequent trimethylaluminum (TMA) dose with an anneal is utilized to maximize the nucleation sites for the high-k atomic layer deposition (ALD) process [29-31]. Compared to a $H_2O(g)$ dose, $H_2O_2(g)$ triples the nucleation density at both 25°C and 120°C. In the present report, each experimental

process is explored using *in-situ* XPS, STM, and scanning tunneling spectroscopy (STS).

3.3 Methods

3.3.1 Experimental methods

P-type $Si_{0.47}Ge_{0.53}$(001) films with 10^{17} cm^{-3} boron (B) doping grown on Si(001) wafers and p-type $Si_{0.5}Ge_{0.5}$(110) films with 10^{15} cm^{-3} B doping grown on Si(110) wafers were supplied by GLOBALFOUNDRIES and diced into 12 × 5 mm^2 pieces. Samples were cleaned via repeated degreasing method using acetone, methanol, and deionized water, then dried with N_2 gas. Samples were loaded into a customized Omicron ultra-high vacuum (UHV) preparation chamber with a base pressure of 2×10^{-10} Torr, and cleaned via sputtering and annealing. The sputter process used a 1.5 kV argon ion (Ar^+) beam (Model 1403 ion gun, Nonsequitur Technologies) with a current of 1 μA and an Ar gas pressure of 6×10^{-7} Torr for 30 min, while the sample temperature was maintained at 500°C via resistive pyrolytic boron nitride (PBN) heating. A 30-min annealing was performed at a sample temperature of 500°C. After repeated sputter and annealing cycles, the chemical, topological, and electronic properties were verified via *in-situ* XPS, STM, and STS.

Sputter-cleaned SiGe(110) samples were exposed to atomic hydrogen in the UHV chamber using a thermal gas cracker (Atomic Hydrogen Source, Veeco). The gas pressure was controlled using a leak valve and measured through an ion gauge; the exposure was calculated in terms of Langmuirs (1 Langmuir (L) = 1×10^{-6} Torr · 1

sec). The reported atomic H dose is based on the H_2 pressure, so the reported dose is the maximum possible dose. During the gas dose, the filament temperature of the thermal gas cracker was maintained between 1800°C and 2200°C, while the SiGe(001) and (110) samples were maintained at 300°C; the cracking efficiency is expected to be 30%, but this could not be verified.

Samples were transferred to an *in-situ* ALD chamber with a base pressure of 2×10^{-8} Torr. H_2O_2(g) and TMA were dosed at 25°C without carrier gas by filling the dosing chamber with the precursor gas at 25°C. Control experiments were also performed in which the substrate temperature was 120°C for a H_2O_2(g) dose. In order to perform a saturation dose on SiGe(001) and (110) surfaces, a 30% solution of H_2O_2(aq) (Fisher Scientific) and TMA (98%, Strem Chemicals) were utilized. It was previously reported that a 30% solution of H_2O_2(aq) results in a vapor of 2.67% H_2O_2(g) at 25°C [32]; therefore, the actual amount of H_2O_2(g) participating in the chemical reaction should be smaller than the reported amount of H_2O_2(g). Due to the possible reactivity of H_2O_2(g) with stainless steel, the H_2O_2(aq) solution was placed in a glass tube and dosed through a Teflon tube and Teflon valve to minimize the decomposition of H_2O_2(g). Additionally, several cycles of H_2O_2(g) were pre-dosed to minimize the chemical reaction with the stainless-steel chamber walls before the samples were introduced to the chamber. The exposure pressures were measured with a convectron gauge and converted into Langmuirs.

After a dose with H_2O_2(g) and/or TMA, samples were transferred to a UHV preparation chamber, followed by a post-deposition annealing at 300°C. In order to

determine the topological and electronic structures on the SiGe(001) and (110) surfaces after each treatment, the samples were transferred to an *in-situ* STM chamber (LT-STM, Omicron Nanotechnology) with a base pressure of 2×10^{-11} Torr. During the operation of the STM and STS at 25°C, constant-current mode (I_{sp} = 200 pA) imaging was performed with a sample bias at –1.8 V to obtain filled-state STM images. Variable-z mode STS was performed using a modulation signal (0.1 V, 650 Hz) from an external lock-in amplifier (SR830 DSP, Stanford Research Systems) while sweeping the sample bias from –1.5 to +1.5 V and simultaneously moving the tip position forward then backward during the scan, so as to gain increased sensitivity to small currents that occur when the sample bias is close to zero volts [33,34]. The tip was modulated with 0.1 V_{ac} and the dI/dV was directly obtained from the lock-in measurement along with the I/V spectra. The I/V data was smoothed using a low-pass filter with energy width of (3.0 eV)/2π (frequency parameter value in filter of (3.0 eV)-1), precisely as described in Fig. 7(b) of Ref. [35]. This procedure resulted in the formation of a broadened I/V, denoted as $\overline{\mathrm{I/V}}$, which forms a suitable normalization quantity for dI/dV [35] (this same procedure was also used in prior work [13], although the description is more explicit in the current manuscript). The ratio (dI/dV)/($\overline{\mathrm{I/V}}$) has the property that band onsets show a linear dependence on voltage, so that they can be fit with a linear function in order to extract the band edge energies [35]. For accurate STS measurements, the (dI/dV)/($\overline{\mathrm{I/V}}$) from each measurement was rescaled from 0 to 1 and subsequently averaged from at least 6 individual spectra; this rescaled and averaged (dI/dV)/($\overline{\mathrm{I/V}}$) was plotted as a single spectrum in the STS figures. A fitting method

was employed as described in previous STM/STS studies to extract the band edge energies for the (dI/dV)/($\overline{I/V}$) spectra [35,36], with a *linear* function and including slight rounding at the onset due to both temperature and AC modulation. The onsets of the linear fits which correspond to the band gaps are calculated with error ranges. Simulated fits to the STS data are included in all STS figures as the dashed lines. The error ranges obtained from the fitting process are standard errors of the least-squares fits.

STS can rigorously show that surfaces are pinned by observation of n-type samples having a Fermi level below mid-gap and p-type samples having a Fermi level above mid-gap. However, to employ STS to rigorously prove unpinning, the Fermi level must be shown to have different positions on n-type and p-type samples. N-type SiGe(110) samples were not available; therefore, in this study "unpinned" means the data is only consistent with unpinning. Furthermore, on Ge(001) and $Si_{0.6}Ge_{0.4}$(001) surfaces, the STS Fermi level positions are never observed to be directly at the VB edge for p-type and the CB edge for n-type even on clean surfaces [13,15,16]; this may be due to intrinsic surface states. Furthermore, quantification of extrinsic surface states are best performed with other techniques such as D_{it} measurements on metal-oxide-semiconductor capacitors (MOSCAP)s.

Chemical analysis after each chemical step was performed with an *in-situ* monochromatic XPS (XM 1000 MkII/SPHERA, Omicron Nanotechnology). A constant analyzer-energy mode with a pass energy of 50 eV and a step width of 0.1 eV, using an Al Kα source (1486.7 eV), were utilized. The detection angle was 30°

from the sample surface, which is close to the surface parallel, and an acceptance angle of + 7° was utilized. For peak shape analysis, a CASA XPS v.2.3 was used through a Shirley background subtraction.

3.3.2 Computational methods

The Density-Functional Theory (DFT) simulations were performed using a Vienna ab-initio simulation package (VASP) for plane-wave DFT simulation with projector augmented-wave (PAW) pseudopotentials [37-42] and a Perdew–Burke–Ernzerhof (PBE) exchange-correlation functional [43]. The SiGe was a regular polymorph with 50% Si and 50% Ge placed in checker-board pattern. The SiGe unit cell was optimized at variable volume with conjugate-gradient algorithm to avoid internal compression/strain. The optimized unit cell was later used to build the SiGe(110) supercell and initial slabs with the desired surfaces. The simulation box included ~12-15 Å of vacuum to avoid spurious interaction through periodic boundary conditions. All slab relaxations were performed using a conjugate-gradient relaxation algorithm with a force tolerance level of 0.05 eV/Å and a Gamma-centered 5 × 7 × 1 K-point grid. During relaxations, the 3 bottom layers of SiGe slabs were permanently fixed in their bulk-like positions and saturated with H atoms with 1 |e| charge to simulate continuous bulk. To avoid artificial field due to periodic boundary conditions, dipole correction in the vertical z direction was applied [39-41]. Due to high computational cost of these simulations including 116 atoms for the clean surface and 144 atoms for the hydroxylated, the 5 × 7 × 1 K-point set and the ~12 Å vacuum layer,

the supercells were limited to 6 SiGe layers. Therefore, instead of modeling all the adatoms in multiple SiGe(110) adatoms structures, a simplified model was employed which retained the highest symmetry adatoms. The cross-sectional area of the simulated slabs is 15.90 × 11.24 $Å^2$. More complex adatom patterns would require much larger cell sizes hardly affordable for DFT simulations. After relaxation, the final samples were rescaled to the higher accuracy Heyd-Scuseria-Ernzerhof (HSE06) exchange-correlation functional lattice constant (different by ~1.1%) and the densities of states were calculated with the HSE06 functional [44-47]. The residual forces in HSE06 force field were inspected to verify that they were less than 0.05 eV/Å.

3.4 Results and Discussion

3.4.1 Clean and H-passivated SiGe surfaces

$Si_{0.47}Ge_{0.53}$(001) and $Si_{0.5}Ge_{0.5}$(110) surfaces were prepared via repeated cycles of sputtering and annealing; afterwards, the cleanliness of the sputter-cleaned surfaces was verified via an *in-situ* XPS (not shown). The surface reconstructions were checked at the atomic level. Fig. 3.1 shows filled-state STM images of sputter-cleaned SiGe(001) and (110) surfaces, followed by 500°C annealed surfaces. Based on previous studies, a clean SiGe(001) surface is known to be terminated with Ge dimers because of Ge segregation to the SiGe(001) surface [48-50]. In addition, based on a previous DFT simulation, a Ge dimer termination is known to be thermodynamically more stable than a Si dimer termination on clean SiGe(001) [13]. In Fig. 3.1(a) and (b), STM shows a surface reconstruction, mainly composed of dimers on SiGe(001), that

is consistent with the schematic diagram in Fig. 3.1(c), and which is identical to the results of a previous study by Kaufman-Osborn et al [13]. As shown in Fig. 3.1(d) and (e), SiGe(110) has a different surface reconstruction with smaller domains and increased disorder compared to the SiGe(001) surface with the same Si/Ge bulk ratio. In addition, the size of the atoms on SiGe(110) looks larger than SiGe(001) because the spacing of adatoms on SiGe(110) is larger compared to the row spacing of Ge dimers on SiGe(001). It is reported that Si and Ge(110) surfaces should have adatom reconstructions as shown by the schematic diagram in Fig. 3.1(f) to lower the surface energy by reducing the number of dangling bonds [51,52]; the number of dangling bonds in Fig. 3.1(f) is reduced by half in a unit cell due to adatom reconstructions. Note this is just one of many nearly degenerate adatom structures.

STS was employed to probe the surface electronic structures, because measurements of (dI/dV)/($\overline{I/V}$) are known to be approximately proportional to the local density of states (LDOS) [33,34]. A clean n-type SiGe(001) surface is known to have an unpinned Fermi level positioned slightly above mid-gap in STS measurements [13]. The position of the Fermi level on a clean n-type SiGe(001) surface is the same as the position of the Fermi level on a clean n-type Ge(001) surface and a clean n-type Si(001) surface, and is consistent with a surface terminated by Ge dimers on SiGe(001) surface [16,53]. A Fermi level position consistent with unpinning was also observed on a clean p-type SiGe(001) surface because the Fermi level is close to the valence band (VB), as shown in Fig. 3.2(a). In contrast, a clean p-type SiGe(110) surface had a pinned Fermi level positioned near the mid-gap between the conduction

and valence band edges, as shown in Fig. 3.2(a); this was consistent with the presence of surface adatoms with half-filled dangling bonds. The surface-pinning effect at the interface between substrate and gate oxides is known to cause undesirable device performance, such as high threshold voltage and subthreshold swing [54]. Therefore, the SiGe(110) surface needs to be unpinned by chemical passivation.

In order to passivate the SiGe(110) surface, atomic H was introduced to remove the dangling bonds. Atomic H was dosed at 3,600 L on a sputter-cleaned SiGe(110) surface using a thermal gas cracker while the substrate temperature was maintained at 300°C; the elevated temperature was employed to prevent Ge preferential etching. Fig. 3.2(a) shows STS measurements before and after an atomic H dose on a clean SiGe(110) surface. Six STS curves were taken at several positions and averaged into one curve, as shown in the graph of Fig. 3.2(a). Additionally, curve fitting of the onsets of VB maximum (VBM) and CB minimum (CBM) were performed to quantitatively determine the band gaps and Fermi level positions [35,36]. Before the atomic H dose, the Fermi level was positioned near mid–gap, which is consistent with SiGe(110) being pinned by adatom dangling bonds. However, after the atomic H dose, the Fermi level was shifted toward the valence band edge (blue arrow). Since the substrate is p-type, the atomic H-dosed SiGe(110) surface having a Fermi level (0 V in STS) near the VB is consistent with unpinning. In Fig. 3.2(b), a filled-state STM image after an atomic H dose shows a uniform and ordered surface with an average row spacing of 7.9 Å, a standard deviation of 0.88 Å, and a standard error of 0.33 Å, as compared to an average row spacing of 8.1 Å on the clean surface,

demonstrating that the adatoms are intact after an atomic H dose. In addition, there were no etch pits on the surface, which was consistent with the prevention of the Ge preferential etching.

3.4.2 H_2O_2(g) dosed SiGe surfaces

In order to functionalize the SiGe(001) and (110) surfaces with hydroxyls, the clean surfaces were exposed to a 1.5×10^6 L dose of H_2O_2(g)/H_2O(g) at 25°C in an *in-situ* ALD chamber without any exposure to ambient air; note that this H_2O_2(g) dose has a maximum value of 40,000 L. Note that the "H_2O_2(g)" dose refers to the dose with the H_2O_2(g)/H_2O(g) mixture, but due to the high reactivity of H_2O_2(g), the results are consistent with the surface functionalization being due to H_2O_2(g), so the dose is denoted as "H_2O_2(g)". In a previous study, a SiGe(001) surface was shown to have all Ge surface atoms bonded to OH (HO-Ge-Ge-OH and HO-Ge-O-Ge-OH bonds) after exposure to a full saturation dose of H_2O_2(g) at 25°C [13]. Furthermore, the Ge-O_xH_y termination (Ge-O_xH_y included a mixture of Ge-OH and HO-Ge-O-Ge-OH sites) after H_2O_2(g) was stable to at least 100°C, in contrast to the combination of Ge-H and Ge-OH termination of Ge(001) from a H_2O dose [16].

Fig. 3.3 shows XPS spectra of Ge 3d and Si 2p peaks of the SiGe(110) surface after each chemical step. Sharp and asymmetric (due to spin-orbit splitting) Si and Ge peaks without any shoulders were observed on a sputter-cleaned SiGe(110) surface consistent with a clean surface; the peaks on clean surfaces showed resolved spin-orbit components consistent with previous studies [55,56]. In addition, the cleanness of the

surface was verified as contaminant-free via XPS and STM analysis. In Fig. 3.3(a), while Si and Ge peaks on a clean surface contained only bulk-like components, a H_2O_2 dosed SiGe(110) surface had shoulder peaks at higher binding energy, corresponding to Si-O_xH_y and Ge-O_xH_y components. As shown in Fig. 3.3(b), the mixture of Si-O_xH_y and Ge-O_xH_y after a 25°C H_2O_2 dose is consistent with Si and Ge atoms coexisting on a clean SiGe(110) surface, while a clean SiGe(001) is terminated with only Ge dimers. After a dose at elevated temperature or annealing, atomic H induced a partial segregation of Si atoms to the surfaces. As shown in Fig 3.3(c), 3,600 L of an atomic H dose at 300°C generated sharp and asymmetric Si and Ge peaks without shoulder peaks, thereby verifying no adsorption of contaminants such as oxygen or hydrocarbons on the surface; the asymmetry was due to the preservation of the spin-orbit splitting, which was consistent with the conservation of a well-order surface. After the 300°C atomic H dose, the Ge 3d and Si 2p peaks were shifted to higher binding energy compared to a sputter-cleaned surface; this was consistent with hydrogen termination at the surface, as shown in the previous report [57]; however, since the shift appears to be nearly equal for both Si and Ge, it is possible some of the shift is due to a change in the work function. Additionally, XPS confirmed the cleanness of the atomic H-dosed surface by showing no carbon and oxygen peaks. However, while the spectra of 25°C H_2O_2(g) that dosed the SiGe(110) surface without atomic H had both higher binding-energy shoulders on the Si and Ge peaks, as would be consistent with Si-O_xH_y and Ge-O_xH_y bonds, the spectra of 25°C H_2O_2(g) dosed SiGe(110)

surface after a 300°C atomic H dose primarily had a higher binding energy peak on Si in Fig. 3.3(d), consistent with preferential formation of Si-O_xH_y bonds.

The H_2O_2(g) dose at 25°C was reactive enough to form hydroxyl bonds on H-terminated SiGe surfaces, consistent with the following mechanism. For the mechanisms below, the reaction enthalpies were estimated using the polyatomic bonds enthalpies [58].

Si-H + H_2O_2(g) → Si-OH + H_2O(g).

$\Delta H = (293 + 210) – (368 + 497) = –362$ kJ/mol

or

Ge-H + H_2O_2(g) → Ge-OH + H_2O(g)

$\Delta H = (263 + 210) – (303 + 497) = –327$ kJ/mol

Since the estimated enthalpies of reaction are negative, the forward reactions are exothermic and are likely to occur. In addition, Bensliman et al. [59] demonstrated that a H_2O_2 dose onto hydrogen-terminated Si(111) surface eliminates Si-H bonds and results in oxidation of the surface as verified using Fourier transform infrared (FTIR) spectra. Based on a previous study, after a H_2O_2(g) dose on SiGe(001), Ge dimers are bonded to two hydroxyls or two hydroxyls with an inserted bridge oxygen atom [13]. In comparison, H_2O_2 dosed SiGe(110) and 300°C atomic H/SiGe(110) have different bonding configurations without dimer bonds, as shown by a proposed model in Fig. 3.4(a). Based on the crystallographic calculation, Si(001) has 6.8 atoms/nm^2 and the unreconstructed Si(110) has 9.6 atoms/nm^2, while the adatom-terminated Si(110) has

4.8 atoms/nm^2 because of 50% reduction of dangling bonds on the surface by adatoms [60]. It is assumed the ratio of spacings is identical on the corresponding SiGe(001) and SiGe(110) surfaces. To just remove the dangling bonds, the Si and Ge adatoms on SiGe(110) need only to be bonded to one hydroxyl group, forming Si-OH and Ge-OH bonds. However, for the O/(Si + Ge) ratio to be nearly identical on H_2O_2 dosed SiGe(001), SiGe(110), and 300°C atomic H/SiGe(110), as shown in Fig. 3.4(b), the H_2O_2(g) dose must partially remove the adatom reconstruction, or else there must be more oxygen insertion into adatom backbonds on SiGe(110) and 300°C atomic H/SiGe(110) compared to oxygen insertion into surface dimers on SiGe(001).

In Fig.3.4(b), XPS analysis of 25°C H_2O_2/SiGe(001), 25°C H_2O_2/SiGe(110), 120°C H_2O_2/SiGe(110), 25°C H_2O_2/300°C atomic H/SiGe(110), and 25°C H_2O/SiGe(110) are shown in terms of oxygen intensities normalized to Si 2p + Ge 3d peaks with standard error ranges of ±0.02. For the precise calculation of the ratios normalized to the SiGe surface, all XPS peaks were normalized by photoelectron cross-sections (Si 2p-0.817, Ge 3d-1.42, O 1s-2.93) using the Hartree-Slater atomic model [61]. Compared to the 25°C H_2O_2/SiGe(001) surface, the oxygen ratios of the 25°C H_2O_2/SiGe(110), 120°C H_2O_2/SiGe(110), and 25°C H_2O_2/300°C atomic H/SiGe(110) surfaces are nearly identical within error ranges, which was consistent with a high coverage of hydroxyls on SiGe(110) and 300°C atomic H/SiGe(110) surfaces. The data are consistent with the 30% H_2O_2 partially removing the adatoms from SiGe(110), additional OH bonding at step edges or defects, or inducing significant oxygen backbond insertion, thereby equalizing the oxygen on SiGe(110)

and SiGe(001). As shown in Figs. 3.3(a) and (c), the shoulder peaks after a H_2O_2(g) dose on clean SiGe(110) and 300°C atomic H/SiGe(110) are positioned between 100.5 eV and 101.5eV for Si mostly corresponding to Si^{2+} (SiO), and between 30.5 eV and 31.5eV for Ge mostly corresponding to Ge^{2+} (GeO), respectively. This demonstrates that the surface is composed mostly of surface atoms with one hydroxyl and an oxygen inserted into a backbond or surface defects atoms (such as step edges) with bonds to two hydroxyls; each shoulder peak at higher binding energy has a wider full width at half maximum (FWHM) compared to a sputter-cleaned surface. This is consistent with a mixture of various surface states. It was previously shown that a 30% H_2O_2 dose results in a second site on Ge(001) and SiGe(001), which is HO-Ge-O-Ge-OH, containing two hydroxyls and an additional bridge oxygen on a Ge dimer [13,16]. On Ge(001), analysis of STM images shows these higher O-content sites are approximately 30% of all sites. In addition, based on the analysis of Ge 2p peaks, a H_2O_2 dose on 300°C atomic H/SiGe(110) results in the formation of a higher binding energy component, corresponding to Ge-OH and X-O-Ge-OH bonding configurations consistent with an additional –OH binding site or an insertion of O into a Si-Ge or Ge-Ge bond. As explained in the supplement, the limited density of GeO_x and the small peak shift in the Ge 2p spectrum prevented definitive assignment of oxidation components Ge^{1+} and Ge^{2+} in the Ge 2p spectrum (see Supplementary Information, Fig. 3.12). More importantly, the oxygen ratios for 25°C H_2O_2/SiGe(110), 120°C H_2O_2/SiGe(110), and 25°C H_2O_2/300°C atomic H/SiGe(110) are 3 times greater than for 25°C H_2O/SiGe(110), consistent with a previous study [16]. This is largely because a

25°C H_2O(g) dose results in a mixture of less than a half monolayer of Si-OH and Ge-OH, and less than a half monolayer of Ge-H and Si-H, while a 25°C H_2O_2(g) dose results in a full monolayer of Si-O_xH_y and Ge-O_xH_y. Based on the model by Seah and Dench [62], the estimated escape depth of electrons in Si 2p and Ge 3d peaks is 1nm with a detection angle of 30° from the sample surface and the estimated coverages of 17% of O/(Si + Ge) for 25°C H_2O_2/SiGe(110) and 5% of O/(Si + Ge) for 25°C H_2O/SiGe(110) correspond to 95% and 31%, respectively. These estimated coverages are calculated based on a simplified model in which the top monolayer on the surface is composed of oxygen atoms and the lower layers are composed of Si and Ge atoms; the attenuation of intensities is obtained through the formula $I = I_0\exp(-t/\lambda)$ (I: intensity in the presence of the overlayer; I_0: intensity in the absence of any overlayer; t: thickness of the covering layer; λ: inelastic mean free path).

The electronic structures of 25°C H_2O_2/SiGe(110) and 25°C H_2O_2/300°C atomic H/SiGe(110) surfaces were verified via the STS curves in Fig. 3.5. At least 6 STS curves were taken on different areas, and all the curves showed a consistent electronic structure. A previous study by Grassman et al. showed that when the p-type Ge(001) surface was exposed to O_2 at 25°C, the STS spectra displayed the same Fermi level position as a sputter-cleaned Ge(001); since the surface was already p-type, the surface dipoles or acceptor surface states induced by an O_2 dose could not further move the Fermi level to the VB in STS measurements [63]. This phenomenon is consistent with the H_2O_2 dosed p-type SiGe(001) surface, which is terminated with Ge-O_xH_y bonds, and has a Fermi level near the VB in the STS measurements, as

shown in Fig. 3.5(a). However, the 25°C H_2O_2/300°C atomic H/SiGe(110) surface (Fig 3.5(b)), which was composed of mainly Si-O_xH_y and partially Ge-O_xH_y bonds, showed a clear shift of the Fermi level in the STS measurements after a 25°C H_2O_2 dose relative to the mid-gap position of the sputter-cleaned surface, and the position of the Fermi level was close to the VB, and similar to the H-terminated SiGe(110) surface. This is consistent with unpinning. It is noted that the bandgap decreased after a H_2O_2 dose on a 300°C atomic H /SiGe(110) surface.

3.4.3 TMA dosed SiGe surfaces

On the SiGe(001) and (110) surfaces that were functionalized by a 25°C H_2O_2 dose, 1.5×10^5 L of TMA was subsequently dosed at 25°C, followed by post-deposition annealing (PDA) at 300°C for 20 min. In a previous report, when a TMA-dosed 25°C H_2O_2/SiGe(001) surface was annealed at 300°C, oxygen atoms that bonded to Ge atoms at the surface were completely transferred to Si atoms, forming Al-O-Si bonds. This is due to the stronger bond strength of Si-O bonds compared to Ge-O bonds [13]. Similarly, when TMA-dosed 25°C H_2O_2/SiGe(110) and 25°C H_2O_2/300°C atomic H/SiGe(110) were annealed at 300°C, the SiGe(110) surfaces were terminated with Al-O-Si bonds, as shown in Fig. 3.6. It is hypothesized that for 25°C H_2O_2/SiGe(110), the thermal energy at 300°C enables the Si atoms to diffuse to the surface to bond with O atoms, releasing Ge atoms to the subsurface on both SiGe(001) and (110).

A previous study on the SiGe(001) surface showed that the 25°C TMA/25°C H_2O_2/SiGe(001) surface showed no significant change in oxygen and aluminum ratios after 300°C annealing, thus demonstrating the thermal stability of Al-O-Si bonds [13]. In order to understand the chemical compositions of the SiGe(110) surface, XPS analysis of 25°C TMA/25°C H_2O_2/300°C atomic H/SiGe(110) before and after 300°C PDA is shown in Fig. 3.7(a), with the carbon, oxygen, and aluminum intensities normalized to Si 2p + Ge 3d peaks (with error ranges of ±0.02). The ratio between Al and O was maintained 2:3 before and after PDA at 300°C, while the C ratio decreased by 50%, as would be consistent with the desorption of methanes or ethanes. In addition, compared to a 25°C H_2O(g) dose, the 25°C H_2O_2(g) dose provided 3 times as great an oxygen ratio, indicating a higher nucleation density for high-k + H_2O_2 ALD process. One possible, simple model consistent with this data is that TMA molecules chemisorb dissociatively on both hydroxyls on the SiGe(110) surface and oxygen backbonded to adatoms, while methanes or ethanes desorb as byproducts, as shown in Fig. 3.7(b). This is consistent with a monolayer of stoichiometric Al_2O_3, indicating a thermal stability up to 300°C.

Fig. 3.8 shows STM image and line trace analysis of SiGe(001) and (110) surfaces dosed with 25°C H_2O_2(g), subsequently dosed with 25°C TMA, and annealed at 300°C. The STM image of the 25°C TMA/25°C H_2O_2/SiGe(001) surface in Fig. 3.8(a) shows vertical rows along the direction of SiGe dimer rows, consistent with Al-O-Si bonds. In order to quantify the vertical rows structure, a line trace was performed in Fig. 3.8(b) at four different locations in the image. Each line in the analysis was

measured at least 5 times. The line traces of the SiGe(001) surface have an average row spacing of 9.0 Å with a standard deviation of 1.1 Å and a standard error of 0.40 Å. The topological image and numerical analysis are almost identical to the results of a previous study [13]. In comparison, the STM image of 25°C TMA/25°C H_2O_2/300°C atomic H/SiGe(110) surface shows different topological structures with lower surface order and larger row spacing in Fig. 3.8(c). The line traces of 25°C TMA/25°C H_2O_2/300°C atomic H/SiGe(110) surface in Fig. 3.8(d) have an average row spacing of 11.8 Å with a standard deviation of 1.2 Å and a standard error of 0.44 Å; the average spacing of the TMA products is slightly greater on SiGe(110) than on SiGe(001). The 11.8 Å average row spacing on SiGe(110) is almost 3/2 of the 8.1Å adatom spacing on a clean SiGe(110), as shown in Fig. 3.1(e). This is consistent with Al atoms being bonded to Si-O ligands with oxygen backbond insertion, as shown in a proposed dissociative chemisorption model in Fig. 3.7(b). The density of Si and Ge atoms is lower on the SiGe(110) surface than on the SiGe(001) surface; this is consistent with the larger row spacing, after TMA functionalization, for SiGe(110) than for SiGe(001). It is noted that the Al/(Si+Ge) ratio after dosing TMA on H_2O_2(g) functionalized SiGe(110) is at least as large as on SiGe(001); this may be due to the more open structure of the SiGe(110) surface allowing TMA bonding with steric hindrance.

To understand the electronic structures, STS measurements were employed, as shown in Fig. 3.9. For the 300°C PDA/25°C TMA/25°C H_2O_2/SiGe(001) and 300°C PDA/25°C TMA/25°C H_2O_2/300°C atomic H/SiGe(110) STS spectra, a black arrow

shows that the 25°C TMA with 300°C PDA moved the Fermi level closer to the conduction band with a slight decrease of the band bending in valence band edge. This result is consistent with the elimination of the surface dipole by the formation of Al-O-Si bonds. In addition, as shown in Fig. 3.9, the Fermi level is positioned below the mid-gap; a result consistent with unpinned surfaces with a larger band gap due to the formation of an Al_2O_3 monolayer. Note, the onsets in the experimental (dI/dV)/(I/V) are slightly greater than the fitted curves; this could be indicative of either site-to-site variations in the Fermi level or a small density of band edge states (sometimes called band tails); in either case, the uncertainty in the band gaps is greater than the standard error.

3.4.4 Density Functional Theory Simulations

Density functional theory (DFT) modeling was employed to understand the proposed bonding configurations and electronic structures. The DFT modeling was performed for clean and hydroxyl-terminated SiGe(110) surfaces, followed by relaxation. In Fig. 3.10(a), a DFT model shows a clean unreconstructed SiGe(110) surface terminated by both tri-coordinated Si and Ge atoms with half-filled dangling bonds. Note this is a simplified structure; as shown by Takeuchi and Stekolnikov et al. [51,52], the real structure has additional adatoms consistent with the large spacing of the adatoms in the STM images in Fig. 3.1(d) and (e); in addition there are multiple nearly degenerate adatoms structures. However, to understand chemical passivation on the surface, the simplified model is sufficient. The DOS of this structure shows states in

the band gap region, and the Fermi level of the surface is pinned as shown in Fig. 3.10(b), which is consistent with the STS measurements in Fig. 3.2(a). This indicates that the surface is pinned near the mid-gap due to the surface dangling bonds.

DFT and DOS simulations were studied on the SiGe(110) surface passivated with hydroxyls after a H_2O_2(g) dose. In Fig. 3.11(a), a SiGe(110) surface is terminated with hydroxyls on both Si and Ge atoms after a H_2O_2(g) dose; this result is consistent with the XPS analysis showing both Si-OH and Ge-OH peaks in Fig. 3.3(a) and (b). In contrast to a clean SiGe(110) surface, the DOS of the hydroxyl-terminated SiGe(110) surface demonstrates the elimination of the states in the band gap region. This is consistent with the STS results showing no mid-gap defect states after a H_2O_2(g) dose in Fig. 3.5. It is anticipated that a similar phenomenon should be demonstrated on an unpinned SiGe(110) surface with H termination after an atomic H dose, as shown in Fig. 3.2(b).

3.5 Conclusion

Chemical, topological, and electronic structures of SiGe(110) and (001) surfaces were compared and analyzed using *in-situ* XPS, STM, and STS. The clean SiGe(110) is terminated with adatoms with a low surface order, while the clean SiGe(001) surface is terminated with Ge dimers with a uniform and well-ordered structure. STS measurements verified that the clean (110) surface is pinned near the mid-gap by adatom dangling bonds, while the clean (001) surface is unpinned. The sputter-cleaned SiGe(110) surface was dosed at 300°C with a 3,600 L dose of atomic

H to passivate the adatom dangling bonds. STS measurements demonstrated that the atomic H-dosed SiGe(110) surface is consistent with unpinning, with a Fermi level near the valence band due to the passivation of the surface adatoms. The 300°C atomic H dose induced a partial Si segregation to the SiGe surfaces because the bond strength of Si-H is larger than that of Ge-H. The Si segregated SiGe(110) and (001) surfaces should be ideal for FinFET structures due to the low defect density of Si/high-*k* dielectric interfaces after a forming gas annealing [64]. It is known that Si termination passivates defects on Ge PMOS transistors that result in a lower D_{it} [12]. The 300°C atomic H/SiGe(110) and (001) surfaces were dosed at 25°C with saturation doses of H_2O_2(g), leaving the SiGe surface terminated with an ordered monolayer of mainly Si-O_xH_y sites on SiGe(110), and only Ge-O_xH_y sites on SiGe(001) surfaces [13]. TMA was subsequently dosed at 25°C on the 25°C H_2O_2/300°C atomic H/SiGe(110) and 25°C H_2O_2/SiGe(001) surfaces. The surfaces were annealed at temperatures up to 300°C, and XPS measurements verified complete Si/Ge place exchange, so that only Al-O-Si bonds are formed on both (110) and (001). This indicates the ability of Si to diffuse to the oxide/SiGe interface and displace Ge, even at modest temperatures. STS measurements indicated that the Fermi levels on both surfaces were consistent with unpinning, leaving an electrically passive, ordered layer, which serves as an ideal template for further high-*k* ALD.

3.6 Acknowledgments

This work was supported in part by the Center for Low Energy Systems Technology (LEAST), one of six centers of STARnet, a Semiconductor Research Corporation program (Grant No. 2013-VJ-2451) sponsored by MARCO and DARPA, NSF DMR 1207213, and Applied Materials. The SiGe wafers were provided by GLOBALFOUNDRIES.

Chapter 3, in part or in full, is a reprint of the following material:
S. W. Park, H. Kim, E. Chagarov, B. Sahu, S. Siddiquui, N. Yoshida, J. Kachian, A. C. Kummel "Formation of Chemically Selective Si-O-Al on SiGe(110) and SiGe(001)" Surface Science (In Press) (2016). The dissertation author was the primary investigator and author of this paper.

3.7 Supplemental materials

In order to provide more accurate analysis of oxygen ratio and O-Ge bonding on SiGe(001) and (110) surfaces, the Ge 2p peaks of 25°C H_2O_2/SiGe(001) and 25°C H_2O_2/300°C atomic H/SiGe(110) were compared and fit (with a resulting error range of ±0.1 eV) to show the bonding configurations.

In Fig. 3.11, the Ge 2p spectra are deconvoluted into several contributions using Gaussian – Lorentzian line shapes based on a previous report [16]. As shown in Fig. 3.11(a), a 25°C H_2O_2(g) dose on the SiGe(001) surface resulted in the formation of two non-bulk bonding configurations normally assigned as Ge^{+1} (red peak) and Ge^{+2} (yellow peak), which correspond to HO-Ge-Ge-OH (red peak) and HO-Ge-O-

Ge-OH (yellow peak) bonding configurations; the ratio of Ge bulk : HO-Ge-Ge-OH : HO-Ge-O-Ge-OH was 8.8 : 2.5 : 1.

Fig. 3.11(b) shows that a 25°C H_2O_2(g) dose on the 300°C atomic H/SiGe(110) surface resulted in the formation of a shoulder peak at high binding energy, corresponding to GeO_x composed of Ge-OH and X-O-Ge-OH bonding configurations. There was no improvement in the fit by separating this shifted component into two peaks. Since this GeO_x had a higher binding-energy shift of 2.1 eV relative to the Ge bulk peak, this GeO_x was assigned as mostly Ge^{2+} (GeO), consistent with Ge-OH with an oxygen inserted into surface backbonds on SiGe(110). The ratio of Ge bulk : GeO_x was 6.3 : 1. Compared to 25°C H_2O_2/SiGe(001), the sum of the shifted Ge components on 300°C atomic H-dosed SiGe(110) is lower, which is consistent with a surface mostly terminated in Si atoms.

To determine the oxidation state of the monolayer of Al_2O_3, Al 2p peaks of 25°C TMA/25°C H_2O_2/300°C atomic H/SiGe(110) and 300°C PDA/25°C TMA/25°C H_2O_2/300°C atomic H/SiGe(110) were provided in Fig. 3.12, and the peaks were positioned between 74.5 eV and 74.7 eV, corresponding to Al^{3+}. This is consistent with a monolayer of stoichiometric Al_2O_3.

Based on a previous study by Linford et al., the hydrogen-terminated Si surface is known to induce the adsorption of alkyl monolayers on the Si surface and the methyl-terminated surface prevents the oxidation of the Si substrate [65]. In Fig. 3.13(a), 25°C TMA was dosed on 300°C atomic H/SiGe(110) and the Al : C ratio was approximately 1 : 3, a result that was consistent with dissociative chemisorption of

TMA on a hydrogen-terminated SiGe(110) surface and resulting in the mainly methyl-terminated surface. In addition, the Al ratio on 25°C TMA/300°C atomic H/SiGe(110) was lower than on 25°C TMA/25°C H_2O_2/300°C atomic H/SiGe(110), demonstrating a hydroxyl-terminated SiGe(110) surface induced higher TMA nucleation density compared to a hydrogen-terminated SiGe(110) surface. In Fig. 3.13(b), 25°C H_2O_2 was dosed on 25°C TMA/300°C atomic H/SiGe(110); no significant change was observed in the Al and C ratios, and the O ratio was less than 2%, showing the stability of the mainly methyl-terminated SiGe(110) surface upon H_2O_2 exposure.

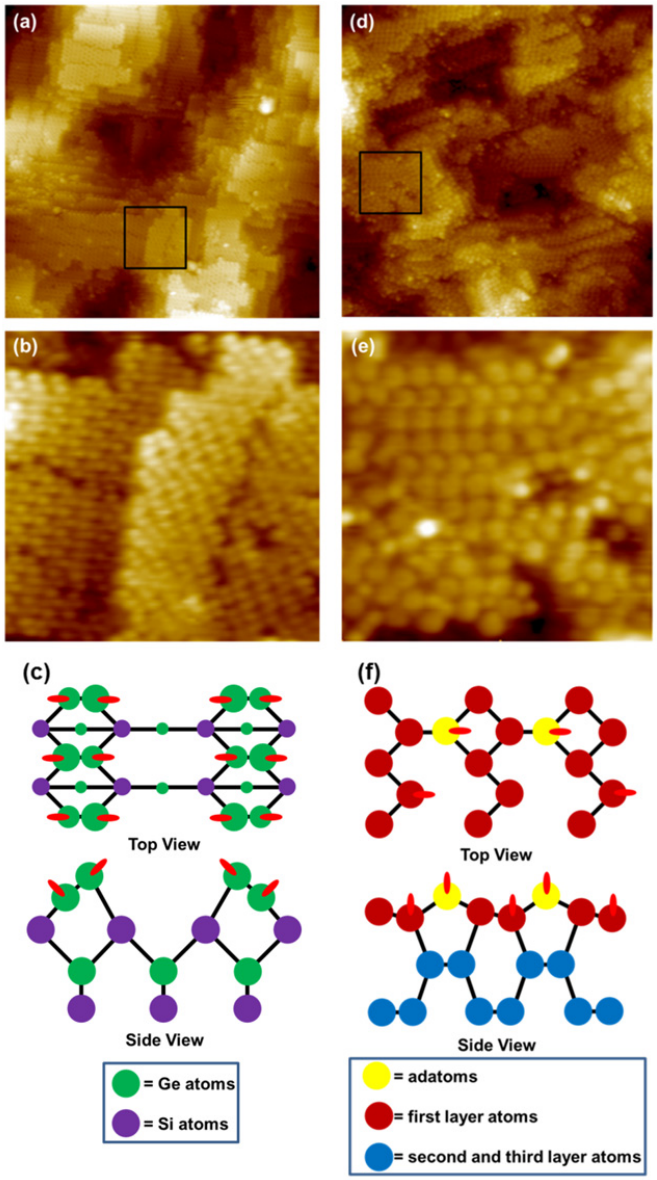

Figure 3.1 STM images and proposed models of sputter-cleaned SiGe(001) and (110) (a) Filled state STM image (50 × 50 nm^2, V_s = –1.8 V, I_t = 200 pA) of sputter-cleaned and 500°C annealed SiGe(001). A clean SiGe(001) surface is terminated with Ge dimers. (b) 10 × 10 nm^2 inset of a black square in (a) to show the surface reconstruction on SiGe(001). (c) Schematic diagram of Ge dimers on SiGe(001). (d) Filled state STM image (50 × 50 nm^2, V_s = –1.8 V, I_t = 200 pA) of sputter-cleaned and 500°C annealed SiGe(110). A clean SiGe(110) surface is terminated with adatoms of both Si and Ge atoms. (e) 10 × 10 nm^2 inset of a black square in (d) to show the surface reconstruction on SiGe(110). (f) Schematic diagram of adatoms on SiGe(110).

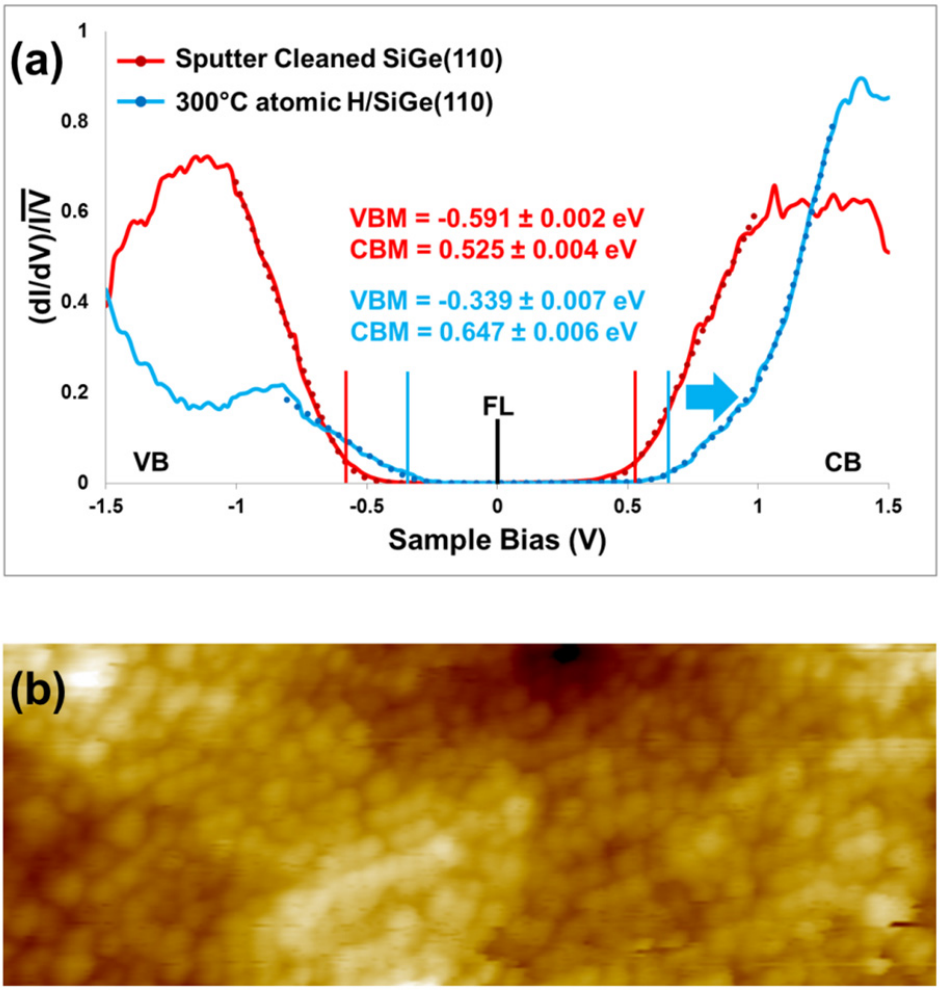

Figure 3.2 STS and STM of 3,600 L of atomic H dosed p-type SiGe(110) surface (a) STS measurements of the p-type SiGe(110) surface before and after an atomic H dose at 300°C. The Fermi level (FL) of the clean SiGe(110) surface (red curve) is pinned near the mid-gap, while the Fermi level of the atomic H dosed SiGe(110) surface (blue curve) is shifted towards the valence band edge, consistent with unpinning. Each STS curve is fit in order to determine the band gaps and Fermi level positions. The range of fitting is -1 to 1V for sputter cleaned SiGe(110) surface and is -0.8 to 1.3 V for 300°C atomic H/SiGe(110) surface. (b) Filled state STM image (40 × 15 nm^2, V_s = –1.8 V, I_t = 200 pA) after an atomic H dose on a clean SiGe(110) surface. The atomic H produces a well-ordered surface structure and no etch pits are observed.

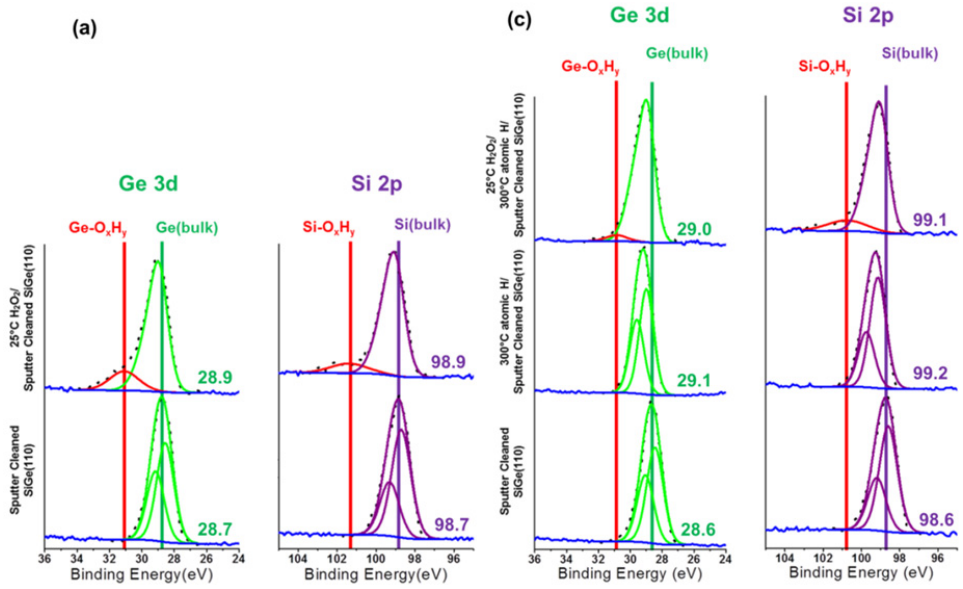

(b)

	GeO$_x$/Ge	SiO$_x$/Si
25°C H$_2$O$_2$/ Sputter Cleaned SiGe(110)	0.15±0.02	0.12±0.01
Sputter Cleaned SiGe(110)	0	0

(d)

	GeO$_x$/Ge	SiO$_x$/Si
25°C H$_2$O$_2$/300°C atomic H/ Sputter Cleaned SiGe(110)	0.03±0.01	0.13±0.01
300°C atomic H/ Sputter Cleaned SiGe(110)	0	0
Sputter Cleaned SiGe(110)	0	0

Figure 3.3 Ge 3d and Si 2p peaks of H_2O_2/SiGe(110) surface with and without an atomic H dose (a) Sputter-cleaned and 500°C-annealed SiGe(110) Ge 3d and Si 2p peaks are composed of sharp and asymmetric bulk components with resolved spin-orbital components consistent with a clean surface without contaminants. When 1.5 × 10^6 L of H_2O_2(g)/H_2O(g) containing a maximum of 40,000 L H_2O_2(g) was dosed at 25°C, XPS data without an atomic H dose showed Ge 3d and Si 2p peaks with shoulder peaks at higher binding energies, corresponding to Ge-O_xH_y and Si-O_xH_y components. (b) The table shows GeO_x/Ge and SiO_x/Si ratios on clean and 25°C H_2O_2(g)/SiGe(110) surfaces. Similar ratios after H_2O_2(g) dosing verify the coexistence of Si and Ge atoms on SiGe(110) surface. (c) XPS data after an atomic H dose at 300°C show the change in the spectra in the Ge 3d and Si 2p peaks. After 3,600 L of an atomic H dose at 300°C, when H_2O_2(g) was dosed at 25°C, the surface was largely composed of Si-O_xH_y bonds, indicating a partial Si segregation to the SiGe(110) surface from the atomic H dose at 300°C. The numerical values in the XPS spectra belong to the peak positions with an error rage of ±0.1 eV. (d) Table shows GeO_x/Ge and SiO_x/Si ratios after 300°C atomic H. The higher ratio of SiO_x/Si verifies a partial Si segregation to the SiGe(110) surface. All errors are standard errors.

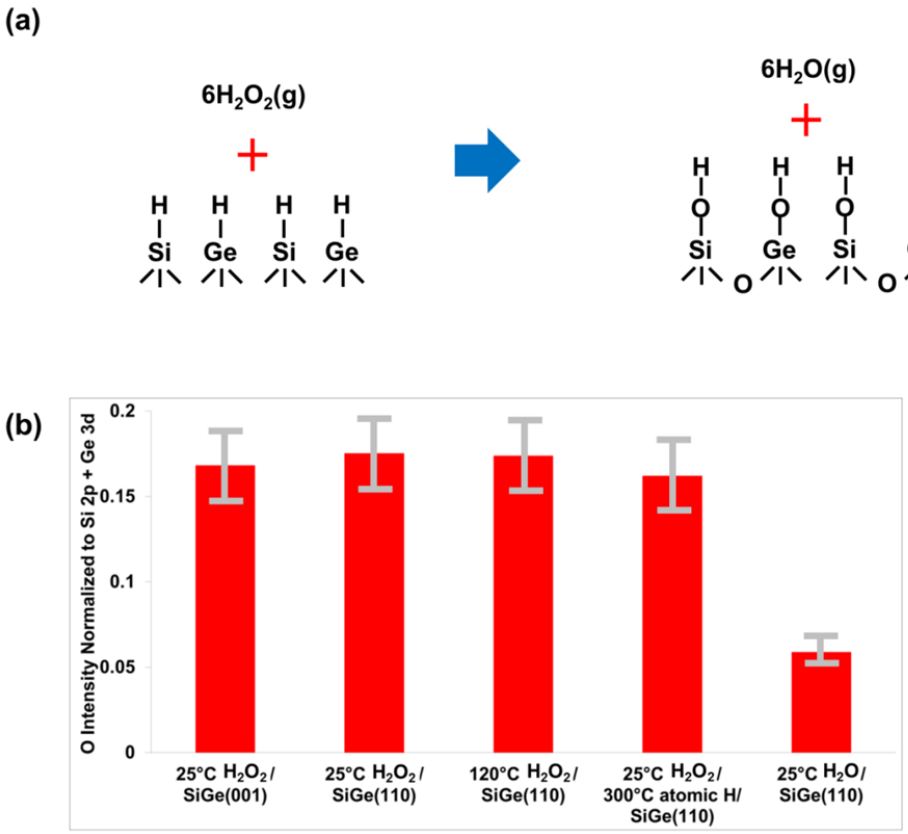

Figure 3.4 Proposed model and XPS analysis of H_2O_2 dosed SiGe(001) and (110) surfaces (a) Proposed dissociative chemisorption model of a 25°C H_2O_2 dose on 300°C atomic H/SiGe(110) surface. H_2O_2(g) molecules dissociatively chemisorb onto hydrogens on SiGe(110) surface, forming surface hydroxyls and oxygen backbond insertion sites, and H_2O(g) desorbs as a byproduct. (b) Intensities of O are normalized to Si 2p + Ge 3d peaks. After 25 and 120°C H_2O_2(g) doses on clean SiGe(001), (110), and 300°C atomic H/SiGe(110) surfaces, the normalized intensities of O are almost the same within the error ranges, and greater than the intensity for 25°C H_2O(g)/SiGe(110) surface. All errors are standard errors.

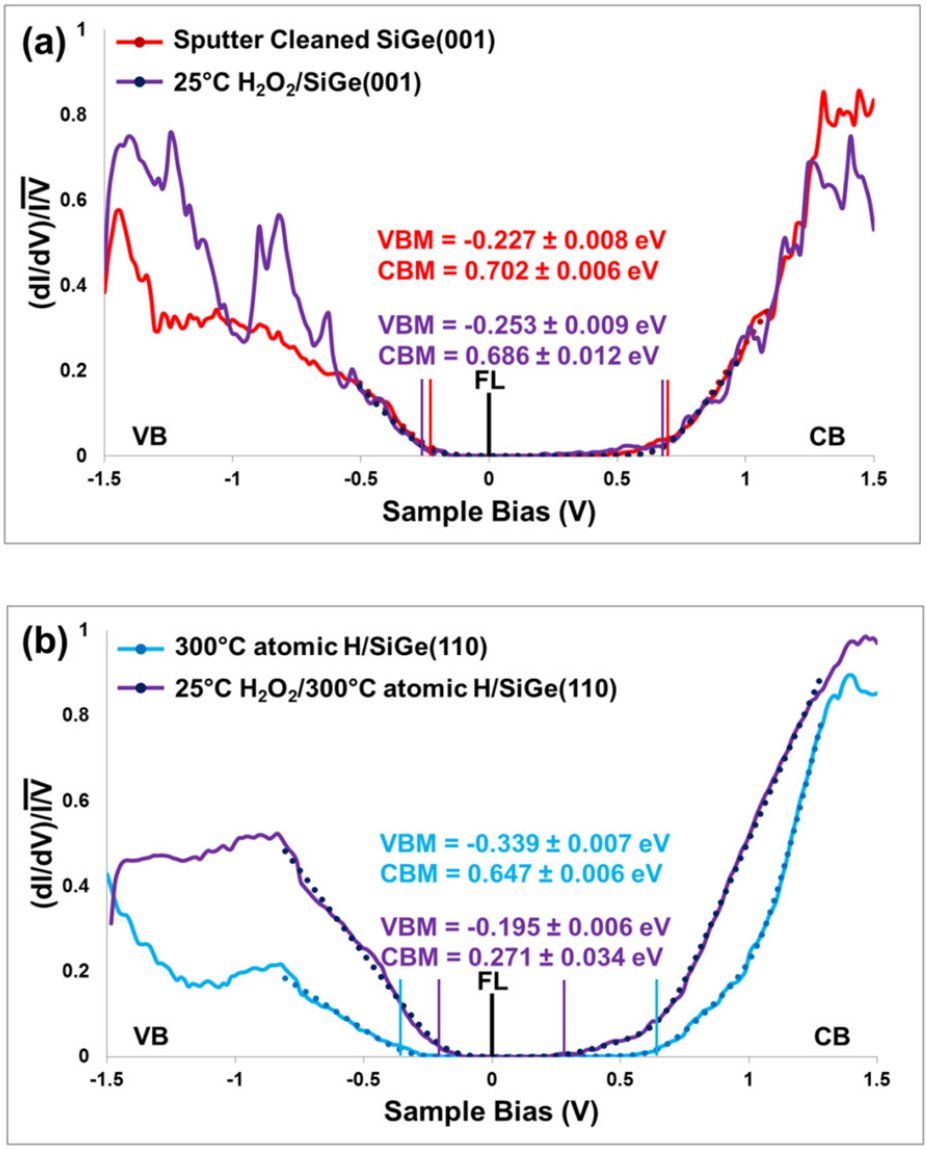

Figure 3.5 STS measurements of H_2O_2 dosed p-type SiGe(001) and (110) surfaces (a) STS measurements of the SiGe(001) surface before and after a H_2O_2 dose at 25°C. The sputter-cleaned surface (red curve) is almost identical to the H_2O_2 dosed surface (purple curve). The range of fitting is -0.5 to 1.1V for sputter cleaned SiGe(001) surface and is -0.5 to 1 V for 25°C H_2O_2/SiGe(110) surface. (b) STS measurements of the 300°C Atomic H/SiGe(110) surface before and after a H_2O_2 dose at 25°C. Each STS curve is fit in order to determine the band gaps and Fermi level positions. The range of fitting is -0.8 to 1.3V for 300°C atomic H/SiGe(110) surface and is -0.8 to 1.3 V for 25°C H_2O_2/300°C atomic H/SiGe(110) surface.

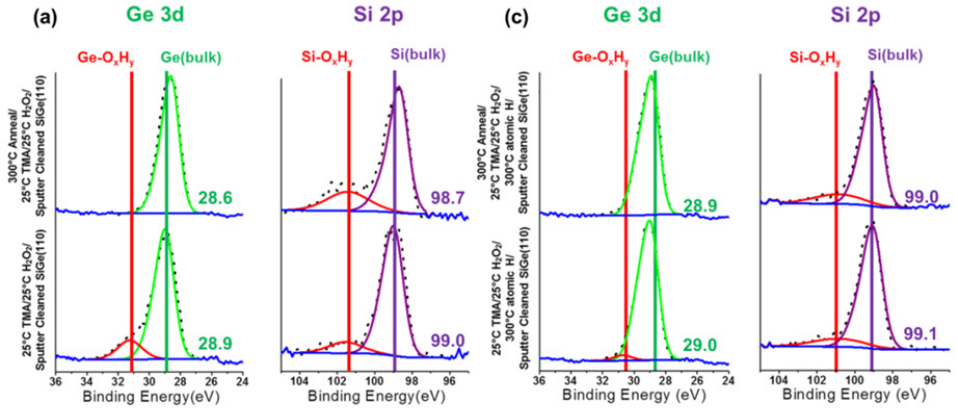

(b)

	GeO_x/Ge	SiO_x/Si
300°C Anneal/ 25°C TMA/25°C H_2O_2/ Sputter Cleaned SiGe(110)	0	0.21±0.03
25°C TMA/25°C H_2O_2/ Sputter Cleaned SiGe(110)	0.15±0.02	0.12±0.01

(d)

	GeO_x/Ge	SiO_x/Si
300°C Anneal/ 25°C TMA/25°C H_2O_2/ 300°C atomic H/ Sputter Cleaned SiGe(110)	0	0.16±0.02
25°C TMA/25°C H_2O_2/ 300°C atomic H/ Sputter Cleaned SiGe(110)	0.03±0.01	0.13±0.01

Figure 3.6 Ge 3d and Si 2p peaks of TMA dosed SiGe(110) surface with and without an atomic H dose (a) After a 25°C TMA dose on the 25°C H_2O_2/SiGe(110) surface, the Ge 3d and Si 2p peaks contain shoulder peaks corresponding to Al-O-Ge and Al-O-Si bonds. Annealing at 300°C eliminates Al-O-Ge bonds and increases Al-O-Si bonds. (b) Table shows GeO_x/Ge and SiO_x/Si ratios without atomic H precleaning. Similar ratios verify the coexistence of Si and Ge atoms on the SiGe(110) surface prior to a H_2O_2 dose. Full Si termination requires H_2O_2 dose and annealing. (c) After a 25°C TMA dose on 25°C H_2O_2/300°C atomic H/SiGe(110) surface, the surface is mainly composed of Al-O-Si bonds. After annealing at 300°C, the surface is completely terminated with Al-O-Si bonds. The numerical values in XPS spectra are the peak positions with an error range of ±0.1 eV. (d) Table shows GeO_x/Ge and SiO_x/Si ratios with 300°C atomic H. The higher ratio of SiO_x/Si verifies a partial Si segregation to the SiGe(110) surface after an atomic H dose. Full Si termination requires an H_2O_2 dose and annealing. All errors are standard errors.

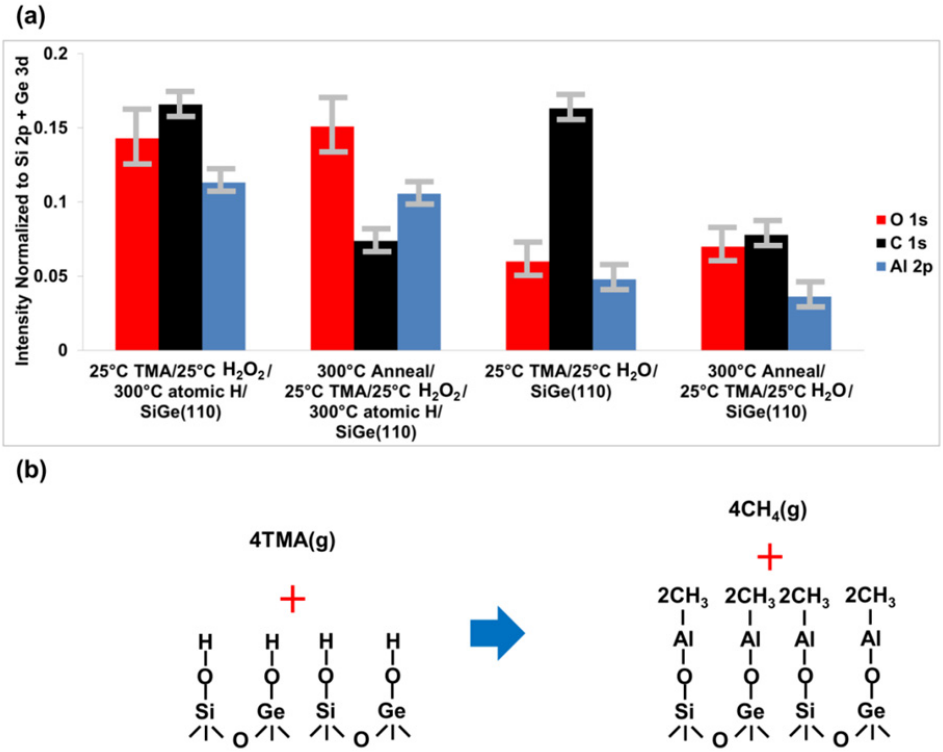

Figure 3.7 XPS analysis and proposed model of dissociation mechanism of a TMA dosed SiGe(110) surface (a) The intensities of O(red), C(black), and Al(blue) are normalized to Si 2p + Ge 3d peaks. After a TMA dose at 25°C, the ratio between Al and O is 2 : 3, consistent with a stoichiometric monolayer of Al_2O_3. After annealing at 300°C, the ratio between Al and O is nearly constant, consistent with thermal stability. The Al intensities after a 25°C H_2O_2(g) dose are 3 times greater than for a 25°C H_2O(g) dose, which is consistent with a nucleation density that is 3 times as great. All errors are standard errors. (b) Proposed dissociative chemisorption model of 25°C TMA dose on 25°C H_2O_2/300°C Atomic H/SiGe(110) surface. TMA molecules dissociatively chemisorb onto hydroxyls on the SiGe(110) surface, with oxygen backbond insertion and methanes desorb as byproducts.

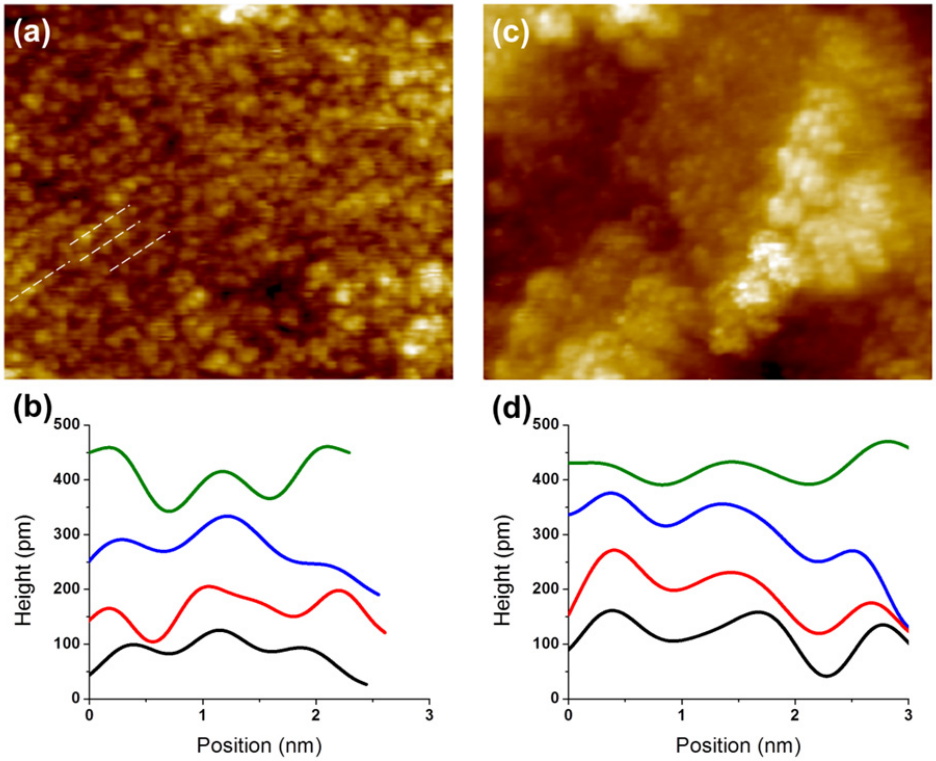

Figure 3.8 STM image and line trace of TMA dosed SiGe(001) and (110) surfaces (a) Filled state STM image (30 × 25 nm^2, V_s = –1.8 V, I_t = 200 pA) after a 25°C TMA dose on 25°C H_2O_2/SiGe(001) surface followed by 300°C annealing. (b) Line trace of four different areas on STM image in (a). The average row spacing is 9.0 Å with a standard error of 0.40 Å. (c) STM image (30 × 25 nm^2, V_s = –1.8 V, I_t = 200 pA) after a 25°C TMA dose on 25°C H_2O_2/atomic H/SiGe(110) surface, followed by 300°C annealing. (d) Line trace of four different areas on STM image in (c). The average row spacing is 11.8 Å with a standard error of 0.44 Å.

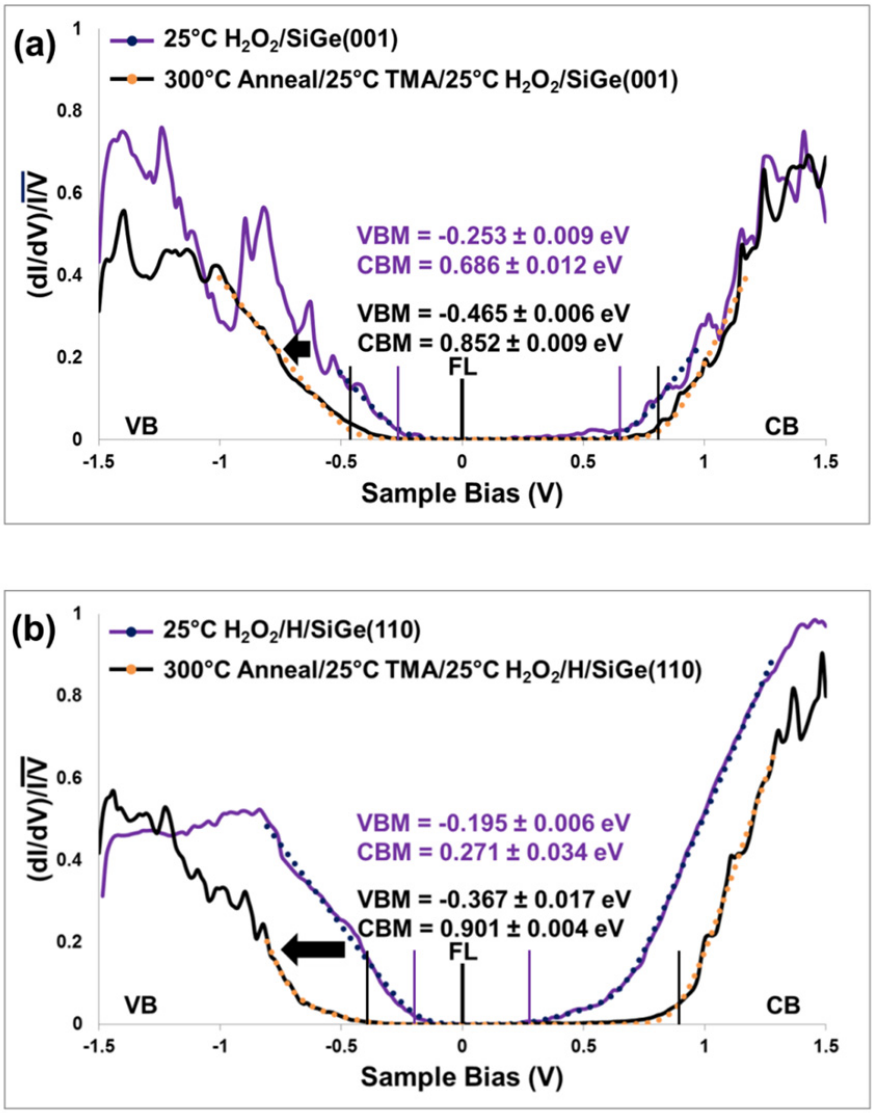

Figure 3.9 STS measurements of TMA dosed p-type SiGe(001) and (110) surfaces (a) The p-type SiGe(001) surface is unpinned after a 25°C TMA dose on 25°C H_2O_2/SiGe(001), followed by 300°C annealing. The black arrow indicates an enlarged band gap due to the formation of Al2O3. The range of fitting is -0.5 to 1 V for 25°C H_2O_2/SiGe(001) surface and is -1 to 1.2 V for 300°C Anneal/25°C TMA/25°C H_2O_2/SiGe(001) surface. (b) The p-type SiGe(110) surface is unpinned after a 25°C TMA dose on 25°C H_2O_2/300°C atomic H/SiGe(110) followed by 300°C annealing. After a TMA dose, the band gap increases and the Fermi level moves toward mid-gap, consistent with the Si-O-Al bonding having smaller dipoles than the Si-OH bonding. Each STS curve is fit in order to determine the band gaps and Fermi level positions. The range of fitting is -0.8 to 1.3V for 25°C H_2O_2/300°C atomic H/SiGe(110) surface and is -0.8 to 1.3 V for 300°C Anneal/25°C TMA/25°C H_2O_2/300°C atomic H/SiGe(110) surface.

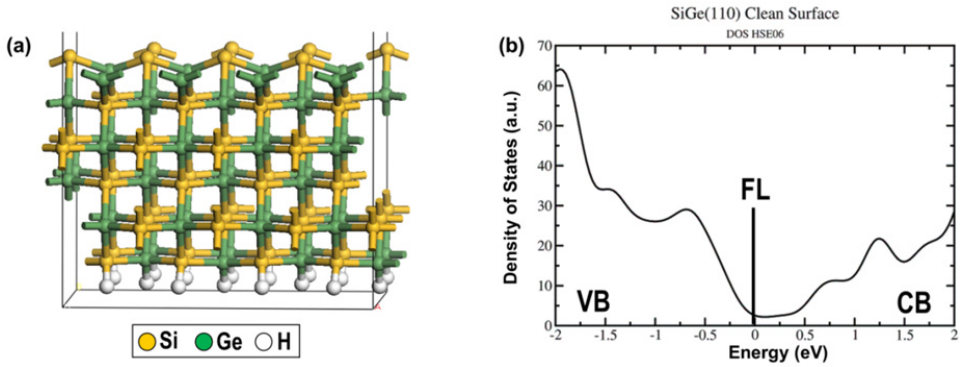

Figure 3.10 DFT Model and HSE06 DOS of a clean SiGe(110) surface (a) The clean SiGe(110) surface is terminated with Si and Ge atoms. Si-yellow, Ge-green, and H-white. (b) The DOS shows states in the band gap, and the clean SiGe(110) surface is pinned.

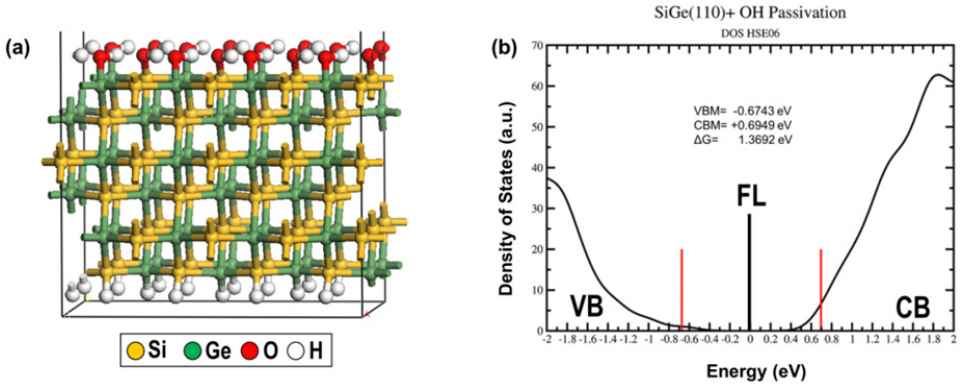

Figure 3.11 DFT Model and HSE06 DOS of H_2O_2 dosed SiGe (110) surface (a) The SiGe(110) surface is terminated with hydroxyls on both Si and Ge atoms after a H_2O_2(g) dose. Si-yellow, Ge-green, O-red, and H- white. (b) The DOS shows the elimination of states in the band gap after the passivation by hydroxyls via a H_2O_2(g) dose.

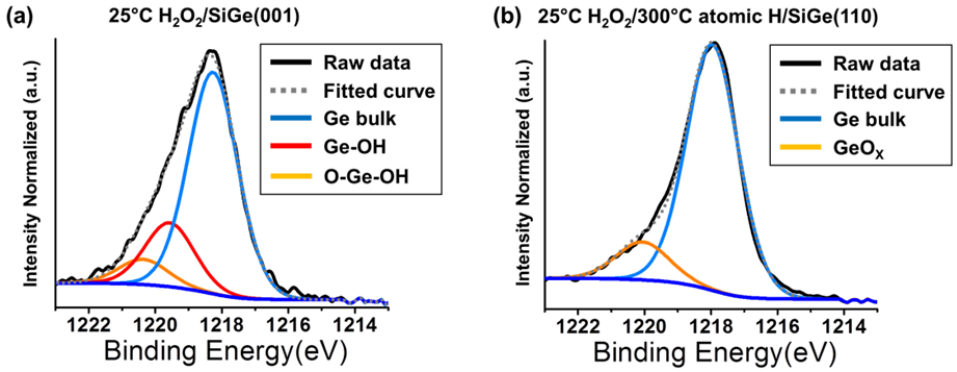

Figure 3.12 Ge 2p peaks of 25°C H_2O_2/SiGe(001) and 25°C H_2O_2/300°C atomic H/SiGe(110) (a) After a 25°C H_2O_2 dose on the SiGe(001) surface, the Ge 2p peak shows the formation of HO-Ge-Ge-OH (red peak) and HO-Ge-O-Ge-OH (yellow peak) components. The ratio of Ge bulk : HO-Ge-Ge-OH : HO-Ge-O-Ge-OH is 8.8 : 2.5 : 1 (b) After a 25°C H_2O_2 dose on a 300°C atomic H/SiGe(110) surface, the Ge 2p peak has a component of GeO_X (yellow peak), including Ge-OH and X-O-Ge-OH bonding configurations. The ratio of Ge bulk : GeO_X is 6.3 : 1.

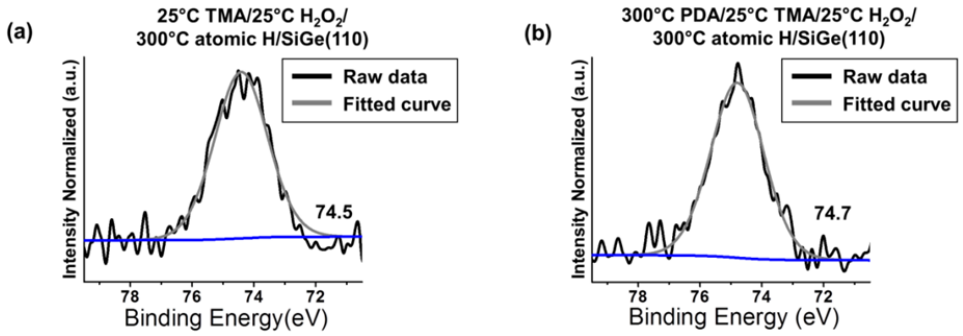

Figure 3.13 Al 2p peaks of 25°C TMA/25°C H_2O_2/300°C Atomic H/SiGe(110) and 300°C PDA/25°C H_2O_2/300°C Atomic H/SiGe(110) (a) After a 25°C TMA dose on the 25°C H_2O_2/300°C atomic H/SiGe(110) surface, the Al 2p peak is positioned at 74.5eV, corresponding to a monolayer of Al_2O_3. (b) After 300°C PDA on the 25°C TMA/25°C H_2O_2/300°C atomic H/SiGe(110) surface, the Al 2p peak is positioned at 74.7eV, consistent with a thermally stable monolayer of Al_2O_3.

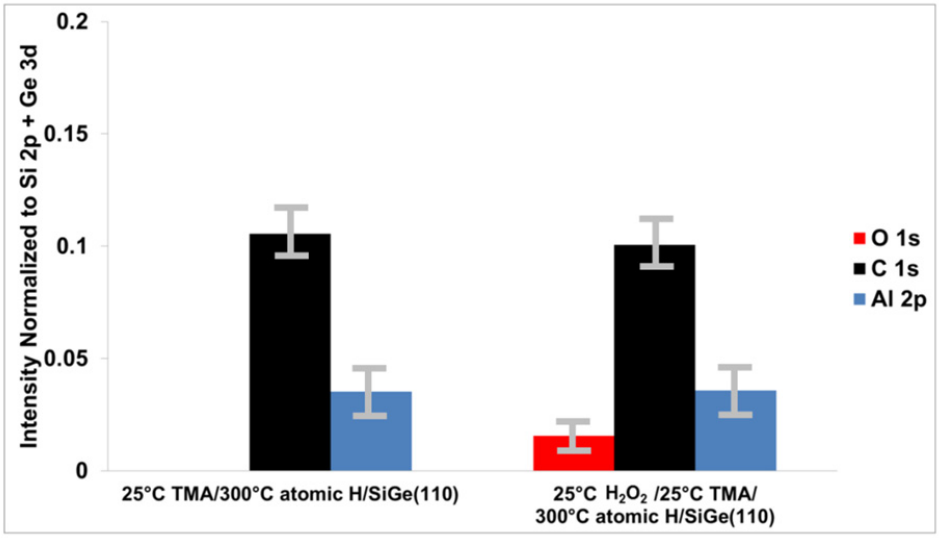

Figure 3.14 XPS analysis of TMA and H_2O_2 dosed SiGe(110) (a) After a 25°C TMA dose on the 300°C atomic H/SiGe(110) surface, the Al : C ratio is approximately 1 : 3 consistent with a dissociative chemisorption of TMA, resulting in the adsorption of alkyl groups. (b) After a 25°C H_2O_2 dose on the 25°C TMA/300°C atomic H/SiGe(110) surface, the Al : C ratio is almost constant and the O ratio is less than 2%, demonstrating that the methyl-terminated SiGe(110) surface is stable upon H_2O_2 exposure.

3.8 References

[1] H. Xuejue, L. Wen-Chin, K. Charles, D. Hisamoto, C. Leland, J. Kedzierski, E. Anderson, H. Takeuchi, C. Yang-Kyu, K. Asano, V. Subramanian, K. Tsu-Jae, J. Bokor, and H. Chenming, in *Sub 50-nm FinFET: PMOS*, 1999, p. 67.

[2] D. Hisamoto, L. Wen-Chin, J. Kedzierski, H. Takeuchi, K. Asano, C. Kuo, E. Anderson, K. Tsu-Jae, J. Bokor, and H. Chenming, Electron Devices, IEEE Transactions on **47,** 2320 (2000).

[3] H. Xuejue, L. Wen-Chin, C. Kuo, D. Hisamoto, L. Chang, J. Kedzierski, E. Anderson, H. Takeuchi, Y.-K. Choi, K. Asano, V. Subramanian, K. Tsu-Jae, J. Bokor, and H. Chenming, Electron Devices, IEEE Transactions on **48,** 880 (2001).

[4] Y. Bin, L. Chang, S. Ahmed, W. Haihong, S. Bell, Y. Chih-Yuh, C. Tabery, H. Chau, X. Qi, K. Tsu-Jae, J. Bokor, H. Chenming, L. Ming-Ren, and D. Kyser, in *FinFET scaling to 10 nm gate length*, 2002, p. 251.

[5] S. Datta, G. Dewey, M. Doczy, B. S. Doyle, B. Jin, J. Kavalieros, R. Kotlyar, M. Metz, N. Zelick, and R. Chau, 2003 Ieee International Electron Devices Meeting, Technical Digest**,** 653 (2003).

[6] S. Datta, J. Brask, G. Dewey, M. Doczy, B. Doyle, B. Jin, J. Kavalieros, M. Metz, A. Majumdar, M. Radosavljevic, and R. Chau, Proceeding of the 2004 Bipolar/Bicmos Circuits and Technology Meeting**,** 194 (2004).

[7] T. Ghani, M. Armstrong, C. Auth, M. Bost, P. Charvat, G. Glass, T. Hoffmann, K. Johnson, C. Kenyon, J. Klaus, B. McIntyre, K. Mistry, A. Murthy, J. Sandford, M. Silberstein, S. Sivakumar, P. Smith, K. Zawadzki, S. Thompson, and M. Bohr, in *A 90nm high volume manufacturing logic technology featuring novel 45nm gate length strained silicon CMOS transistors*, 2003, p. 11.6.1.

[8] T. Mizuno, S. Takagi, N. Sugiyama, H. Satake, A. Kurobe, and A. Toriumi, Ieee Electron Device Letters **21,** 230 (2000).

[9] T. Mizuno, N. Sugiyama, H. Satake, and S. Takagi, 2000 Symposium on Vlsi Technology, Digest of Technical Papers**,** 210 (2000).

[10] M. L. Lee, C. W. Leitz, Z. Cheng, A. J. Pitera, T. Langdo, M. T. Currie, G. Taraschi, E. A. Fitzgerald, and D. A. Antoniadis, Applied Physics Letters **79,** 3344 (2001).

[11] K. J. Kuhn, A. Murthy, R. Kotlyar, and M. Kuhn, Sige, Ge, and Related Compounds 4: Materials, Processing, and Devices **33,** 3 (2010).

[12] M. Caymax, F. Leys, J. Mitard, K. Martens, L. J. Yang, G. Pourtois, W. Vandervorst, M. Meuris, and R. Loo, Journal of the Electrochemical Society **156,** H979 (2009).

[13] T. Kaufman-Osborn, E. A. Chagarov, S. W. Park, B. Sahu, S. Siddiqui, and A. C. Kummel, Surface Science **630,** 273 (2014).

[14] D. Kuzum, T. Krishnamohan, A. J. Pethe, A. K. Okyay, Y. Oshima, Y. Sun, J. P. McVittie, P. A. Pianetta, P. C. McIntyre, and K. C. Saraswat, Electron Device Letters, IEEE **29,** 328 (2008).

[15] J. S. Lee, T. Kaufman-Osborn, W. Melitz, S. Lee, and A. Kummel, Surface Science **605,** 1583 (2011).

[16] T. Kaufman-Osborn, E. A. Chagarov, and A. C. Kummel, Journal of Chemical Physics **140** (2014).

[17] H. Takeuchi, T. Matsuura, and J. Murota, Applied Physics Letters **77,** 1828 (2000).

[18] Y. Zhang, G. S. Oehrlein, E. de Frésart, and J. W. Corbett, Journal of Applied Physics **71,** 1936 (1992).

[19] T. D. Bestwick, G. S. Oehrlein, Y. Zhang, G. M. W. Kroesen, and E. de Frésart, Applied Physics Letters **59,** 336 (1991).

[20] G. S. Oehrlein, G. M. W. Kroesen, E. de Frésart, Y. Zhang, and T. D. Bestwick, Journal of Vacuum Science & Technology A **9,** 768 (1991).

[21] E. Rudkevich, F. Liu, D. E. Savage, T. F. Kuech, L. McCaughan, and M. G. Lagally, Physical Review Letters **81,** 3467 (1998).

[22] K. Nakagawa, A. Nishida, Y. Kimura, and T. Shimada, Japanese Journal of Applied Physics Part 2-Letters **33,** L1331 (1994).

[23] M. Copel and R. M. Tromp, Applied Physics Letters **58,** 2648 (1991).

[24] D. A. Grutzmacher, T. O. Sedgwick, A. Powell, M. Tejwani, S. S. Iyer, J. Cotte, and F. Cardone, Applied Physics Letters **63,** 2531 (1993).

[25] Y. J. Zheng, P. F. Ma, and J. R. Engstrom, Journal of Applied Physics **90,** 3614 (2001).

[26] J. Y. Lee, S. J. Jung, J. Y. Maeng, Y. E. Cho, S. Kim, and S. K. Jo, Applied Physics Letters **84,** 5028 (2004).

[27] A. P. Webb and S. Vepřek, Chemical Physics Letters **62,** 173 (1979).

[28] A. Stesmans, Applied Physics Letters **68,** 2076 (1996).

[29] M. L. Reed and J. D. Plummer, Journal of Applied Physics **63,** 5776 (1988).

[30] K. L. Brower, Applied Physics Letters **53,** 508 (1988).

[31] K. L. Brower, Physical Review B **38,** 9657 (1988).

[32] S. L. Manatt and M. R. R. Manatt, Chemistry – A European Journal **10,** 6540 (2004).

[33] R. M. Feenstra, J. A. Stroscio, and A. P. Fein, Surface Science **181,** 295 (1987).

[34] R. M. Feenstra, Surface Science **299–300,** 965 (1994).

[35] R. M. Feenstra, J. Y. Lee, M. H. Kang, G. Meyer, and K. H. Rieder, Physical Review B **73,** 035310 (2006).

[36] R. M. Feenstra, Physical Review B **50,** 4561 (1994).

[37] G. Kresse and J. Hafner, Physical Review B **47,** 558 (1993).

[38] G. Kresse and J. Hafner, Physical Review B **49,** 14251 (1994).

[39] G. Kresse and J. Furthmüller, Computational Materials Science **6,** 15 (1996).

[40] G. Kresse and J. Furthmuller, Phys Rev B Condens Matter **54,** 11169 (1996).

[41] P. E. Blochl, Phys Rev B Condens Matter **50,** 17953 (1994).

[42] G. Kresse and D. Joubert, Physical Review B **59,** 1758 (1999).

[43] J. P. Perdew, K. Burke, and M. Ernzerhof, Physical Review Letters **77,** 3865 (1996).

[44] J. Heyd, G. E. Scuseria, and M. Ernzerhof, The Journal of Chemical Physics **118,** 8207 (2003).

[45] J. Heyd and G. E. Scuseria, The Journal of Chemical Physics **121,** 1187 (2004).

[46] J. Heyd, G. E. Scuseria, and M. Ernzerhof, The Journal of Chemical Physics **124,** 219906 (2006).

[47] A. V. Krukau, O. A. Vydrov, A. F. Izmaylov, and G. E. Scuseria, The Journal of Chemical Physics **125,** 224106 (2006).

[48] D. J. Godbey and M. G. Ancona, Applied Physics Letters **61,** 2217 (1992).

[49] D. J. Godbey and M. G. Ancona, Journal of Vacuum Science & Technology B **11,** 1392 (1993).

[50] G. G. Jernigan, P. E. Thompson, and C. L. Silvestre, Surface Science **380,** 417 (1997).

[51] N. Takeuchi, Surface Science **494,** 21 (2001).

[52] A. A. Stekolnikov, J. Furthmuller, and F. Bechstedt, Physical Review B **70** (2004).

[53] A. J. Mayne, A. R. Avery, J. Knall, T. S. Jones, G. A. D. Briggs, and W. H. Weinberg, Surface Science **284,** 247 (1993).

[54] C. C. Hobbs, L. R. C. Fonseca, A. Knizhnik, V. Dhandapani, S. B. Samavedam, W. J. Taylor, J. M. Grant, L. G. Dip, D. H. Triyoso, R. I. Hegde, D. C. Gilmer, R. Garcia, D. Roan, M. L. Lovejoy, R. S. Rai, E. A. Hebert, T. Hsing-Huang, S. G. H. Anderson, B. E. White, and P. J. Tobin, Electron Devices, IEEE Transactions on **51,** 978 (2004).

[55] P. D. Kirsch, C. S. Kang, J. Lozano, J. C. Lee, and J. G. Ekerdt, Journal of Applied Physics **91,** 4353 (2002).

[56] M. Edmonds, T. Kent, E. Chagarov, K. Sardashti, R. Droopad, M. Chang, J. Kachian, J. H. Park, and A. Kummel, Journal of the American Chemical Society (2015).

[57] Y. Sun, Z. Liu, S. Y. Sun, and P. Pianetta, Journal of Vacuum Science & Technology A **26,** 1248 (2008).

[58] Y.-R. Luo, *Comprehensive handbook of chemical bond energies* (CRC press, 2007).

[59] F. Bensliman, Y. Sawada, K. Tsujino, and M. Matsumura, Journal of the Electrochemical Society **154,** F102 (2007).

[60] W. C. O'Mara, R. B. Herring, and L. P. Hunt, in *Materials science and process technology series* (Noyes Publications,, Park Ridge, N.J., 1990), p. xx.

[61] J. H. Scofield, Journal of Electron Spectroscopy and Related Phenomena **8,** 129 (1976).

[62] M. P. Seah and W. A. Dench, Surface and Interface Analysis **1,** 2 (1979).

[63] T. J. Grassman, S. R. Bishop, and A. C. Kummel, Surface Science **602,** 2373 (2008).

[64] K. Onishi, C. S. Kang, R. Choi, H.-J. Cho, S. Gopalan, R. E. Nieh, S. A. Krishnan, and J. C. Lee, Electron Devices, IEEE Transactions on **50,** 384 (2003).

[65] M. R. Linford, P. Fenter, P. M. Eisenberger, and C. E. D. Chidsey, Journal of the American Chemical Society **117,** 3145 (1995).

Chapter 4

Formation of atomically ordered and chemically selective Si-O-Ti monolayer on $Si_{0.5}Ge_{0.5}$(110) for a MIS structure via H_2O_2(g) functionalization

4.1 Abstract

$Si_{0.5}Ge_{0.5}$(110) surfaces were passivated and functionalized using atomic H, hydrogen peroxide (H_2O_2), and either tetrakis(dimethylamino)titanium (TDMAT) or titanium tetrachloride ($TiCl_4$), and studied *in-situ* with multiple spectroscopic techniques. To passivate the dangling bonds, atomic H and H_2O_2(g) were utilized and scanning tunneling spectroscopy (STS) demonstrated unpinning of the surface Fermi level. The H_2O_2(g) could also be used to functionalize the surface for metal atomic layer deposition (ALD). After subsequent TDMAT or $TiCl_4$ dosing followed by a post deposition annealing (PDA), scanning tunneling microscopy (STM) demonstrated that a thermally stable and well-ordered monolayer of TiO_x was deposited on $Si_{0.5}Ge_{0.5}$(110) and X-ray photoelectron spectroscopy (XPS) verified the interfaces only contained Si-O-Ti bonds and a complete absence of GeO_x. STS measurements confirmed a TiO_x monolayer without mid-gap and conduction band (CB) edge states, which should be an ideal ultrathin insulating layer in a metal-insulator-semiconductor (MIS) structure. Regardless of the Ti precursors, the final Ti density and electronic structure were identical since the Ti bonding is limited by the high coordination of Ti to O.

4.2 Introduction

As the size of Si-based complimentary metal-oxide semiconductor (CMOS) devices decreases, new materials have been developed to enhance device performance. Silicon-germanium (SiGe) has received much attention due to its applications in strain engineering and higher mobility [1-3]. The larger lattice constant of SiGe has been utilized in n-type MOS transistors to improve electron mobility by applying a biaxial tensile stress into Si channels [4,5]. Alternatively, when SiGe materials were employed in the source or drain areas, a compressive stress was utilized for the enhancement of hole mobility in p-type MOS transistors [6,7]. Furthermore, due to the higher mobility of SiGe compared to silicon, SiGe has been employed as a channel material in p-type MOS transistors [8]. However, to utilize SiGe in the source and drain in very large scale integrated (VLSI) technology, source/drain resistance must be minimized [9].

While few studies have looked at passivation of SiGe as a contact material, many studies have reported passivation of SiGe and Ge as channel materials. Extensive studies have been reported to passivate the channel surfaces with low interface state density (D_{it}) and unpinned Fermi level. Passivation of Ge via ozone oxidation below 400°C resulted in low D_{it} by suppressing the formation of Ge suboxide in favor of GeO_2 [10]. Lee et al. [11] demonstrated that water (H_2O) was effective in passivating Ge(001) surfaces as verified by scanning tunneling microscopy (STM) and scanning tunneling spectroscopy (STS) measurements. Recent studies verified that hydrogen peroxide vapor ($H_2O_2(g)$) formed a more stable passivation layer and a higher nucleation density for atomic layer deposition (ALD) than $H_2O(g)$ on Ge(001)

[12], SiGe(001) [13], and SiGe(110) [14] surfaces thereby improving the formation of high-k dielectrics.

Extremely thin insulator interfaces have been used to form unpinned contacts on Ge and SiGe substrates. Kobayashi et al. [15] deposited an ultrathin tunnel barrier of Si_3N_4 between the contact metal and a Ge substrate to form a metal-insulator-semiconductor (MIS) structure. However, the insulating layer of Si_3N_4 introduced a large tunneling resistance due to the significant conduction band offset (CBO) to the Ge substrate. Lieten et al. [16] formed a thin Ge_3N_4 layer on Ge substrates for ohmic contacts, and this layer passivated Ge surface states. Lin et al. [17] employed 7.1 nm-thick TiO_2 interfacial layer in a MIS structure to reduce the tunneling resistance by having nearly zero CBO. The TiO_2 films deposited on SiGe(001) for MIS capacitors minimized D_{it} as demonstrated by capacitance-voltage and conductance-voltage measurements [18].

In this report, the topological, electronic, and chemical properties of $Si_{0.5}Ge_{0.5}$(110) were studied for application as a MIS structure. Exposure of atomic H or H_2O_2(g) passivated the dangling bonds on sputter-cleaned $Si_{0.5}Ge_{0.5}$(110) with hydrogen atoms or hydroxyl groups resulting in an unpinned Fermi level. H_2O_2(g) also was utilized to form a high density of OH sites which is advantageous for the formation of a high density ultrathin insulating layer in a MIS structure. Subsequent tetrakis(dimethylamino)titanium (TDMAT) or titanium tetrachloride ($TiCl_4$) dosing via ALD functionalized the hydroxyl-terminated $Si_{0.5}Ge_{0.5}$(110) with Ti atoms, thereby forming a monolayer of TiO_x on $Si_{0.5}Ge_{0.5}$(110) surfaces. Annealing studies

demonstrated the thermal and electronic stability of a TiO_x monolayer on $Si_{0.5}Ge_{0.5}$(110) surfaces and the complete absence of GeO_x at the interface; instead the interface was composed solely of Si-O-Ti bonds. Each experimental process was probed using *in-situ* STM, STS, and X-ray photoelectron spectroscopy (XPS).

4.3 Methods

P-type $Si_{0.5}Ge_{0.5}$(110) films with 10^{15} cm^{-3} B doping grown on Si(110) wafers were provided by GLOBALFOUNDRIES and diced into 10.5 × 5.5 mm^2 pieces. Each sample was repeatedly cleaned via a degreasing method using acetone, methanol, and deionized water then dried with N_2 gas. Samples were loaded into a customized Omicron ultra-high vacuum (UHV) preparation chamber with a base pressure of 1×10^{-10} Torr, and prepared by combined sputtering and annealing processes. The sputtering process utilized a 1.5 kV argon ion (Ar^+) beam (Model 1403 ion gun, Nonsequitur Technologies) with a current of 0.9 μA and an Ar gas pressure of 6×10^{-7} Torr for 30 min, while the sample temperature was maintained at 500°C using resistive pyrolytic boron nitride (PBN) heating. An annealing process was performed at a sample temperature of 500°C for 30 min. After repeated sputter and annealing cycles, the chemical, topological, and electronic characteristics were studied via *in-situ* XPS, STM, and STS.

Sputter-cleaned $Si_{0.5}Ge_{0.5}$(110) samples were reacted with atomic hydrogen in the UHV preparation chamber using a thermal gas cracker (Atomic Hydrogen Source, Veeco). The gas pressure was controlled via a leak valve and measured with an ion

gauge; the exposure was calculated in terms of Langmuirs (1 Langmuir (L) = 1×10^{-6} Torr · 1 sec). During the atomic hydrogen dose, the temperature of filament was maintained between 1800 and 2200°C, while the temperature of $Si_{0.5}Ge_{0.5}(110)$ samples was maintained at 300°C; the cracking efficiency was expected to be 30%, but the reported amount of atomic H dose was estimated based solely on the H_2 pressure, so the actual amount of atomic H dose should be smaller compared to the reported value. During the experiment, H_2 was dosed at 1 x 10^{-5} Torr for 360 sec; this is reported below as 3,600 L of atomic H.

To avoid air exposure, samples were transferred to an *in-situ* ALD chamber with a base pressure of 1×10^{-7} Torr. $H_2O_2(g)$, TDMAT, and $TiCl_4$ were dosed at 25°C surface temperature by filling the dosing chamber at 25°C without a carrier gas. As a control experiment, $Si_{0.5}Ge_{0.5}(110)$ samples were also dosed with $H_2O(g)$ at 25°C. To achieve saturated nucleation on $Si_{0.5}Ge_{0.5}(110)$ surfaces, a 30% solution of $H_2O_2(aq)$ (Fisher Scientific), TDMAT (99%, Strem Chemicals), and $TiCl_4$ (99%, Strem Chemicals) were utilized. In this paper, the "$H_2O_2(g)$" refers to the mixture of $H_2O_2(g)/H_2O(g)$; the $H_2O_2(aq)$ solution was composed of both components and the H2O2(g) reaction should be dominant due to its high reactivity. Based on a previous report, a 30% solution of $H_2O_2(aq)$ resulted in a vapor of 2.67% $H_2O_2(g)$ at 25°C [19]; therefore, the actual amount of $H_2O_2(g)$ involved in the chemical reaction should be smaller than the reported amount of total vapor below. During the experiment, $H_2O_2(aq)$ was dosed at 30 mTorr for 150 sec to provide 4.5×10^6 L of total vapor from $H_2O_2(aq)$; the maximum amount of $H_2O_2(g)$ should be 120,000 L. Before the samples

were transferred to the ALD chamber, the chamber was baked overnight by heating the chamber walls to 120°C to minimize the background O and H_2O contaminations. In addition, several cycles of H_2O_2(g), TDMAT, and $TiCl_4$ were pre-dosed to minimize the chemical reaction with the stainless-steel chamber walls during the actual experiments.

Chemical properties from each experimental step were studied with an in-situ monochromatic XPS (XM 1000 MkII/SPHERA, Omicron Nanotechnology). For the XPS studies, an Al Kα source (1486.7 eV) was utilized as an anode material; spectra were measured with constant analyzer-energy (CAE) mode with a pass energy of 50 eV and a step width of 0.1 eV. The take-off angle between the analyzer axis and the sample normal was 60° and the analyzer-acceptance angle was 7°. For peak shape analysis, a CASA XPS v.2.3 program was utilized via a Shirley background subtraction.

The samples were transferred to an in-situ STM chamber (LT-STM, Omicron Nanotechnology) with a base pressure of 1×10^{-11} Torr to probe the topological and electronic properties on the $Si_{0.5}Ge_{0.5}$(110) surface after each experimental process. Constant-current mode (Isp = 200 pA) STM was performed with a sample bias between –2.0 and –1.8 V to obtain filled-state STM images. Variable-z mode STS was performed with a modulation signal (0.1 Vac, 650 Hz) through an external lock-in amplifier (SR830 DSP, Stanford Research Systems) to directly obtain the dI/dV along with the I/V spectra while varying the sample bias from –1.5 to +1.5 V and simultaneously moving the tip position forward then backward during the scan to

increase the sensitivity with regard to small currents [20,21]. As described in a previous report [14,22], the raw I/V data were smoothed through a low-pass filter with energy width of (3.0 eV)/2 (frequency parameter value in filter of $(3.0\ eV)^{-1}$). This smoothing step led to a broadened I/V, denoted as $\overline{I/V}$, which forms a suitable normalization quantity for dI/dV [22]. For the precise STS measurements, at least 5 individual spectra of $(dI/dV)/(\overline{I/V})$ were rescaled from 0 to 1 and subsequently averaged into a single spectrum in the STS figures. Since the $(dI/dV)/(\overline{I/V})$ spectrum have the property that band onsets have a linear dependence on the sample bias, they were fit with a linear function to extract the band edge energies [22]. Based on previous STS studies [22,23], a fitting method was performed to extract the band edge energies for the $(dI/dV)/(\overline{I/V})$ spectra using a linear function depending on both operational temperature and alternating current (AC) modulation. The calculated linear fits for each STS measurement were included as the solid lines and the onsets of the linear fits corresponding to the band edge energies were calculated with error ranges. The obtained error ranges from the fitting method were standard errors of the least-squares fits and did not reflect thermal broadening nor inaccuracies due to band edge states.

4.4 Results and Discussion

$Si_{0.5}Ge_{0.5}(110)$ surfaces were cleaned via repeated sputtering and annealing processes at 500°C and the cleanness of the surfaces were verified by an *in-situ* XPS showing no carbon and oxygen at the surfaces. As explained in the supplement, a sputter-cleaned $Si_{0.5}Ge_{0.5}(110)$ should be terminated with adatoms, which induce a

pinned Fermi level due to the half-filled dangling bonds. To form an unpinned Fermi level, 3,600 L of atomic H was dosed onto $Si_{0.5}Ge_{0.5}(110)$ while the substrate temperature was maintained at 300°C. Afterwards, sputter-cleaned or atomic H dosed $Si_{0.5}Ge_{0.5}(110)$ samples were transferred to an *in-situ* ALD chamber to functionalize the surfaces with hydroxyls. For the saturation reaction, 4.5×10^6 L of vapor from $H_2O_2(aq)$, which was composed of approximately 120,000 L $H_2O_2(g)$ and the balance $H_2O(g)$, was dosed onto the samples at 25°C and this amount was expected to be a saturation dose which would fully react with $Si_{0.5}Ge_{0.5}(110)$ surfaces.

To understand the surface reaction after atomic H or $H_2O_2(g)$ dosing of $Si_{0.5}Ge_{0.5}(110)$ surfaces, schematic models were proposed based on the XPS studies in the supplement. XPS data showed that a full saturation dose of $H_2O_2(g)$ at 25°C resulted in an O/(Si + Ge) ratio of 19 %, which corresponded to ~1.05 monolayers (see supplement Fig. 4.9). For a 25°C H_2O_2 dose on H-terminated $Si_{0.5}Ge_{0.5}(110)$, the O/(Si + Ge) ratio was identical to 25°C $H_2O_2/Si_{0.5}Ge_{0.5}(110)$ demonstrating a strong reactivity of 25°C $H_2O_2(g)$ on H-terminated $Si_{0.5}Ge_{0.5}(110)$ to replace H atoms with hydroxyls. In addition, the chemical shifts of Ge-O_xH_y and Si-O_xH_y on 25°C H_2O_2 /$Si_{0.5}Ge_{0.5}(110)$ and 25°C H_2O_2/300°C atomic H/$Si_{0.5}Ge_{0.5}(110)$ surfaces mainly corresponded to Ge^{2+} and Si^{2+} (see supplement Fig. 4.11). Fig. 4.1 presents schematic diagrams for 25°C $H_2O_2(g)$ reactions with clean or H-terminated $Si_{0.5}Ge_{0.5}(110)$ surfaces. As shown in Fig. 4.1(a), a saturation $H_2O_2(g)$ dose on a clean $Si_{0.5}Ge_{0.5}(110)$ surface, which was terminated with half-filled dangling bonds from adatoms, formed hydroxyls on dangling bonds along with oxygen inserted into adatom backbonds with

H_2(g) as a byproduct. Similarly, when a H-terminated $Si_{0.5}Ge_{0.5}$(110) surface was dosed with a saturation H_2O_2(g) at 25°C, H_2O_2(g) was sufficiently reactive to replace H atoms with hydroxyls on $Si_{0.5}Ge_{0.5}$(110) and to insert additional oxygen atoms into Si-Ge backbonds, producing H_2O(g) as a byproduct as shown in Fig. 4.1(b). In sum, when a clean or H-terminated $Si_{0.5}Ge_{0.5}$(110) surface was exposed to a saturation dose of H_2O_2(g) at 25°C, the top surface should be terminated with hydroxyls and additional oxygen atoms were likely to break the backbonds resulting in oxygen insertion consistent with the XPS intensities and chemical shifts corresponding to Ge^{2+} and Si^{2+} in the supplement.

The electronic properties of 25°C $H_2O_2/Si_{0.5}Ge_{0.5}$(110) and 25°C H_2O_2/300°C atomic $H/Si_{0.5}Ge_{0.5}$(110) surfaces were studied through STS measurements in Fig. 4.2. STS measurements of $(dI/dV)/(\overline{I/V})$ are known to be proportional to the local density of states (LDOS) [21,22]; therefore, STS measurements were performed to understand the electronic structures of the surfaces. STS spectra of 25°C $H_2O_2/Si_{0.5}Ge_{0.5}$(110) surface (black) demonstrated the nearly identical electronic structure to 25°C H_2O_2/300°C atomic $H/Si_{0.5}Ge_{0.5}$(110) surface (yellow) with ±0.1V difference with regard to valence band maximum (VBM) and conduction band minimum (CBM), respectively. While the clean p-type $Si_{0.5}Ge_{0.5}$(110) surface had a Fermi level pinned near mid-gap (as demonstrated in the supplement Fig. 4.8), the Fermi levels of 25°C $H_2O_2/Si_{0.5}Ge_{0.5}$(110) and 25°C H_2O_2/300°C atomic $H/Si_{0.5}Ge_{0.5}$(110) surfaces were positioned closer to the VB edge consistent with Fermi level unpinning. In addition, the bandgaps were decreased due to the increased density of states near VB and CB

edges. Based on STS analysis, it was demonstrated that a 25°C H_2O_2(g) dosing on clean or H terminated $Si_{0.5}Ge_{0.5}$(110) resulted in electronically identical surfaces.

To functionalize the surfaces with Ti atoms for the TiO_x formation, the 25°C H_2O_2/$Si_{0.5}Ge_{0.5}$(110) and 25°C H_2O_2/300°C atomic H/$Si_{0.5}Ge_{0.5}$(110) surfaces were dosed with 4.5×10^5 L of TDMAT or 4.5×10^5 L of $TiCl_4$ without carrier gas at 25°C in an *in-situ* ALD chamber. Fig. 4.3 shows the chemical compositions after a saturation dose of TDMAT or $TiCl_4$ followed by 300°C post-deposition annealing (PDA); the Ge 3d and Si 2p peaks are also presented. Based on the Hartree-Slater model [24], all elemental intensities were corrected using photoelectron cross-sections (Si 2p-0.817, Ge 3d-1.42, Ti 2p-7.81, O 1s-2.93, C 1s-1, Cl 2p-2.29) and normalized to the combination of Si 2p and Ge 3d peaks to estimate the ratios of each chemical components on the surfaces. As shown in Fig. 4.3(a), when 25°C TDMAT was dosed onto 25°C H_2O_2/300°C atomic H/$Si_{0.5}Ge_{0.5}$(110) surface, the ratios of Ti : O : C were 1 : 3 : 2 and no N signal was observed. In addition, the shoulder peaks of Si 2p and Ge 3d in Fig. 4.3(b) had the identical binding energies as those on the H_2O_2 dosed $Si_{0.5}Ge_{0.5}$(110) surfaces (shown in the supplement Fig. 4.11); this demonstrated that Si-O-Ti and Ge-O-Ti bonds formed by H_2O_2 remained intact after low temperature TDMAT dosing.

After 300°C PDA, the ratio of Ti and O remained constant demonstrating a thermally stable TiO_x monolayer while the C ratio was decreased. To explain these results, it was proposed that, upon annealing, Ti-O-Ti bonds were formed allowing C_2H_6 desorption. In addition, the shoulder peak of Si 2p was increased while the

shoulder peak Ge 3d was disappeared consistent with the $Si_{0.5}Ge_{0.5}(110)$ surfaces being terminated with only Si-O-Ti bonds. It was expected that the thermal energy at 300°C activated the Si atoms to diffuse to the top surface to bond with oxygen atoms and drove the Ge atoms to the subsurface due to the stronger bonds between Si and O compared to the bonds between Ge and O. Furthermore, the shoulder peak of Si 2p was shifted toward the higher binding by 1.0 eV after 300°C PDA (between 101.5 and 102.5 eV) corresponding to Si^{3+} on 300°C anneal/25°C TDMAT/25°C H_2O_2/300°C atomic H/$Si_{0.5}Ge_{0.5}(110)$; this was consistent with the Si atoms making additional Si-O bonds upon annealing.

$TiCl_4$, an inorganic precursor, was also dosed onto 25°C $H_2O_2/Si_{0.5}Ge_{0.5}(110)$ surface at 25°C to provide a comparison between an inorganic precursor and TDMAT, an organometallic precursor. Fig. 4.3(d) showed that the ratios of Ti : O : Cl were 1 : 3 : 2 after a $TiCl_4$ dose at 25°C on 25°C $H_2O_2/Si_{0.5}Ge_{0.5}(110)$ consistent with the results of TDMAT dosed 25°C $H_2O_2/Si_{0.5}Ge_{0.5}(110)$. Moreover, the shoulder peaks of Si 2p and Ge 3d in Fig. 4.3(e) had identical binding energies as 25°C TDMAT/25°C H_2O_2/300°C atomic H/$Si_{0.5}Ge_{0.5}(110)$ in Fig. 4.3(c). This demonstrated that each Ti atom was likely to form Ti-O bonds by replacing two ligands with two oxygen atoms at the surface regardless of Ti precursors.

For the 25°C $TiCl_4$/25°C $H_2O_2/Si_{0.5}Ge_{0.5}(110)$, a subsequent PDA at 300°C demonstrated that the monolayer of TiO_x was thermally stable as shown by the constant Ti and O ratios; however, the ratio of Cl was decreased due to the desorption of $Cl_2(g)$. In addition, as demonstrated in Fig. 4.3(e), the shoulder peaks of Si spectra

showed a shift to higher binding energy while the shoulder peaks of Ge spectra were removed from the interface upon 300°C PDA consistent with the results of 300°C anneal/25°C TDMAT/25°C H_2O_2/300°C atomic H/$Si_{0.5}Ge_{0.5}$(110) in Fig. 4.3(b).

In Fig. 4.4, STS and XPS chemical shift measurements were performed to understand the electronic and chemical characteristics of a TiO_x monolayer on $Si_{0.5}Ge_{0.5}$(110) surfaces. STS measurements in Fig. 4.4(a) verified identical electronic properties for 300°C anneal/25°C TDMAT/25°C H_2O_2/300°C atomic H/$Si_{0.5}Ge_{0.5}$(110) (red) and 300°C anneal/25°C $TiCl_4$/25°C H_2O_2/$Si_{0.5}Ge_{0.5}$(110) (green) surfaces with ±0.1 V difference near VB and CB edges. To achieve more accurate onsets near VB edges, the outer and inner VB edges were obtained from a bilinear fit; a bilinear fit was employed for these spectra since there were obvious band edge states. The bilinear fit of VB edge states results in calculation of two onsets. The two VB onsets were -0.578 ± 0.030 and -0.257 ± 0.065 V for 300°C anneal/25°C TDMAT/25°C H_2O_2/300°C atomic H/$Si_{0.5}Ge_{0.5}$(110), and -0.513 ± 0.016 and -0.196 ± 0.076 V for 300°C anneal/25°C $TiCl_4$/25°C H_2O_2/$Si_{0.5}Ge_{0.5}$(110), respectively. Based on the results, it was concluded that a monolayer of TiO_x without mid-gap and CB edge states was formed on $Si_{0.5}Ge_{0.5}$(110) surfaces using TDMAT or $TiCl_4$. Additionally, compared to $Si_{0.5}Ge_{0.5}$(110) surfaces dosed with a 25°C H_2O_2(g), the STS spectra after TDMAT or $TiCl_4$ dose showed that state density near CB edge were largely decreased due to the formation of a TiO_x monolayer.

Fig. 4.4(b) presented XPS spectra of Ti 2p peaks on TDMAT or $TiCl_4$ dosed $Si_{0.5}Ge_{0.5}$(110) surfaces to investigate the oxidation states. The positions of Ti 2p 3/2

and 1/2 spin-orbit components between two different $Si_{0.5}Ge_{0.5}(110)$ surfaces were almost same with an error range of ±0.1 eV. Furthermore, the positions of Ti 2p 3/2 peaks were located in 459.3 eV, and this binding energy corresponded to Ti^{4+} consistent with a proposed model of Ti atoms bonded to two O atoms with two other Ti-O or Ti-Cl bonds, which have stronger electronegativity than Ti atoms, as shown in detail below.

Proposed models of TDMAT or TiCl4 dosed $Si_{0.5}Ge_{0.5}(110)$ surfaces followed by 300°C PDA are shown in Fig. 4.5. A proposed model in Fig. 4.5(a) shows that TDMAT molecules reacted with surface hydroxyl groups forming one Ti atom bonded to two oxygen atoms on $Si_{0.5}Ge_{0.5}(110)$ surface, two other ligands reacted with weakly bound hydroxyl groups from the surface forming two Ti-O-CH_3 bonds, and $NH(CH_3)_3$ or $NH_2(CH_3)_2$ desorbed as byproducts; note that it was proposed that the back bonded oxygens remained intact and this was consistent with the XPS peak intensities and shifts in Fig. 4.3 and 4.4. Moreover, a proposed model including Ti-O-CH_3 bonds was consistent with the previous report [25]. After 300°C PDA, O=Ti-CH_3 bonds and additional Si-O-Si bonds were formed and $C_2H_6(g)$ desorb as a byproduct consistent with the XPS peak intensities and shifts; however, the experimental ratio between Ti : O was 1 : 3, while the proposed model in Fig. 4.3 had a Ti : O ratio of 1 : 5. In order to explain the ratio difference, a model must consider that many of oxygens are located at the subsurface and the emitted electrons should be affected by an exponential attenuation function according to the depth [26]. The electron escape depths for Ti and O peaks are 2nm at normal incidence and decreased to 1nm at 60° take-off

angle [26], which is the experimental condition during the XPS measurements. Based on the proposed model in which the depths of oxygen are assumed to be 0, 3, and 6Å, a simple attenuation estimate using the electron escape depth of 1nm provides a Ti and O ratio of 1 : 4, which is closer to the experimental results.

A model is also provided for the $TiCl_4$ reaction, as shown in Fig. 4.5(b), $TiCl_4$ molecules reacted with hydroxyl groups resulting in the formation of one Ti atom bonded to two oxygen atoms on $Si_{0.5}Ge_{0.5}(110)$ surface while a HCl(g) desorbed as a byproduct. After 300°C PDA, annealing induced the formation of Ti-O-Ti bonds allowing Cl_2(g) desorption and surface Si atoms formed additional Si-O backbonds. Note that proposed models were highly simplified to provide explanations with regard to the chemical compositions.

To compare the topology of $Si_{0.5}Ge_{0.5}(110)$ surfaces dosed with TDAMT or $TiCl_4$ followed by 300°C PDA, STM images and line trace analyses are presented in Fig. 4.6. In Fig. 4.6(a), 300°C anneal/25°C TDMAT/25°C H_2O_2/300°C atomic H/$Si_{0.5}Ge_{0.5}(110)$ surface showed consistent vertical rows. To analyze the row spacing, four different areas in the STM image were analyzed and line traces were performed as shown in Fig. 4.6(b). Line traces of 300°C anneal/25°C TDMAT/25°C H_2O_2/300°C atomic H/$Si_{0.5}Ge_{0.5}(110)$ surface showed an average row spacing of 18.0 Å with a standard deviation of 1.7 Å and a standard error of 0.60 Å. This row spacing was more than twice the 8.0 Å of adatom spacing on a sputter-cleaned $Si_{0.5}Ge_{0.5}(110)$ surface consistent with the proposed models in Fig. 4.5(a), in which one Ti atom is bonded to two oxygen atoms on $Si_{0.5}Ge_{0.5}(110)$ surface with the oxygen backbond insertion. In

comparison, Fig. 4.6(c) shows the STM image of 300°C anneal/25°C $TiCl_4$/25°C H_2O_2/$Si_{0.5}Ge_{0.5}$(110) surface. The line traces in Fig. 4.6(d) show an average row spacing of 18.2 Å with a standard deviation of 1.3 Å and a standard error of 0.47 Å. Therefore, there is an identical row spacing for TDMAT and $TiCl_4$ dosing followed by PDA within an error range demonstrated the formation of TiO_x monolayer with the same surface structure independent of precursors. Compared to the 11.8 Å average row spacing of a monolayer of Al_2O_3 on $Si_{0.5}Ge_{0.5}$(110) surface, in which one Al atom was bonded to one oxygen atom with the ratio of Al : O to be 2 : 3 on $Si_{0.5}Ge_{0.5}$(110) [14], the TiO_x row spacing was larger as shown in the proposed model in Fig. 4.5(a) and (b) for Ti making two bonds to surface O atoms.

4.5 Conclusion

Clean or H-terminated $Si_{0.5}Ge_{0.5}$(110) surfaces were dosed with H_2O_2(g) at 25°C to functionalize the surfaces with hydroxyls. STS measurements demonstrated that H_2O_2(g) resulted in the identical electronic and –OH terminated molecular structures on both clean and H-terminated $Si_{0.5}Ge_{0.5}$(110) surfaces. To form a monolayer of TiO_x on hydroxyl-terminated $Si_{0.5}Ge_{0.5}$(110) surfaces, TDMAT or $TiCl_4$ were subsequently dosed at 25°C on 25°C H_2O_2/300°C atomic H/$Si_{0.5}Ge_{0.5}$(110) and 25°C H_2O_2/$Si_{0.5}Ge_{0.5}$(001) surfaces. XPS indicated that the ratio between Ti and O was 1 : 3 and remained constant upon 300°C PDA demonstrating a thermally stable monolayer of TiO_x regardless of Ti-based precursors. STM images showed the row spacing of TiO_x monolayer on $Si_{0.5}Ge_{0.5}$(110) surfaces was more than twice the

adatom spacing on a clean $Si_{0.5}Ge_{0.5}(110)$ verifying a proposed chemisorption model. XPS analysis verified that a monolayer of TiO_x was composed of only Si-O-Ti bonds after PDA indicating the complete segregation of Si atoms. Furthermore, STS measurements were consistent with the monolayer of TiO_x having no mid-gap and CB edge states, which should be an ideal ultrathin insulating layer for a MIS structure.

4.6 Acknowledgments

This work was supported in part by the Center for Low Energy Systems Technology (LEAST), one of six centers of STARnet, a Semiconductor Research Corporation program (Grant No. 2013-VJ-2451) sponsored by MARCO and DARPA, NSF DMR 1207213, GLOBALFOUNDRIES, and Applied Materials. The $Si_{0.5}Ge_{0.5}$ wafers were provided by GLOBALFOUNDRIES.

Chapter 4, in part or in full, is a reprint of the following material:
S. W. Park, J. Y. Choi, B. Sahu, S. Siddiquui, N. Yoshida, J. Kachian, A. C. Kummel "Formation of atomically ordered and chemically selective Si-O-Ti monolayer on $Si_{0.5}Ge_{0.5}(110)$ for a MIS structure via $H_2O_2(g)$" (Manuscript in preparation). The dissertation author was the primary investigator and author of this paper.

4.7 Supplemental materials

The structures of a sputter-cleaned $Si_{0.5}Ge_{0.5}(110)$ surface are shown in Fig. 4.7. The filled-state STM images of $Si_{0.5}Ge_{0.5}(110)$ in Fig. 4.7(a) and (b) show that the surface reconstructions were mainly composed of adatoms. To estimate the row

spacing of adatoms, four different areas were analyzed in line traces as shown in Fig. 4.7(d). The average row spacing of adatoms was 8.0 Å with a standard deviation of 0.92 Å, and a standard error of 0.33 Å. Based on the previous studies, Si(110) and Ge(110) surfaces are likely to form adatom reconstructions to decrease the surface energy by minimizing the number of dangling bonds at the surface [27,28]. As shown by a schematic diagram in Fig. 4.7(c), the number of dangling bonds at the surface was reduced by half due to the formation of adatom reconstructions. The STM images of adatom reconstructions on $Si_{0.5}Ge_{0.5}$(110) were consistent with the previous report [14].

Fig. 4.8(a) demonstrates that the Fermi level of a clean p-type $Si_{0.5}Ge_{0.5}$(110) was located near mid-gap between conduction and valence band edges consistent with surface pinning. It was expected that the half-filled dangling bonds of tri-coordinated Ge and Si adatoms on a clean $Si_{0.5}Ge_{0.5}$(110) surface created defect states resulting in a pinned Fermi level. To passivate the half-filled dangling bonds of surface adatoms by forming Ge-H and Si-H sigma bonds, a sputter-cleaned $Si_{0.5}Ge_{0.5}$(110) surface was exposed to 3,600 L of atomic H. During the exposure, the substrate temperature was maintained at 300°C to avoid Ge preferential etching, which occurs below 250°C [29,30]. As shown by the STS spectra in Fig. 4.8(a), after atomic H dosing, the Fermi level was shifted toward the valence band edge (blue arrow) becoming p-type consistent with surface unpinning because the B-doped $Si_{0.5}Ge_{0.5}$(110) substrate was p-type. Since surface pinning causes undesirable device performance such as a high subthreshold swing and a shifted threshold voltage in metal-oxide-semiconductor field-effect

transistors (MOSFETs) [31], an unpinned Fermi level should be advantageous for the formation of gate oxides.

As shown by a STM image in Fig. 4.8(b), the $Si_{0.5}Ge_{0.5}$(110) surface after atomic H dosing was well-ordered and uniform without any Ge preferential etching or etch pits. Additionally, as shown in Fig. 4.8(c), the average row spacing was 7.9 Å with a standard deviation of 1.1 Å, and a standard error of 0.40 Å, which was almost identical to a sputter-cleaned $Si_{0.5}Ge_{0.5}$(110) surface. In sum, the atomic H was effective in passivating the dangling bonds of adatoms indicating an unpinned Fermi level of $Si_{0.5}Ge_{0.5}$(110) while maintaining the surface uniformity.

Sputter-cleaned or atomic H dosed $Si_{0.5}Ge_{0.5}$(110) surfaces were transferred to an *in-situ* ALD chamber and dosed with a saturation dose of H_2O_2(g) at 25°C. To verify the identical surface termination between the 25°C $H_2O_2/Si_{0.5}Ge_{0.5}$(110) and 25°C H_2O_2/300°C atomic $H/Si_{0.5}Ge_{0.5}$(110) surfaces, the chemical structures were studied by an *in-situ* XPS. In Fig. 4.9, XPS demonstrated the oxygen ratios normalized to Si 2p + Ge 3d peaks with error ranges of ±0.02 for 25°C 1X $H_2O_2/Si_{0.5}Ge_{0.5}$(110), 2X 25°C $H_2O_2/Si_{0.5}Ge_{0.5}$(110), 1X 25°C H_2O_2/300°C atomic $H/Si_{0.5}Ge_{0.5}$(110), and 1X 25°C $H_2O/Si_{0.5}Ge_{0.5}$(110) surfaces, in which 4.5×10^6 L of vapor of H_2O was dosed. Here, 1X H_2O_2 was H_2O_2(g), 4.5×10^6 L of vapor from H_2O_2(aq) (approximately 120,000 L of H_2O_2(g)), while 2X H_2O_2 was 9.0×10^6 L of vapor from H_2O_2(aq) (approximately 240,000 L of H_2O_2(g)) The oxygen ratio of 2X 25°C $H_2O_2/Si_{0.5}Ge_{0.5}$(110) was almost same as 1X 25°C $H_2O_2/Si_{0.5}Ge_{0.5}$(110) indicating a saturation dose of H_2O_2(g). In addition, the 1X 25°C $H_2O_2/Si_{0.5}Ge_{0.5}$(110) surface and

1X 25°C H_2O_2/300°C atomic H/$Si_{0.5}Ge_{0.5}$(110) had identical oxygen ratios consistent with a high reactivity of 25°C H_2O_2(g) on H-terminated $Si_{0.5}Ge_{0.5}$(110) forming a saturated layer of hydroxyls by removing H atoms at the surface. A previous Fourier Transform Infrared Spectroscopy (FTIR) study by Bensliman et al. [32] showed that hydrogen peroxide was effective in oxidizing H-terminated Si(111). In comparison with 1X 25°C H_2O/$Si_{0.5}Ge_{0.5}$(110) surface, a H_2O_2(g) dose produced a nearly three times higher oxygen consistent with previous studies on Ge(001) and $Si_{0.5}Ge_{0.5}$(110) [12,14].

To estimate the approximate coverage, a model, in which the top surface was composed of only oxygen atoms while the underlying layers were composed of Si and Ge atoms, was employed along with an exponential attenuation function of $I = I_0\exp(-t/\lambda)$ (I: intensity in the presence of the overlayer; I_0: intensity in the absence of any overlayer; t: thickness of the covering layer; λ: inelastic mean free path). According to the database of electron inelastic mean free paths (IMFP) [33], the escape depth of Si 2p, Ge 3d, and O 1s peaks was approximately 1nm for a 60° take-off angle relative to the surface normal. Based on the these calculations, the 19% O ratio of 25°C H_2O_2/$Si_{0.5}Ge_{0.5}$(110) surface corresponded to 1.05 monolayer whereas the 6% O ratio of 25°C H_2O/$Si_{0.5}Ge_{0.5}$(110) surface corresponded to 0.32 monolayer. Therefore, a H_2O_2(g) dose should be able to provide higher nucleation density than H_2O(g) for subsequent reaction with metal precursors to form an ultrathin insulating MIS structure.

To analyze the effect of a H_2O_2(g) dose at elevated temperature, H_2O(g) or H_2O_2(g) were dosed onto clean $Si_{0.5}Ge_{0.5}$(110) surfaces at 150°C. As shown in Fig. 4.10, a 150°C H_2O(g) dose resulted in the greater GeO_x/Ge formation compared to SiO_x/Si formation. However, when H_2O_2(g) was dosed at 150°C onto $Si_{0.5}Ge_{0.5}$(110), there was greater SiO_x/Si than GeO_x/Ge formation. Therefore, a H_2O_2(g) dose at 150°C induced a partial segregation of Si atoms thereby forming more Si-O_xH_y bonds at the surface and pushing the Ge atoms to the subsurface.

To perform more accurate analysis of bonding configurations on $Si_{0.5}Ge_{0.5}$(110) surfaces, the Ge 3d and Si 2p peaks were compared and fit with an error range of ±0.1 eV for each chemical step. In Fig. 4.11(a) and (c), the Ge 3d and Si 2p peaks on clean SiGe(110) showed sharp and asymmetric features due to the spin-orbit splitting consistent with previous studies [14,34]. When a sputter-cleaned $Si_{0.5}Ge_{0.5}$ (110) surface was dosed with H_2O_2(g) at 25°C, as shown in Fig. 4.11(a) and (b), the shoulder peaks were formed at higher binding energy (red) on both Si and Ge peaks, corresponding to Si-O_xH_y and Ge-O_xH_y bonds. These results verified that clean $Si_{0.5}Ge_{0.5}$ (110) was terminated with both Ge and Si atoms. In comparison, when a 300°C atomic H/$Si_{0.5}Ge_{0.5}$(110) surface was dosed with H_2O_2(g) at 25°C, as shown in Fig. 4.11(c) and (d), there was much greater ratio of SiO_x/Si than GeO_x/Ge consistent with the preferential formation of Si-O_xH_y bonds. This was consistent with atomic H above 250°C inducing a partial Si segregation to the top surface due to the higher bond energy of Si-H compared to Ge-H as demonstrated in previous studies [29,35]. Furthermore, the shoulder peaks of 25°C H_2O_2/$Si_{0.5}Ge_{0.5}$(110) and 25°C H_2O_2/300°C

atomic H/$Si_{0.5}Ge_{0.5}$(110) were located between 100.5 and 101.5 eV for Si 2p peaks mainly belonging to Si^{2+} and between 30.5 and 31.5 eV for Ge 3d peaks mainly belonging to Ge^{2+} with a wider full width at half maximum (FWHM) compared to Si and Ge bulk peaks. This was consistent with surface Si and Ge atoms being bonded to one hydroxyl and an oxygen atom inserted into backbonds demonstrating the proposed models in Fig. 4.1.

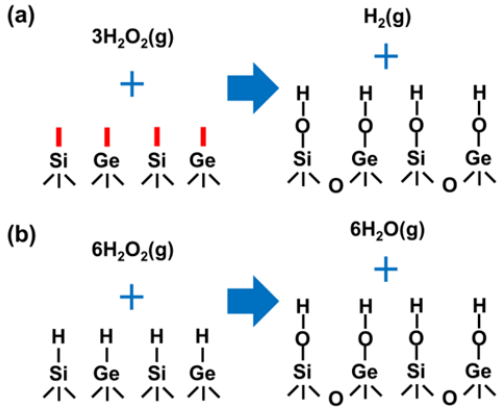

Figure 4.1 Proposed models of clean and H-terminated $Si_{0.5}Ge_{0.5}(110)$ surfaces dosed with 25°C $H_2O_2(g)$. (a) A schematic diagram of a 25°C $H_2O_2(g)$ dosing of a clean $Si_{0.5}Ge_{0.5}(110)$ surface terminated with dangling bonds (red). The surface was terminated with hydroxyls with O insertion into backbonds and the byproduct is $H_2(g)$. (b) A schematic diagram of a 25°C $H_2O_2(g)$ dose on a H-terminated $Si_{0.5}Ge_{0.5}(110)$ surface. $H_2O_2(g)$ was sufficiently reactive to form hydroxyl termination at the surface with $H_2O(g)$ as byproduct.

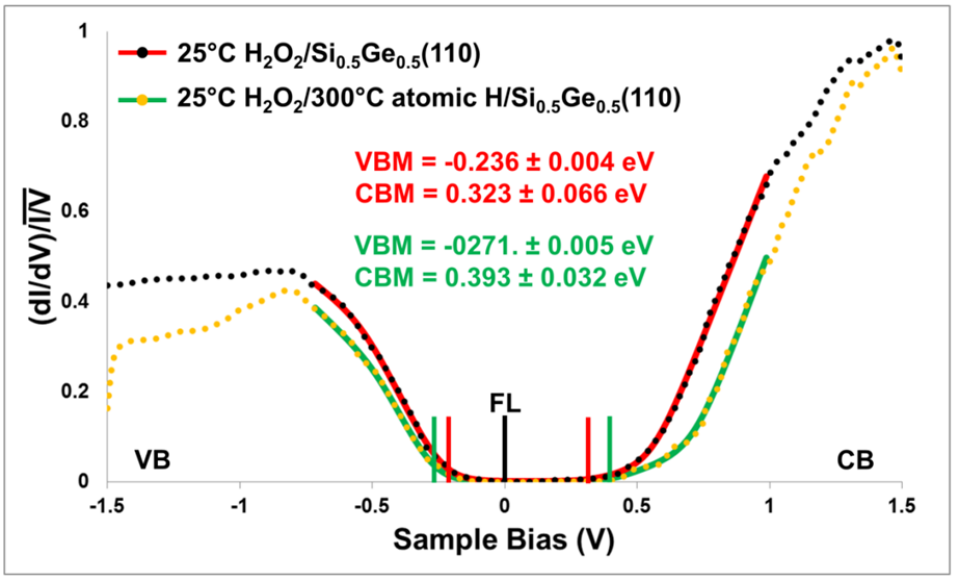

Figure 4.2 STS of H_2O_2 dosed $Si_{0.5}Ge_{0.5}(110)$ surfaces. STS spectra with fits to estimate VB and CB edges. After a 25°C H_2O_2(g) dose, the electronic structures are nearly identical with an unpinned Fermi level regardless of an atomic H dose.

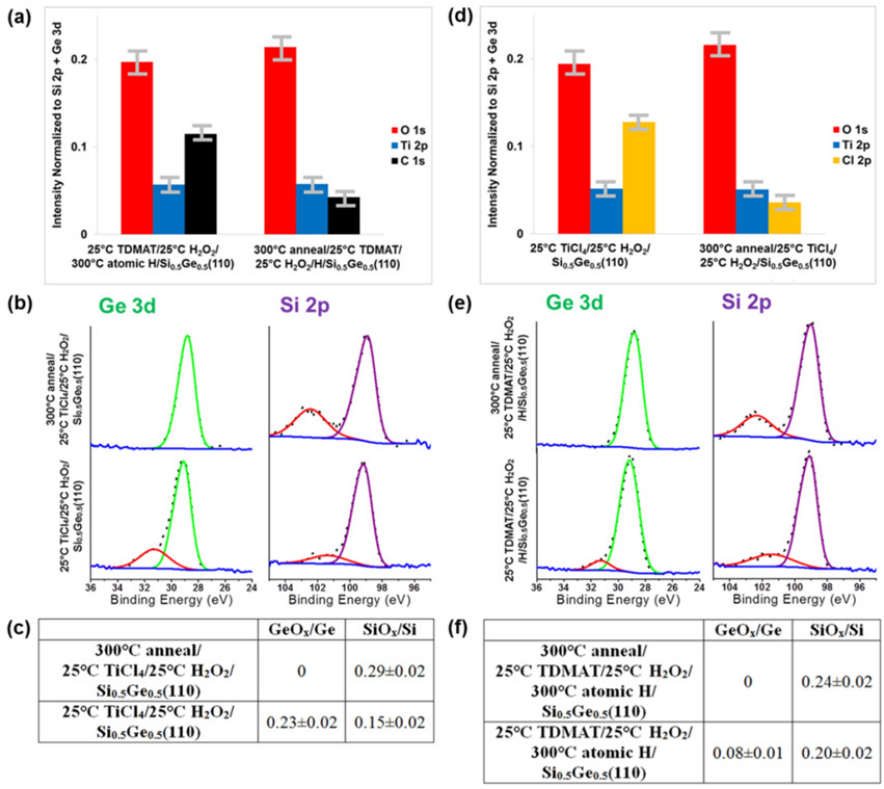

(c)

	GeO_x/Ge	SiO_x/Si
300°C anneal/ 25°C $TiCl_4$/25°C H_2O_2/ $Si_{0.5}Ge_{0.5}$(110)	0	0.29±0.02
25°C $TiCl_4$/25°C H_2O_2/ $Si_{0.5}Ge_{0.5}$(110)	0.23±0.02	0.15±0.02

(f)

	GeO_x/Ge	SiO_x/Si
300°C anneal/ 25°C TDMAT/25°C H_2O_2/ 300°C atomic H/ $Si_{0.5}Ge_{0.5}$(110)	0	0.24±0.02
25°C TDMAT/25°C H_2O_2/ 300°C atomic H/ $Si_{0.5}Ge_{0.5}$(110)	0.08±0.01	0.20±0.02

Figure 4.3 XPS chemical compositions and Si 2p and Ge 3d spectra of TDMAT or $TiCl_4$ dosed Si.5Ge.5(110) surfaces (a) Chemical intensities normalized to Si 2p + Ge 3d peaks upon a 25°C TDMAT dose. Ti : O : C ratios were 1 : 3 : 2 with error ranges of ±0.02 and no N peak was observed. After 300°C annealing, Ti and O ratios were constant consistent with a thermally stable TiO_x monolayer while C was decreased due to desorption of methanes or ethanes. (b) Ge 3d (green) and Si 2p (purple) peaks upon a 25°C $TiCl_4$ dose followed by 300°C PDA. After a $TiCl_4$ dose at 25°C, XPS showed shoulder peaks (red) on both Ge 3d and Si 2p peaks corresponding to Ge-O-Ti and Si-O-Ti components. After annealing at 300°C, Ge-O-Ti bonds disappeared and Si-O-Ti bonds increased. The shoulder peak of Si was shifted toward the higher binding energy by 1.0 eV after 300°C PDA. (c) The table showed the ratios of GeO_x/Ge and SiO_x/Si with standard errors after 25°C $TiCl_4$ dose and 300°C PDA. 300°C PDA removed GeO_x and increased SiO_x resulting in exclusively Si-O-Ti termination on SiGe(110). (d) Chemical intensities normalized to Si 2p + Ge 3d peaks upon a 25°C $TiCl_4$ dose. Ti : O : Cl ratios were 1 : 3 : 2 and after 300°C annealing, Ti and O ratios were constant while Cl was decreased by a HCl(g) desorption. This data was consistent with a thermally stable TiO_x monolayer while Cl was decreased due to the desorption of HCl. (e) XPS spectra upon a 25°C TDMAT dose followed by 300°C PDA. The change in shoulder peaks after 300°C PDA was identical with (b). (f) The table shows the ratios of GeO_x/Ge and SiO_x/Si with standard errors after 25°C TDMAT dose and 300°C PDA. The surface was also composed of Si-O-Ti bonds after 300°C PDA.

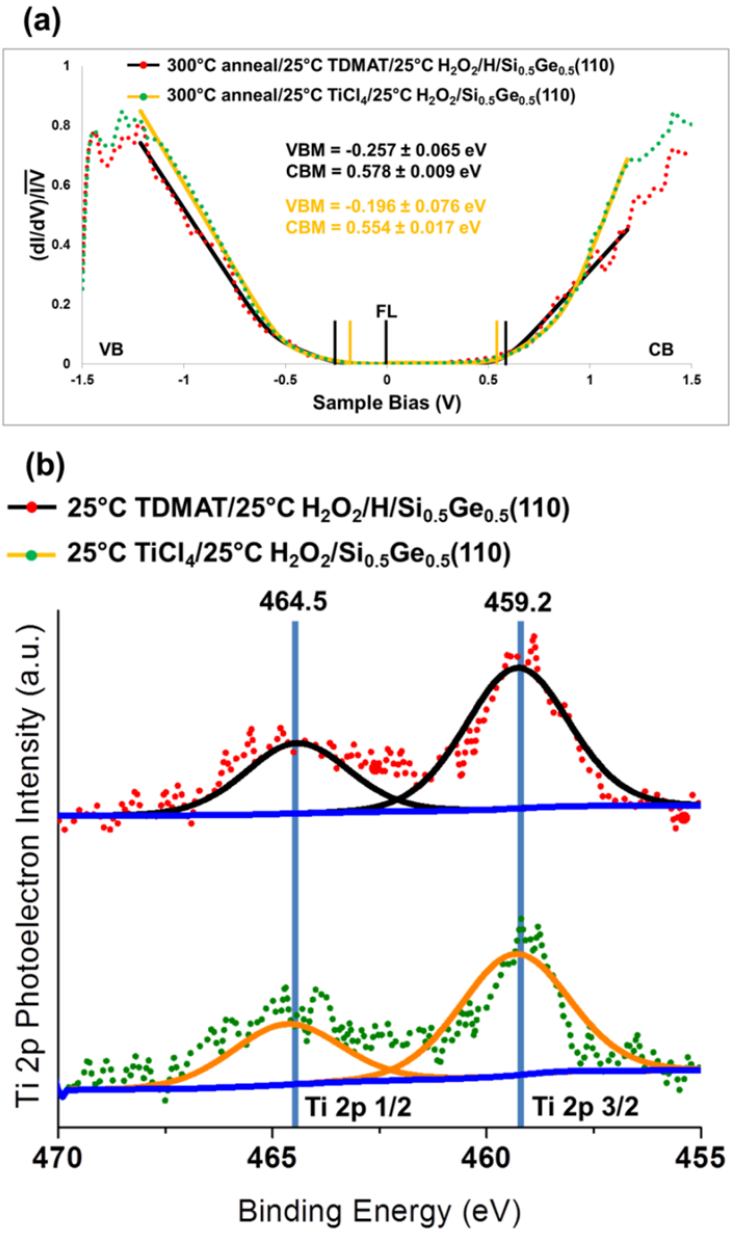

Figure 4.4 STS measurements and Ti 2p peaks of TDMAT or $TiCl_4$ dosed $Si_{0.5}Ge_{0.5}(110)$ surfaces (a) STS measurements of 300°C anneal/25°C TDMAT/25°C H_2O_2/300°C atomic $H/Si_{0.5}Ge_{0.5}(110)$ and 300°C anneal/25°C $TiCl_4$/25°C $H_2O_2/Si_{0.5}Ge_{0.5}(110)$ surfaces. The Fermi level was positioned closer to VB edge on both surfaces consistent with the unpinning effect. Note: a bilinear fit was used for the VB side of the STS due to the band edge states. The reported VB positions are for the inner band gap. (b) Ti 2p peaks of TDMAT or $TiCl_4$ dosed $Si_{0.5}Ge_{0.5}(110)$. The Ti 2p 3/2 peaks on both surfaces were positioned at 459.2 eV corresponding to Ti^{4+}.

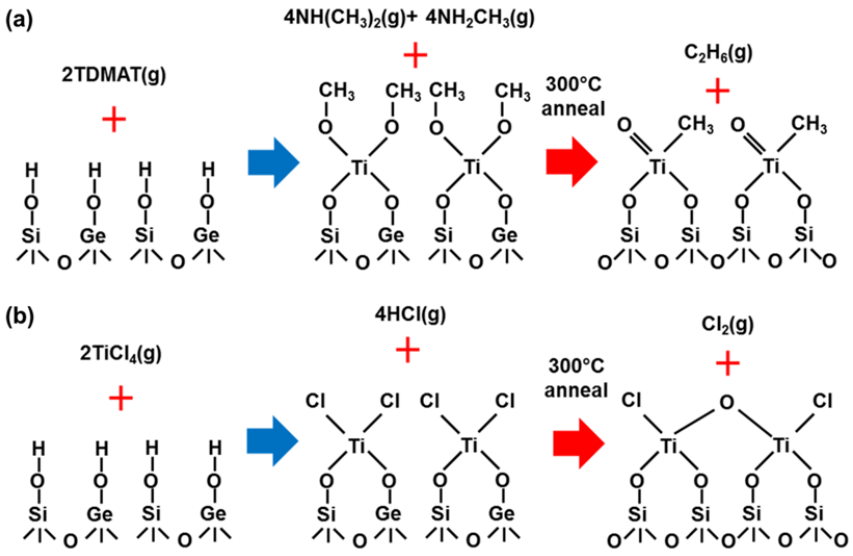

Figure 4.5 Proposed models of $TiCl_4$ or TDMAT dosed $H_2O_2/Si_{0.5}Ge_{0.5}(110)$ surfaces (a) A proposed model of the 25°C TDMAT reaction + PDA. TDMAT molecules dissociatively chemisorbed to form one Ti atom bonded with two O atoms at the $Si_{0.5}Ge_{0.5}(110)$ surface along with two Ti-O-CH_3 bonds while $NH(CH_3)_3$ or $NH_2(CH_3)_2$ desorbed as byproducts. After 300°C annealing, the model surface was composed of only Si-O-Ti and Si-O-Si bonds while ethane desorbed as a byproduct. (b) A proposed model of the 25°C $TiCl_4$ reaction + PDA. $TiCl_4$ molecules were also likely to form one Ti atom bonded with two O atoms at the $Si_{0.5}Ge_{0.5}(110)$ surface while a byproduct desorbed as HCl(g). After 300°C annealing, the model surface was composed of only Si-O-Ti and Si-O-Si bonds while Cl_2 desorbed as a byproduct; Ti-O-Ti bridge bonds formed to maintain the oxidation state (Ti^{4+}).

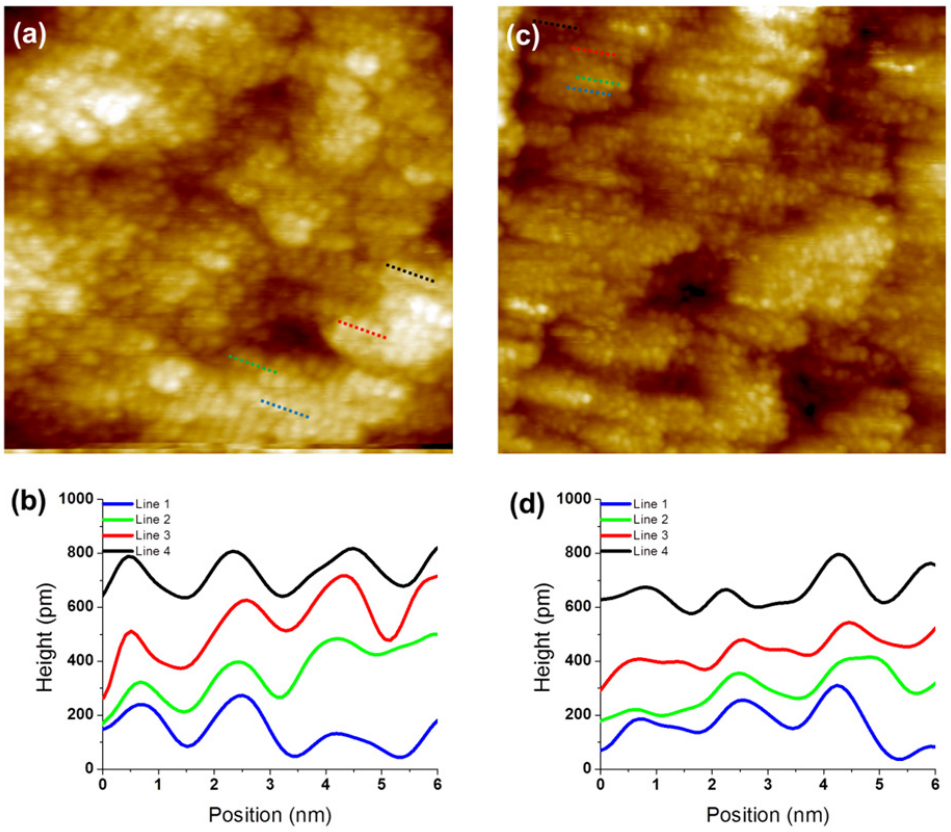

Figure 4.6 STM images and line traces of TDMAT or $TiCl_4$ dosed $Si_{0.5}Ge_{0.5}(110)$ surfaces (a) Filled state STM image (50 × 50 nm^2, V_s = –1.8 V, I_t = 200 pA) of 300°C anneal/25°C TDMAT/25°C H_2O_2/300°C atomic H/$Si_{0.5}Ge_{0.5}(110)$ surface. (b) Line traces to estimate the row spacing in (a). The average row spacing was 18.0 Å with a standard deviation of 1.7 Å. (c) Filled state STM image (50 × 50 nm^2, V_s = –1.8 V, I_t = 200 pA) of 300°C anneal/25°C $TiCl_4$/25°C H_2O_2/$Si_{0.5}Ge_{0.5}(110)$ surface. (d) Line traces to estimate the row spacing in (c). The average row spacing was 18.2 Å with a standard deviation of 1.3 Å.

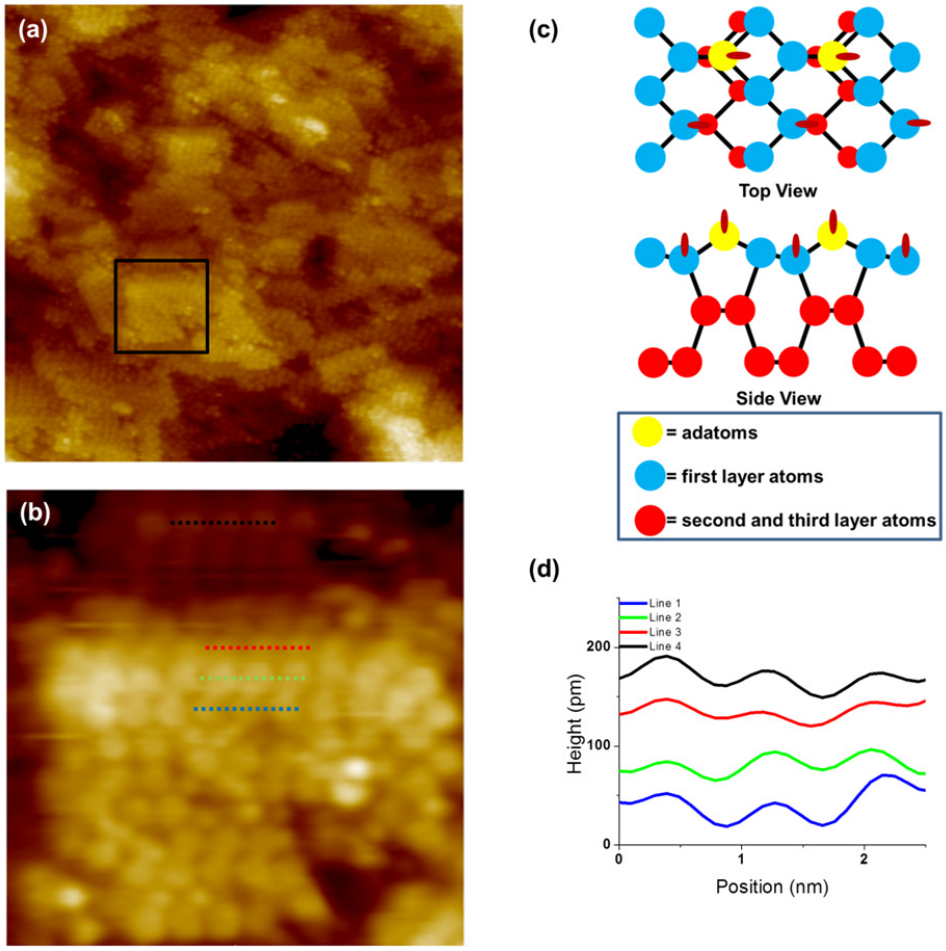

Figure 4.7 STM image and proposed model of a sputter-cleaned $Si_{0.5}Ge_{0.5}$(110) (a) A filled state STM image (50 × 50 nm^2, Vs = –1.8 V, It = 200 pA) of a sputter-cleaned $Si_{0.5}Ge_{0.5}$(001). A clean $Si_{0.5}Ge_{0.5}$(110) surface was terminated with Si and Ge adatoms. (b) 10 × 10 nm^2 inset of a black square in (a) to show the surface reconstruction on $Si_{0.5}Ge_{0.5}$(110). (c) A proposed model of a clean $Si_{0.5}Ge_{0.5}$(110) surface terminated with adatoms. The surface reconstruction via Si and Ge adatoms reduced the number of dangling bonds. The adatoms were tri-coordinated and had half-filled dangling bonds. (d) Line traces to estimate the row spacing in (a) and (b). The average row spacing was 8.0 Å with a standard deviation of 0.92 Å.

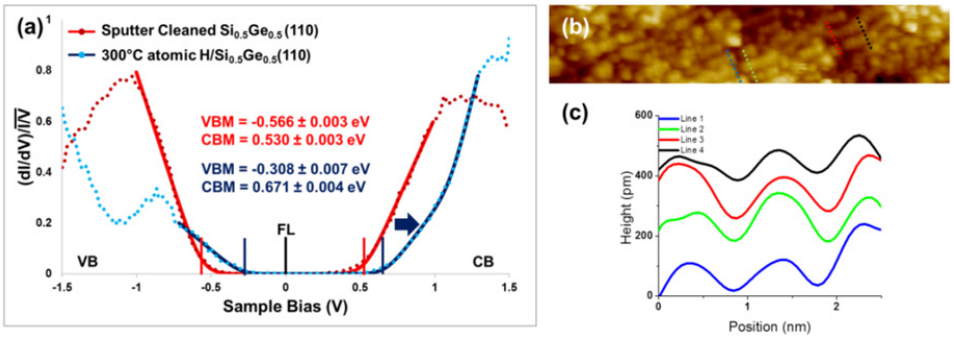

Figure 4.8 STS and STM after 3,600 L of atomic H dose on p-type $Si_{0.5}Ge_{0.5}$(110) (a) STS measurements of the p-type $Si_{0.5}Ge_{0.5}$(110) surface before and after an atomic H dose at 300°C. The Fermi level (0V position) of the clean $Si_{0.5}Ge_{0.5}$(110) surface (red curve) was pinned near the mid-gap, while the Fermi level of the atomic H dosed $Si_{0.5}Ge_{0.5}$(110) surface (blue curve) was shifted towards the valence band edge, consistent with unpinning. Each STS curve was fit to determine the band gaps and Fermi level positions. The range of fitting was -1 to 1V for sputter cleaned $Si_{0.5}Ge_{0.5}$(110) surface and was -0.7 to 1.3 V for 300°C atomic H/$Si_{0.5}Ge_{0.5}$(110) surface. (b) Filled state STM image (30 × 6 nm^2, V_s = –1.8 V, I_t = 200 pA) after an atomic H dose on a clean $Si_{0.5}Ge_{0.5}$(110) surface. The atomic H produced a well-ordered surface structure and no etch pits were observed; however, the adatom reconstruction of the clean $Si_{0.5}Ge_{0.5}$(110) was removed. (c) Line traces to estimate the row spacing in (b). The average row spacing was 7.9 Å with a standard deviation of 1.1 Å.

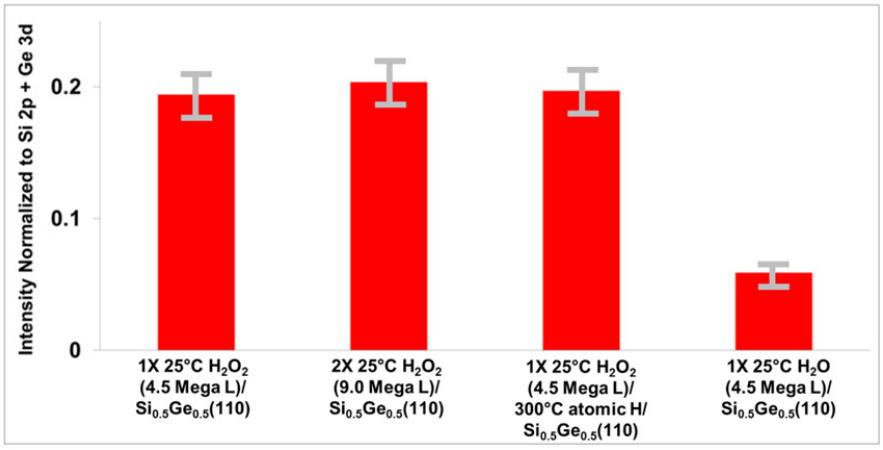

Figure 4.9 XPS of H_2O_2 dosed $Si_{0.5}Ge_{0.5}(110)$ surfaces. Ratios of O normalized to Si 2p + Ge 3d peaks. The oxygen ratio of 2X 25°C $H_2O_2/Si_{0.5}Ge_{0.5}(110)$, in which the double amount of $H_2O_2(g)$ compared to 1X 25°C $H_2O_2/Si_{0.5}Ge_{0.5}(110)$ was exposed, was nearly same as 1X 25°C $H_2O_2/Si_{0.5}Ge_{0.5}(110)$ consistent with a saturation dose of $H_2O_2(g)$. The O intensities of 1X 25°C $H_2O_2/Si_{0.5}Ge_{0.5}(110)$ and 1X 25°C H_2O_2/300°C atomic $H/Si_{0.5}Ge_{0.5}(110)$ surfaces were almost identical and three times larger than the O intensity of the 1X 25°C $H_2O(g)/Si_{0.5}Ge_{0.5}(110)$ surface consistent with a strong reactivity and a higher nucleation site density induced by $H_2O_2(g)$.

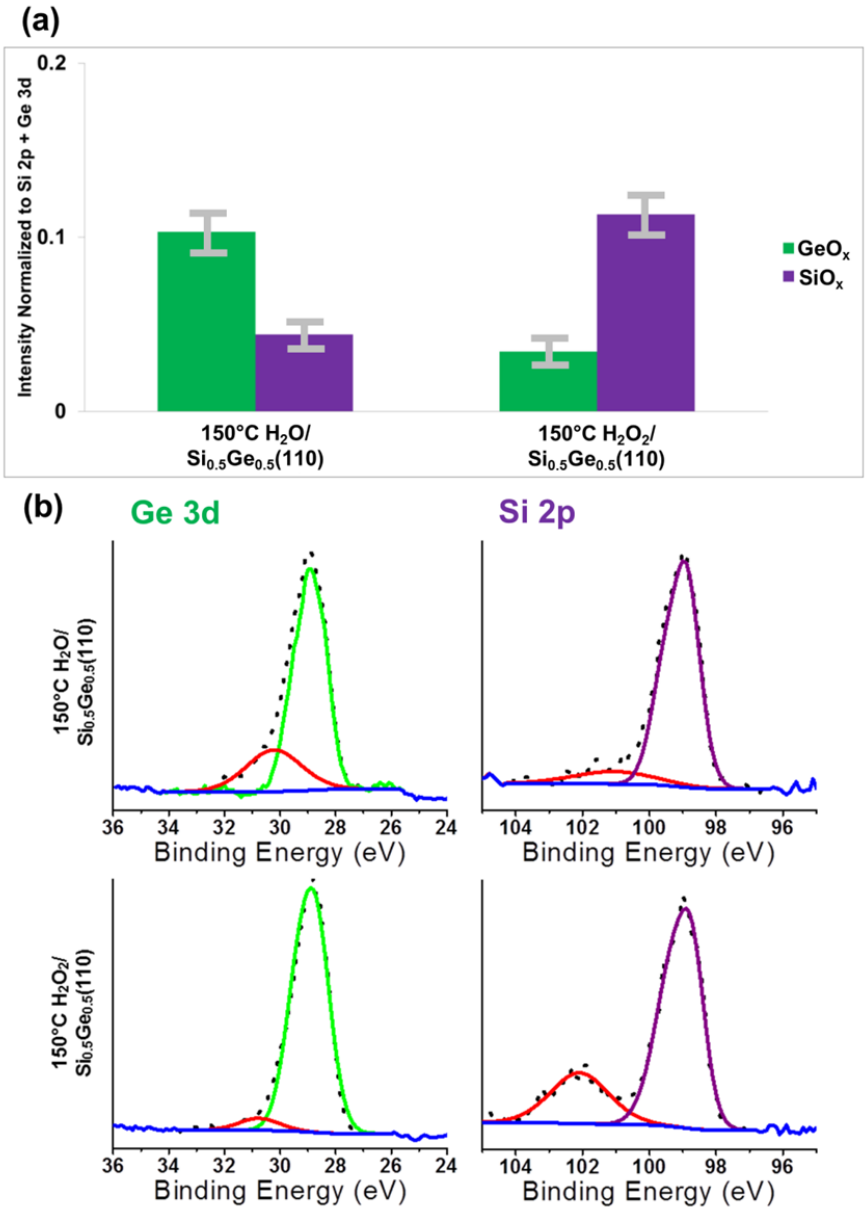

Figure 4.10 XPS of 150°C H_2O or H_2O_2 dosed $Si_{0.5}Ge_{0.5}(110)$ surfaces (a) Ratios of GeO_x and SiO_x normalized to Si 2p + Ge 3d peaks. When $H_2O(g)$ was dosed onto $Si_{0.5}Ge_{0.5}(110)$ at 150°C, the ratio of GeO_x/Ge was larger than SiO_x/Si. In comparison, a $H_2O_2(g)$ dose at 150°C resulted in the higher ratio of SiO_x/Si compared to GeO_x/Ge demonstrating a partial Si segregation induced by a 150°C $H_2O_2(g)$ dose. (b) Ge 3d (green) and Si 2p (purple) peaks after a $H_2O(g)$ or $H_2O_2(g)$ dose at 150°C. The ratio of GeO_x/Ge was larger than SiO_x/Si on 150°C $H_2O/Si_{0.5}Ge_{0.5}(110)$ while SiO_x/Si was higher compared to GeO_x/Ge on 150°C $H_2O_2/Si_{0.5}Ge_{0.5}(110)$.

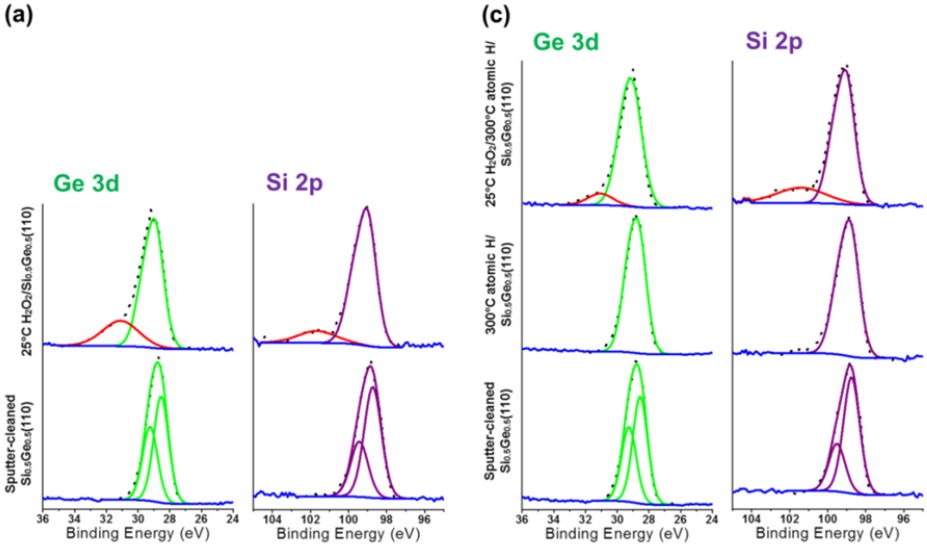

(b)

	GeO_x/Ge	SiO_x/Si
25°C H_2O_2/ $Si_{0.5}Ge_{0.5}$(110)	0.25±0.02	0.13±0.02
Sputter-cleaned $Si_{0.5}Ge_{0.5}$(110)	0	0

(d)

	GeO_x/Ge	SiO_x/Si
25°C H_2O_2/300°C atomic H/ $Si_{0.5}Ge_{0.5}$(110)	0.09±0.01	0.21±0.02
300°C atomic H/ $Si_{0.5}Ge_{0.5}$(110)	0	0
Sputter-cleaned $Si_{0.5}Ge_{0.5}$(110)	0	0

Figure 4.11 Ge 3d and Si 2p peaks of H_2O_2 dosed $Si_{0.5}Ge_{0.5}$(110) surfaces (a) Ge 3d (green) and Si 2p (purple) peaks after a H_2O_2(g) dose at 25°C. Peaks on a sputter-cleaned $Si_{0.5}Ge_{0.5}$(110) are asymmetric and sharp due to the orbit-splitting. After a H_2O_2(g) dose on clean $Si_{0.5}Ge_{0.5}$(110) at 25°C, XPS showed the formation of shoulder peaks (red) in the Ge 3d and Si 2p peaks corresponding to Ge-O_xH_y and Si-O_xH_y. (b) A table to show the ratios of GeO_x/Ge and SiO_x/Si with standard errors after a 25°C H_2O_2(g) dose. The formation of both GeO_x and SiO_x demonstrated that Ge and Si atoms coexisted on $Si_{0.5}Ge_{0.5}$(110) surface. (c) XPS spectra after 300°C atomic H and 25°C H_2O_2(g) dose. After a 25°C H_2O_2(g) dose on 300°C atomic H/$Si_{0.5}Ge_{0.5}$(110), the formation of Si-O_xH_y was larger than Ge-O_xH_y indicating a partial Si segregation to the top surface induced by 300°C atomic H dose. (d) A table to show the ratios of GeO_x/Ge and SiO_x/Si with standard errors after 300°C atomic H and 25°C H_2O_2(g). On 25°C H_2O_2/300°C atomic H/$Si_{0.5}Ge_{0.5}$(110) surface, the ratio of SiO_x/Si was higher compared to the ratio of GeO_x/Ge, verifying a partial Si segregation induced by 300°C atomic H.

4.8 References

[1] F. Schaffler, Semiconductor Science and Technology **12,** 1515 (1997).

[2] D. J. Paul, Semiconductor Science and Technology **19,** R75 (2004).

[3] M. L. Lee, E. A. Fitzgerald, M. T. Bulsara, M. T. Currie, and A. Lochtefeld, Journal of Applied Physics **97** (2005).

[4] B. G. Streetman and S. Banerjee, *Solid state electronic devices*, 6th ed. (Pearson Prentice Hall, Upper Saddle River, N.J., 2006).

[5] M. Lundstrom, *Fundamentals of carrier transport*, 2nd ed. (Cambridge University Press, Cambridge, U.K. ; New York, 2000).

[6] M. L. Lee, C. W. Leitz, Z. Cheng, A. J. Pitera, T. Langdo, M. T. Currie, G. Taraschi, E. A. Fitzgerald, and D. A. Antoniadis, Applied Physics Letters **79,** 3344 (2001).

[7] T. Ghani, M. Armstrong, C. Auth, M. Bost, P. Charvat, G. Glass, T. Hoffmann, K. Johnson, C. Kenyon, J. Klaus, B. McIntyre, K. Mistry, A. Murthy, J. Sandford, M. Silberstein, S. Sivakumar, P. Smith, K. Zawadzki, S. Thompson, and M. Bohr, in *A 90nm high volume manufacturing logic technology featuring novel 45nm gate length strained silicon CMOS transistors*, 2003, p. 11.6.1.

[8] S. Verdonckt-Vandebroek, E. F. Crabbe, B. S. Meyerson, D. L. Harame, P. J. Restle, J. M. C. Stork, and J. B. Johnson, IEEE Transactions on Electron Devices **41,** 90 (1994).

[9] J. P. Snyder, C. R. Helms, and Y. Nishi, Applied Physics Letters **67,** 1420 (1995).

[10] D. Kuzum, T. Krishnamohan, A. J. Pethe, A. K. Okyay, Y. Oshima, Y. Sun, J. P. McVittie, P. A. Pianetta, P. C. McIntyre, and K. C. Saraswat, Electron Device Letters, IEEE **29,** 328 (2008).

[11] J. S. Lee, T. Kaufman-Osborn, W. Melitz, S. Lee, and A. Kummel, Surface Science **605,** 1583 (2011).

[12] T. Kaufman-Osborn, E. A. Chagarov, and A. C. Kummel, Journal of Chemical Physics **140** (2014).

[13] T. Kaufman-Osborn, E. A. Chagarov, S. W. Park, B. Sahu, S. Siddiqui, and A. C. Kummel, Surface Science **630,** 273 (2014).

[14] S. W. Park, H. Kim, E. Chagarov, S. Siddiqui, B. Sahu, N. Yoshida, J. Kachian, R. Feenstra, and A. C. Kummel, Surface Science.

[15] M. Kobayashi, A. Kinoshita, K. Saraswat, H.-S. P. Wong, and Y. Nishi, Journal of Applied Physics **105,** 023702 (2009).

[16] R. R. Lieten, S. Degroote, M. Kuijk, and G. Borghs, Applied Physics Letters **92,** 022106 (2008).

[17] J.-Y. J. Lin, A. M. Roy, A. Nainani, Y. Sun, and K. C. Saraswat, Applied Physics Letters **98,** 092113 (2011).

[18] S. Chakraborty, M. K. Bera, P. K. Bose, and C. K. Maiti, Semiconductor Science and Technology **21,** 335 (2006).

[19] S. L. Manatt and M. R. R. Manatt, Chemistry – A European Journal **10,** 6540 (2004).

[20] R. M. Feenstra, J. A. Stroscio, and A. P. Fein, Surface Science **181,** 295 (1987).

[21] R. M. Feenstra, Surface Science **299–300,** 965 (1994).

[22] R. M. Feenstra, J. Y. Lee, M. H. Kang, G. Meyer, and K. H. Rieder, Physical Review B **73,** 035310 (2006).

[23] R. M. Feenstra, Physical Review B **50,** 4561 (1994).

[24] J. H. Scofield, Journal of Electron Spectroscopy and Related Phenomena **8,** 129 (1976).

[25] F. Bini, C. Rosier, R. P. Saint-Arroman, E. Neumann, C. Dablemont, A. de Mallmann, F. Lefebvre, G. P. Niccolai, J.-M. Basset, M. Crocker, and J.-K. Buijink, Organometallics **25,** 3743 (2006).

[26] D. Briggs and M. P. Seah, D. Briggs, & M. P. Seah,(Editors), John Wiley & Sons, Chichester 1983, xiv+ 533 (1983).

[27] N. Takeuchi, Surface Science **494,** 21 (2001).

[28] A. A. Stekolnikov, J. Furthmuller, and F. Bechstedt, Physical Review B **70** (2004).

[29] Y. J. Zheng, P. F. Ma, and J. R. Engstrom, Journal of Applied Physics **90,** 3614 (2001).

[30] J. Y. Lee, S. J. Jung, J. Y. Maeng, Y. E. Cho, S. Kim, and S. K. Jo, Applied Physics Letters **84,** 5028 (2004).

[31] C. C. Hobbs, L. R. C. Fonseca, A. Knizhnik, V. Dhandapani, S. B. Samavedam, W. J. Taylor, J. M. Grant, L. G. Dip, D. H. Triyoso, R. I. Hegde, D. C. Gilmer, R. Garcia, D. Roan, M. L. Lovejoy, R. S. Rai, E. A. Hebert, T. Hsing-Huang, S. G. H. Anderson, B. E. White, and P. J. Tobin, Electron Devices, IEEE Transactions on **51,** 978 (2004).

[32] F. Bensliman, Y. Sawada, K. Tsujino, and M. Matsumura, Journal of the Electrochemical Society **154,** F102 (2007).

[33] M. P. Seah and W. A. Dench, Surface and Interface Analysis **1,** 2 (1979).

[34] M. Edmonds, T. Kent, E. Chagarov, K. Sardashti, R. Droopad, M. Chang, J. Kachian, J. H. Park, and A. Kummel, Journal of the American Chemical Society (2015).

[35] E. Rudkevich, F. Liu, D. E. Savage, T. F. Kuech, L. McCaughan, and M. G. Lagally, Physical Review Letters **81,** 3467 (1998).